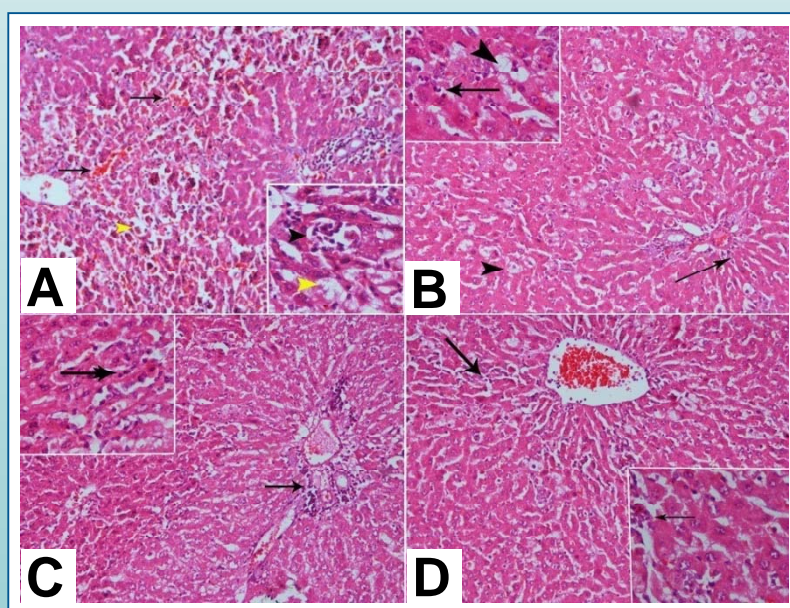


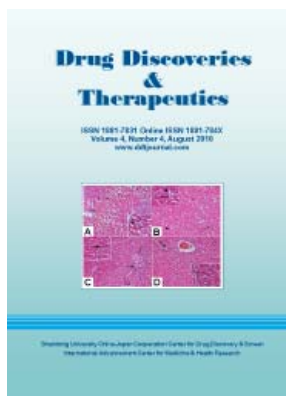
Drug Discoveries & Therapeutics

ISSN 1881-7831 Online ISSN 1881-784X
Volume 4, Number 4, August 2010
www.ddtjournal.com



Shandong University China-Japan Cooperation Center for Drug Discovery & Screen
International Advancement Center for Medicine & Health Research

Drug Discoveries & Therapeutics



Editor-in-Chief:

Kazuhisa SEKIMIZU
(The University of Tokyo, Tokyo, Japan)

Associate Editor:

Norihiro KOKUDO
(The University of Tokyo, Tokyo, Japan)

Drug Discoveries & Therapeutics is a peer-reviewed international journal published bimonthly by *Shandong University China-Japan Cooperation Center for Drug Discovery & Screen (SDU-DDSC)* and *International Advancement Center for Medicine & Health Research Co., Ltd. (IACMHR Co., Ltd.)*.

Drug Discoveries & Therapeutics mainly publishes articles related to basic and clinical pharmaceutical research such as pharmaceutical and therapeutical chemistry, pharmacology, pharmacy, pharmacokinetics, industrial pharmacy, pharmaceutical manufacturing, pharmaceutical technology, drug delivery, toxicology, and traditional herb medicine. Studies on drug-related fields such as biology, biochemistry, physiology, microbiology, and immunology are also within the scope of this journal.

Subject Coverage: Basic and clinical pharmaceutical research including Pharmaceutical and therapeutical chemistry, Pharmacology, Pharmacy, Pharmacokinetics, Industrial pharmacy, Pharmaceutical manufacturing, Pharmaceutical technology, Drug delivery, Toxicology, and Traditional herb medicine.

Language: English

Issues/Year: 6

Published by: IACMHR and SDU-DDSC

ISSN: 1881-7831 (Online ISSN 1881-784X)

CODEN: DDTRBX

Editorial and Head Office

Wei TANG, MD PhD
Executive Editor
Drug Discoveries & Therapeutics
Pearl City Koishikawa 603,
2-4-5 Kasuga, Bunkyo-ku,
Tokyo 112-0003, Japan
Tel: 03-5840-9697
Fax: 03-5840-9698
E-mail: office@ddtjournal.com
URL: www.ddtjournal.com



Drug Discoveries & Therapeutics

Editorial Board

Editor-in-Chief:

Kazuhisa SEKIMIZU (*The University of Tokyo, Tokyo, Japan*)

Associate Editor:

Norihiro KOKUDO (*The University of Tokyo, Tokyo, Japan*)

Executive Editor:

Wei TANG (*The University of Tokyo, Tokyo, Japan*)

Managing Editor:

Munehiro NAKATA (*Tokai University, Kanagawa, Japan*)

Web Editor:

Yu CHEN (*The University of Tokyo, Tokyo, Japan*)

English Editors:

Curtis BENTLEY (*Roswell, GA, USA*)

Thomas R. LEBON (*Los Angeles Trade Technical College, Los Angeles, CA, USA*)

China Office:

Wenfang XU (*Shandong University, Shandong, China*)

Editorial Board Members:

Yoshihiro ARAKAWA (<i>Tokyo, Japan</i>)	Yuxiu LIU (<i>Nanjing, China</i>)
Santad CHANPRAPAPH (<i>Bangkok, Thailand</i>)	Hongxiang LOU (<i>Jinan, China</i>)
Fen-Er CHEN (<i>Shanghai, China</i>)	Ken-ichi MAFUNE (<i>Tokyo, Japan</i>)
Zhe-Sheng CHEN (<i>Queens, NY, USA</i>)	Norio MATSUKI (<i>Tokyo, Japan</i>)
Zilin CHEN (<i>Wuhan, China</i>)	Tohru MIZUSHIMA (<i>Kumamoto, Japan</i>)
Guanhua DU (<i>Beijing, China</i>)	Abdulla M. MOLOKHIA (<i>Alexandria, Egypt</i>)
Chandradhar DWIVEDI (<i>Brookings, SD, USA</i>)	Masahiro MURAKAMI (<i>Osaka, Japan</i>)
Mohamed F. EL-MILIGI (<i>Cairo, Egypt</i>)	Yoshinobu NAKANISHI (<i>Ishikawa, Japan</i>)
Harald HAMACHER (<i>Tuebingen, Germany</i>)	Yutaka ORIHARA (<i>Tokyo, Japan</i>)
Hiroshi HAMAMOTO (<i>Tokyo, Japan</i>)	Xiao-Ming OU (<i>Jackson, MS, USA</i>)
Xiaojiang HAO (<i>Kunming, China</i>)	Weisan PAN (<i>Shenyang, China</i>)
Waseem HASSAN (<i>Santa Maria, RS, Brazil</i>)	Rakesh P. PATEL (<i>Gujarat, India</i>)
Langchong HE (<i>Xi'an, China</i>)	Shafiqur RAHMAN (<i>Brookings, SD, USA</i>)
David A. HORNE (<i>Duarte, CA, USA</i>)	Shivanand P. PUTHLI (<i>Mumbai, India</i>)
Yongzhou HU (<i>Hangzhou, China</i>)	Adel SAKR (<i>Cincinnati, OH, USA</i>)
Wei HUANG (<i>Shanghai, China</i>)	Abdel Aziz M. SALEH (<i>Cairo, Egypt</i>)
Yu HUANG (<i>Hong Kong, China</i>)	Tomofumi SANTA (<i>Tokyo, Japan</i>)
Hans E. JUNGINGER (<i>Phitsanulok, Thailand</i>)	Yasufumi SAWADA (<i>Tokyo, Japan</i>)
Amrit B. KARMARKAR (<i>Mumbai, India</i>)	Brahma N. SINGH (<i>Commack, NY, USA</i>)
Toshiaki KATADA (<i>Tokyo, Japan</i>)	Hongbin SUN (<i>Nanjing, China</i>)
Gagan KAUSHAL (<i>Charleston, WV, USA</i>)	Benny K. H. TAN (<i>Singapore, Singapore</i>)
Ibrahim S. KHATTAB (<i>Safat, Kuwait</i>)	Renxiang TAN (<i>Nanjing, China</i>)
Hiromichi KIMURA (<i>Tokyo, Japan</i>)	Chandan M. THOMAS (<i>Bradenton, FL, USA</i>)
Shiroh KISHIOKA (<i>Wakayama, Japan</i>)	Murat TURKOGLU (<i>Istanbul, Turkey</i>)
Kam Ming KO (<i>Hong Kong, China</i>)	Zhengtao WANG (<i>Shanghai, China</i>)
Nobuyuki KOBAYASHI (<i>Nagasaki, Japan</i>)	Stephen G. WARD (<i>Bath, UK</i>)
Toshiro KONISHI (<i>Tokyo, Japan</i>)	Takako YOKOZAWA (<i>Toyama, Japan</i>)
Masahiro KUROYANAGI (<i>Hiroshima, Japan</i>)	Liangren ZHANG (<i>Beijing, China</i>)
Chun Guang LI (<i>Victoria, Australia</i>)	Jianping ZUO (<i>Shanghai, China</i>)
Hongmin LIU (<i>Zhengzhou, China</i>)	
Jikai LIU (<i>Kunming, China</i>)	

(as of August 25, 2010)

Review

- 223 - 234 **Bioactive constituents of Corni Fructus: The therapeutic use of morroniside, loganin, and 7-O-galloyl-D-sedoheptulose as renoprotective agents in type 2 diabetes.**
Takako Yokozawa, Ki Sung Kang, Chan Hum Park, Jeong Sook Noh, Noriko Yamabe, Naotoshi Shibahara, Takashi Tanaka

Brief Reports

- 235 - 239 **Stability of MALAT-1, a nuclear long non-coding RNA in mammalian cells, varies in various cancer cells.**
Hidenori Tani, Yo Nakamura, Kenichi Ijiri, Nobuyoshi Akimitsu
- 240 - 245 **Alkyne- and 1,6-elimination-succinimidyl carbonate-terminated heterobifunctional poly(ethylene glycol) for reversible "Click" PEGylation.**
Yumei Xie, Shaofeng Duan, M. Laird Forrest

Original Articles

- 246 - 256 **Di(hetero)arylamines in the benzo[b]thiophene series as novel potent antioxidants.**
João P. Silva, Vera A. Machado, Ricardo C. Calhelha, Maria-João R. P. Queiroz, Olga P. Coutinho
- 257 - 266 **Development of a microemulsion-based formulation to improve the availability of poorly water-soluble drug.**
Fathy I. Abd-Allah, Hamdy M. Dawaba, Ahmed M. S. Ahmed
- 267 - 275 **Preparation, characterization, and stability studies of piroxicam-loaded microemulsions in topical formulations.**
Fathy I. Abd-Allah, Hamdy M. Dawaba, Ahmed M. S. Ahmed
- 276 - 284 **The potential therapeutic effect of nitric oxide modulators in experimentally-induced gastric ulcers.**
Ebtehal El-Demerdash, Hala O. El-Mesallamy, Noha M. Abu-Zaid, Mohamed Z. Gad

CONTENTS

(Continued)

- 285 - 297 **Effect of trazodone and nefazodone on hepatic injury induced by carbon tetrachloride.**
Omar M. E. Abdel Salam, Amany A. Sleem, Nermeen Shafee

Guide for Authors

Copyright

Review**Bioactive constituents of Corni Fructus: The therapeutic use of morroniside, loganin, and 7-O-galloyl-D-sedoheptulose as renoprotective agents in type 2 diabetes****Takako Yokozawa^{1,*}, Ki Sung Kang¹, Chan Hum Park¹, Jeong Sook Noh¹, Noriko Yamabe¹, Naotoshi Shibahara¹, Takashi Tanaka²**¹ Institute of Natural Medicine, University of Toyama, Toyama, Japan;² Graduate School of Biomedical Sciences, Nagasaki University, Nagasaki, Japan.

ABSTRACT: Corni Fructus, the fruit of *Cornus officinalis* Sieb. et Zucc. (Cornaceae), is an important crude herb used in Chinese medicine to exhibit several biological activities, including hypoglycemic, antineoplastic, and antimicrobial effects, and to improve liver and kidney functions. We have been investigating the mechanism and bioactive constituents of Corni Fructus using diabetic animal models. Morroniside, loganin, and 7-O-galloyl-D-sedoheptulose, the main active compounds of Corni Fructus, exhibit the same lowering effects of elevated triglyceride, oxidative stress and advanced glycation endproduct (AGE) formation in the kidney of *db/db* mice. The effects of morroniside and 7-O-galloyl-D-sedoheptulose were mediated through modulation by renal sterol regulatory element binding proteins and nuclear factor-kappa B expression, but the effect of loganin was presumably mediated by hypoglycemic and antioxidant effects in the kidney, and also indirectly by the amelioration of metabolic disorders in other organs such as the liver. These findings led us to conclude that morroniside, loganin, and 7-O-galloyl-D-sedoheptulose would synergistically contribute to the inhibition of metabolic disorders (hyperglycemia and dyslipidemia), oxidative stress, inflammation, as well as AGE formation in the diabetic kidney.

Keywords: Corni Fructus, morroniside, loganin, 7-O-galloyl-D-sedoheptulose, *db/db* mice

1. Introduction

Diabetes mellitus is a major cause of mortality and morbidity worldwide, and its prevalence is increasing at an alarming rate. The prevalence of type 2 diabetes mellitus has been predicted to increase markedly during the next few years, reaching 300 million by 2025 (1). The increasing prevalence of diabetes is largely due to the rapid spread of obesity, which is considered the most important risk factor for type 2 diabetes mellitus (2). Type 2 diabetes, a predominant type of diabetes mellitus accounting for 90% of cases, is characterized by abnormal insulin secretion caused by impaired pancreatic β -cell function and insulin resistance in hepatic, adipose, and peripheral tissues (3). As a result of insulin resistance, aggravations of hyperglycemia and dyslipidemia occur, and, consequently, progressive damage to various tissues is induced in type 2 diabetes. Chronic hyperglycemia and dyslipidemia cause oxidative stress and inflammatory responses through the formation of advanced glycation endproducts (AGEs) (4,5), activation of the protein kinase C pathway (6,7), increased glucose flux through the polyol pathway (8), and the accelerated generation of reactive oxygen species (ROS) (9,10). The resulting glycative, glycoxidative, and carbonyl lipotoxicity and oxidative stress can play a key role in the pathogenesis of diabetes (11-14). Therefore, the attenuation of oxidative stress and regulation of hyperlipidemia have been considered as ways to alleviate diabetes and diabetic complications.

Clinical evidence has suggested that the appropriate use of traditional Chinese medicines with modern Western medicinal, or mainstream antidiabetic drugs, can prevent or ameliorate the development of diabetic complications. Many diabetic patients choose alternative therapeutic approaches such as herbal or traditional Chinese medicine along with mainstream antidiabetic drugs, thus making alternative therapy for diabetes very popular (15). However, these medicines

*Address correspondence to:

Dr. Takako Yokozawa, Institute of Natural Medicine, University of Toyama, 2630 Sugitani, Toyama 930-0194, Japan.
e-mail: yokozawa@inm.u-toyama.ac.jp

usually have an insufficient scientific basis and the exact mechanisms behind their beneficial effects are unknown. Therefore, recently, based on a large number of chemical and pharmacological research studies, numerous bioactive compounds have been identified in Chinese medicinal plants for diabetes (16), and we have investigated the mechanism and bioactive constituents of Corni Fructus, the fruit of *Cornus officinalis Sieb. et Zucc.* (Cornaceae), in diabetic animal models.

Corni Fructus is an important crude herb used in Chinese medicine. It is considered to be one of the 25 plant-based drugs most frequently used in China, Japan, and Korea. It is known to exhibit several biological activities, including hypoglycemic, antineoplastic, and antimicrobial effects, and to improve liver and kidney functions (17-19). We previously reported that treatment with Corni Fructus for 10 days suppressed hyperglycemia, proteinuria, renal AGE formation, and related protein expressions, *i.e.*, receptor for AGEs (RAGE), nuclear factor-kappa B (NF- κ B), transforming growth factor-beta1, and *N*^ε-(carboxymethyl)lysine (CML), in the same way as with aminoguanidine. However, improvement of the renal function, shown *via* serum creatinine and creatinine clearance, was superior to aminoguanidine treatment (20). In addition, the administration of Corni Fructus inhibited the elevation of both systolic and diastolic blood pressures, and lowered serum total cholesterol levels with a decrease in esterified cholesterol in the diet-induced hypercholesterolemia rat model (21). Moreover, the atherogenic index was decreased in a dose-dependent manner, suggesting its protective role against cardiovascular disease through regulating cholesterol and lipoprotein levels (21). Therefore, Corni Fructus was suggested to have beneficial effects on diabetes and diabetic complications.

The discovery of efficacious components is essential for clarification of the precise mechanisms of herbal medicines. However, studies on the biological activities of the active components in Corni Fructus are limited. Therefore, we have isolated the major active components of Corni Fructus by employing activity-guided fractionation (Figure 1), and the effects of morroniside, loganin, and 7-*O*-galloyl-D-sedoheptulose (Figure 2) were assessed on glucose metabolism, AGE formation, oxidative stress, and inflammation in type 2 diabetic kidney damage to identify their effects and mechanism of action in type 2 diabetes. This paper gives a review of our recent findings, with emphasis on the therapeutic potential of the active constituents of Corni Fructus against diabetic renal damage.

2. Effect of morroniside on renal damage in type 2 diabetic mice

To investigate the effect of morroniside on type 2 diabetic renal damage, we employed *db/db* mice. As

an experimental model of obesity-associated type 2 diabetes mellitus, *db/db* mice are widely used and well-established (22,23). C57BLKS/J *db/db* mice develop diabetes due to a mutation of the mouse diabetes (*db*) gene that encodes a receptor for leptin. The lack of leptin-receptor signaling results in increased food intake in combination with a phenotype of reduced energy expenditure, reminiscent of the neuroendocrine starvation response (24). Consequently, homozygotes (*db/db*) after birth show uncontrolled eating behavior, become obese, and by 3-6 months after birth, develop severe insulin resistance associated with hyperinsulinemia, hyperglycemia, and hyperlipidemia. The *db/db* vehicle-treated group ($n = 10$) was orally administered water, while the other two groups ($n = 10$ per group) were orally administered morroniside at a dose of 20 or 100 mg per kg body weight per day for 8 weeks, respectively. The non-diabetic *m/m* mice ($n = 6$) as a normal group were compared with the diabetic groups.

Consistent with an earlier report (25), the body weight, food intake, and water intake of *db/db* mice in this study were markedly higher than those of *m/m* mice due to augmented food consumption in *db/db* mice. The administration of morroniside for 8 weeks led to no difference in body weight and food intake; however, the water intake was significantly reduced in morroniside 100 mg/kg-treated mice (Table 1). These results suggest that the oral administration of morroniside may improve the typical diabetic symptom, an excessive intake of water. The serum glucose, triglyceride, and total cholesterol levels of *db/db* mice were markedly higher than those of *m/m* mice, but no significant changes in the glucose and total cholesterol levels were shown on morroniside administration (Table 2). On the other hand, the elevated serum triglyceride level was significantly decreased in morroniside-treated *db/db* mice in a dose-dependent manner (Table 2).

Abnormal renal lipid metabolism is a major symptom of type 2 diabetes (26), and the renal glucose uptake is also markedly increased in type 2 diabetes (27). This could explain the accumulation of glucose and fatty acids noted in diabetic kidneys, and may play a role in the development of diabetic nephropathy (27). Sun *et al.* (28) reported that sterol regulatory element binding protein-1 (SREBP-1) expression was increased in the kidney cortex, resulting in the up-regulation of enzymes responsible for fatty acid synthesis and a high renal triglyceride content as a consequence, which was associated with mesangial expansion and glomerulosclerosis. The transcriptional activation of SREBP-1 can be up-regulated by insulin (29), glucose (10), and liver X receptor (30). The treatment of morroniside led to significant reductions of renal glucose, triglyceride, and total cholesterol contents in *db/db* mice (Figures 3A-3C), which suggested that morroniside effectively prevented the excessive

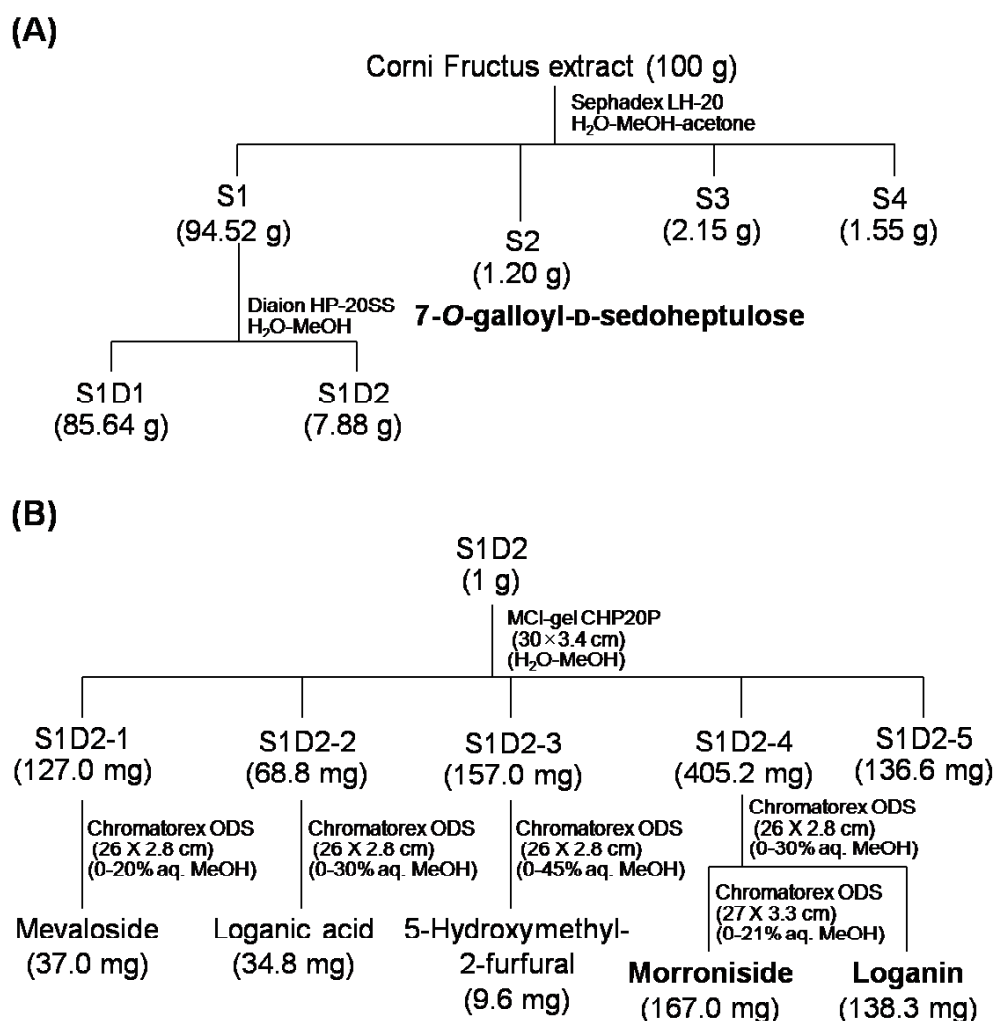


Figure 1. Isolation of morroniside, loganin and 7-O-galloyl-D-sedoheptulose from (A) Corni Fructus extract and (B) fraction S1D2. The extract of *Cornus officinalis* (100 g), which was produced by Tsumura & Co. (Tokyo, Japan) was fractionated by Sephadex™ LH-20 column chromatography (32 × 5 cm) with water containing increasing proportions of methanol (0-100%, 10% stepwise gradient elution) and finally 60% acetone to give four fractions: S1 (94.52 g), S2 (1.20 g), S3 (2.15 g), and S4 (1.55 g). The fraction S1 was further separated by Diaion™ HP-20SS column chromatography (28 × 5 cm) with water-methanol (0-100%, 10% stepwise gradient elution) to give S1D1 (85.64 g) and S1D2 (7.88 g). The structures of morroniside, loganin and 7-O-galloyl-D-sedoheptulose were confirmed by the further purification and spectrometric identification.

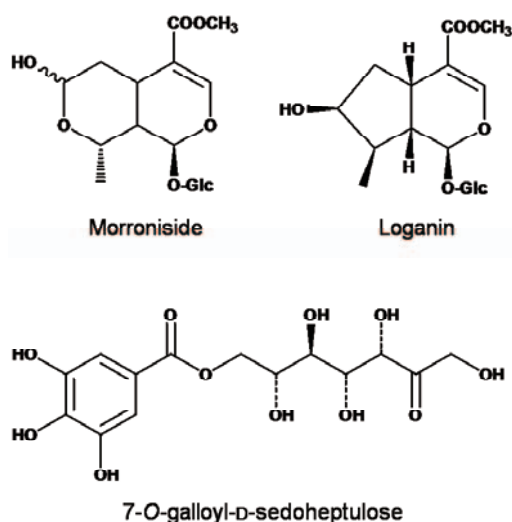


Figure 2. Chemical structure of morroniside, loganin and 7-O-galloyl-D-sedoheptulose.

glucose supply and abnormal lipid accumulation in the kidney. Compared with vehicle-treated *db/db* mice, no alteration in PPAR α expressions of renal tissue was shown in *m/m* mice (Figure 3D). However, morroniside administration significantly lowered the expression of proteins associated with lipid homeostasis, SREBP-1 and SREBP-2, in the kidney of *db/db* mice (Figures 3E and 3F).

Subsequently, the effects of morroniside on factors related to ROS and inflammation in renal tissues were investigated. Increased thiobarbituric acid-reactive substance (TBARS) formation and oxidative stress induced by ROS production and a reduced ratio of reduced glutathione (GSH) to oxidized glutathione (GSSG) are known to decrease insulin sensitivity and increase renal inflammation (31). In this study, TBARS and ROS levels also markedly increased in vehicle-treated *db/db* mice, and these biochemical

Table 1. Body weight, food intake and water intake

Group	Body weight			Food intake (g/day)	Water intake (mL/day)
	Initial (g)	Final (g)	Gain (g/8 weeks)		
<i>m/m</i>	18.6 ± 1.8***	25.4 ± 0.9**	6.4 ± 0.1**	2.7 ± 0.2**	4.1 ± 0.2**
<i>db/db</i>					
Veh	41.4 ± 0.3	55.2 ± 2.4	13.8 ± 1.2	7.0 ± 0.2	15.4 ± 1.2
M-20	42.5 ± 0.7	57.9 ± 1.3	15.4 ± 0.7	7.4 ± 0.1	15.4 ± 0.5
M-100	41.6 ± 0.4	57.5 ± 1.3	15.9 ± 0.5	6.6 ± 0.2	11.6 ± 0.9*

m/m, misty; Veh, vehicle-treated *db/db* mice; M-20, morroniside 20 mg/kg body weight-treated *db/db* mice; M-100, morroniside 100 mg/kg body weight-treated *db/db* mice. * $p < 0.05$, ** $p < 0.01$, *** $p < 0.001$ vs. vehicle-treated *db/db* mice values.

Table 2. Hematological analyses

Item	<i>m/m</i>	<i>db/db</i>		
		Veh	M-20	M-100
Glucose (mg/dL)	219.7 ± 12.0***	765.2 ± 44.8	753.8 ± 34.2	713.6 ± 32.3
Triglyceride (mg/dL)	89.6 ± 5.7***	298.7 ± 24.6	229.8 ± 24.8*	175.4 ± 19.1**
Total cholesterol (mg/dL)	74.0 ± 1.3***	168.5 ± 8.3	160.4 ± 11.2	173.8 ± 4.2

m/m, misty; Veh, vehicle-treated *db/db* mice; M-20, morroniside 20 mg/kg body weight-treated *db/db* mice; M-100, morroniside 100 mg/kg body weight-treated *db/db* mice. * $p < 0.05$, ** $p < 0.01$, *** $p < 0.001$ vs. vehicle-treated *db/db* mice values.

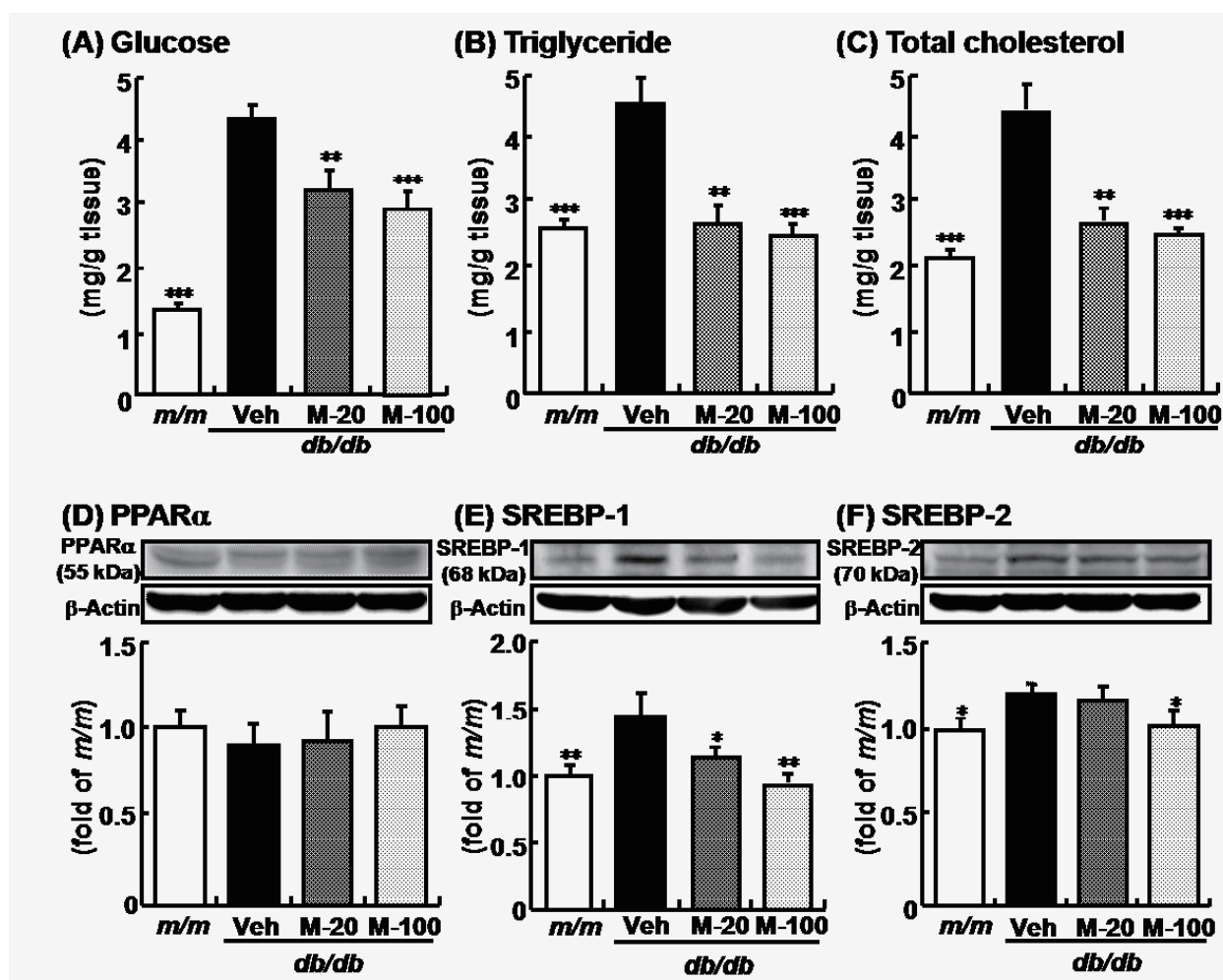


Figure 3. The glucose, triglyceride and total cholesterol contents and the protein expressions related to lipid metabolism in the kidney. (A) Glucose content, (B) triglyceride content, (C) total cholesterol content, (D) PPAR α expression, (E) SREBP-1 expression, (F) SREBP-2 expression. *m/m*, misty; Veh, vehicle-treated *db/db* mice; M-20, morroniside 20 mg/kg body weight-treated *db/db* mice; M-100, morroniside 100 mg/kg body weight-treated *db/db* mice. The results are presented as the means \pm S.E. ($n = 6$ or 10). * $p < 0.05$, ** $p < 0.01$, *** $p < 0.001$ vs. vehicle-treated *db/db* mice values.

factors were significantly reduced by oral morroniside administration in a dose-dependent manner (Table 3). Also, the reduced ratio of GSH/GSSG in vehicle-treated *db/db* mice in the kidney was increased by morroniside treatment almost to the level of *m/m* normal control mice (Table 3).

Hyperglycemia also causes oxidative stress due to the increased mitochondrial production of superoxide, including the depletion of NADPH and consequent disturbance of glutathione and nitric oxide metabolism. These oxidative stresses are responsible for the regulation of the transcriptional pathways of NF- κ B (32), which is a transcription factor thought to play an important role in the onset of inflammation (33). NF- κ B activation can lead to the enhanced expression of proinflammatory cytokines, chemokines, adhesion molecules, inflammatory receptors, and inflammatory enzymes such as inducible nitric oxide synthase (iNOS) and cyclooxygenase-2 (COX-2) (34-36). Therefore, the modulation of NF- κ B activation may provide a direct way of inhibiting inflammatory mediators (37). From the analysis of renal protein expression, the administration of morroniside could reduce the

elevated renal NF- κ Bp65, COX-2, and iNOS levels (Figure 4). These results suggest that the administration of morroniside can alleviate renal damage induced by ROS through the deactivation of NF- κ B and subsequent restoration of the antioxidative state.

In summary, morroniside has beneficial effects against type 2 diabetic renal damage mediated by a decrease in augmented concentrations of glucose, triglyceride, and cholesterol *via* the down-regulation of SREBP-1 and SREBP-2 proteins in the kidney of *db/db* mice. Also, morroniside ameliorated oxidative stress and its related inflammation in the kidney. Consequently, the protective role of morroniside against type 2 diabetic renal damage was suggested to be mediated by the amelioration of metabolic disorders including dyslipidemia, oxidative stress, and the inflammatory response.

3. Effect of loganin on renal damage in type 2 diabetic mice

To identify the effect of loganin on type 2 diabetic renal damage, *db/db* mice ($n = 10$ per group) were orally

Table 3. Biomarkers associated with oxidative stress in kidney

Item	<i>m/m</i>	<i>db/db</i>		
		Veh	M-20	M-100
TBARS (nmol/mg protein)	1.24 ± 0.03***	1.90 ± 0.09	1.54 ± 0.07**	1.30 ± 0.06*
ROS (Fluorescence/min/mg protein)	2,168 ± 33***	3,086 ± 185	2,017 ± 93***	1,769 ± 53*
GSH (μmol/mg protein)	7.44 ± 0.25***	4.45 ± 0.15	6.61 ± 0.30**	7.41 ± 0.26***
GSSG (μmol/mg protein)	6.29 ± 0.43*	5.12 ± 0.31	6.24 ± 0.19*	6.33 ± 0.10*
GSH/GSSG	1.20 ± 0.05***	0.89 ± 0.05	1.07 ± 0.06**	1.17 ± 0.03***

m/m, misty; Veh, vehicle-treated *db/db* mice; M-20, morroniside 20 mg/kg body weight-treated *db/db* mice; M-100, morroniside 100 mg/kg body weight-treated *db/db* mice. * $p < 0.05$, ** $p < 0.01$, *** $p < 0.001$ vs. vehicle-treated *db/db* mice values.

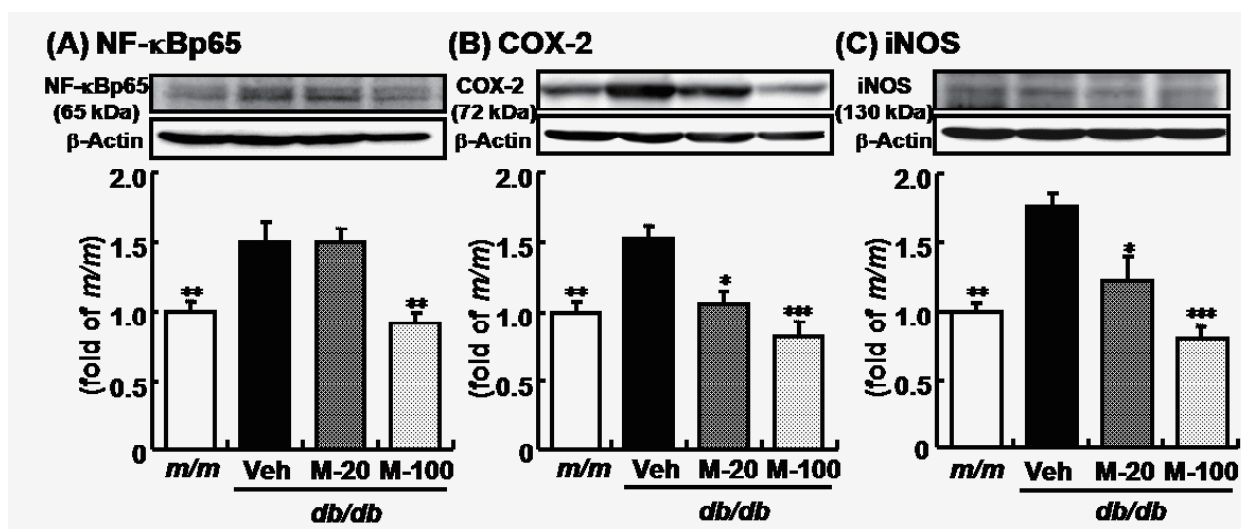


Figure 4. The protein expressions related inflammation in the kidney. (A) NF- κ Bp65 expression, (B) COX-2 expression, (C) iNOS expression. *m/m*, misty; Veh, vehicle-treated *db/db* mice; M-20, morroniside 20 mg/kg body weight-treated *db/db* mice; M-100, morroniside 100 mg/kg body weight-treated *db/db* mice. The results are presented as the means \pm S.E. ($n = 6$ or 10). * $p < 0.05$, ** $p < 0.01$, *** $p < 0.001$ vs. vehicle-treated *db/db* mice values.

administered loganin at a dose of 20 or 100 mg per kg body weight per day for 8 weeks, respectively. The non-diabetic *m/m* mice ($n = 6$) as a normal group were compared with the diabetic groups.

The *db/db* mice displayed typical phenotypes of obesity-induced diabetes with a marked increase in body weight gain, and food and water intakes. Although there were no changes in the body weight and water intake, food consumption was significantly reduced in loganin-treated groups after an 8-week experimental period (Table 4). The serum glucose, triglyceride and total cholesterol levels of *db/db* mice were markedly higher than those of *m/m* mice (Table 5). The loganin 100 mg/kg-treated *db/db* mice showed a decrease in serum glucose (Table 5) presumably caused by the reduced food intake. Several studies have shown that just few days of caloric restriction can induce marked improvements in glycemic control (39). Furthermore, the 8-week administration of loganin to *db/db* mice significantly improved the serum lipid profile with dose-dependent reductions of triglyceride; however, the total cholesterol level remained unchanged (Table 5). The levels of glucose, triglyceride, and total cholesterol in the kidney of vehicle-treated *db/db* mice were significantly elevated compared to those of *m/m* mice (Figures 5A-5C), but loganin administration at 100 mg/kg led to a marked decrease in the triglyceride level in the kidney of *db/db* mice (Figure 5B). However, compared with vehicle-treated *db/db* mice, no alteration in PPAR α expressions of renal tissue was shown in *m/m* mice (Figure 5D). SREBP-1 and SREBP-2 protein expressions were markedly elevated in the kidney of vehicle-treated *db/db* compared with *m/m* mice (Figures 5E and 5F), but there were no changes on loganin treatment. These results suggest that the lipid-lowering

effect of loganin may be mediated by its effect on other organs such as the liver.

As shown in Table 6, the levels of TBARS and ROS in the kidney of vehicle-treated *db/db* mice were higher than those of *m/m* mice, whereas these enhanced levels were significantly reduced by loganin treatment nearly to the level of *m/m* mice. The *db/db* vehicle group showed significantly decreased GSH/GSSG ratios in the kidney compared with the *m/m* group, which resulted from the decreased GSH and increased GSSG, but this reduction in the GSH/GSSG ratio recovered nearly to the level of *m/m* mice on loganin treatment.

The two distinctive AGEs, CML and *N*^ε-(carboxyethyl)lysine (CEL), are formed on proteins by glycoxidation and/or lipid peroxidation pathways. CML accumulates with TBARS in glomerular lesions, resulting in structural and functional alterations in extracellular matrix proteins (39). In addition, RAGE is activated by AGEs, and AGE-RAGE interaction increases ROS formation, with the subsequent activation of NF- κ B and release of pro-inflammatory cytokines (40). In the present study, the enhanced renal protein expressions of NF- κ B, COX-2, and iNOS in the kidney of *db/db* mice remained unchanged on loganin administration in *db/db* mice (Figures 6A-6C). The protein expressions of AGE-related proteins were enhanced in the kidneys of *db/db* mice at the age of 17 weeks, but the oral administration of loganin attenuated the increase in CML accumulation (Figure 6E). Therefore, loganin was suggested to have no effect on the inflammatory damage in the kidney, but inhibited AGE accumulation possibly through hypoglycemic effect.

In summary, loganin has a milder effect than morroniside against type 2 diabetic renal damage.

Table 4. Body weight, food intake and water intake

Group	Body weight			Food intake (g/day)	Water intake (mL/day)
	Initial (g)	Final (g)	Gain (g/8 weeks)		
<i>m/m</i>	21.4 ± 0.5**	27.1 ± 0.9**	5.2 ± 0.6**	3.2 ± 0.2**	3.8 ± 0.3**
<i>db/db</i>					
Veh	39.6 ± 0.3	52.7 ± 1.6	13.7 ± 1.1	7.0 ± 0.1	19.4 ± 4.0
L-20	38.6 ± 0.6	52.2 ± 1.4	13.5 ± 0.9	6.2 ± 0.1*	13.2 ± 0.1
L-100	38.5 ± 0.4	50.9 ± 0.9	11.6 ± 0.6	5.7 ± 0.1*	12.8 ± 0.1

m/m, misty; Veh, vehicle-treated *db/db* mice; L-20, loganin 20 mg/kg body weight-treated *db/db* mice; L-100, loganin 100 mg/kg body weight-treated *db/db* mice. * $p < 0.05$, ** $p < 0.001$ vs. vehicle-treated *db/db* mice values.

Table 5. Hematological analyses

Item	<i>m/m</i>	<i>db/db</i>		
		Veh	L-20	L-100
Glucose (mg/dL)	206.2 ± 6.5**	854.9 ± 24.3	809.5 ± 25.9	739.8 ± 38.1*
Triglyceride (mg/dL)	87.4 ± 5.4**	303.4 ± 24.5	163.2 ± 16.7**	151.8 ± 14.2**
Total cholesterol (mg/dL)	82.4 ± 6.2**	165.0 ± 11.2	174.6 ± 9.7	156.9 ± 4.9

m/m, misty; Veh, vehicle-treated *db/db* mice; L-20, loganin 20 mg/kg body weight-treated *db/db* mice; L-100, loganin 100 mg/kg body weight-treated *db/db* mice. * $p < 0.01$, ** $p < 0.001$ vs. vehicle-treated *db/db* mice values.

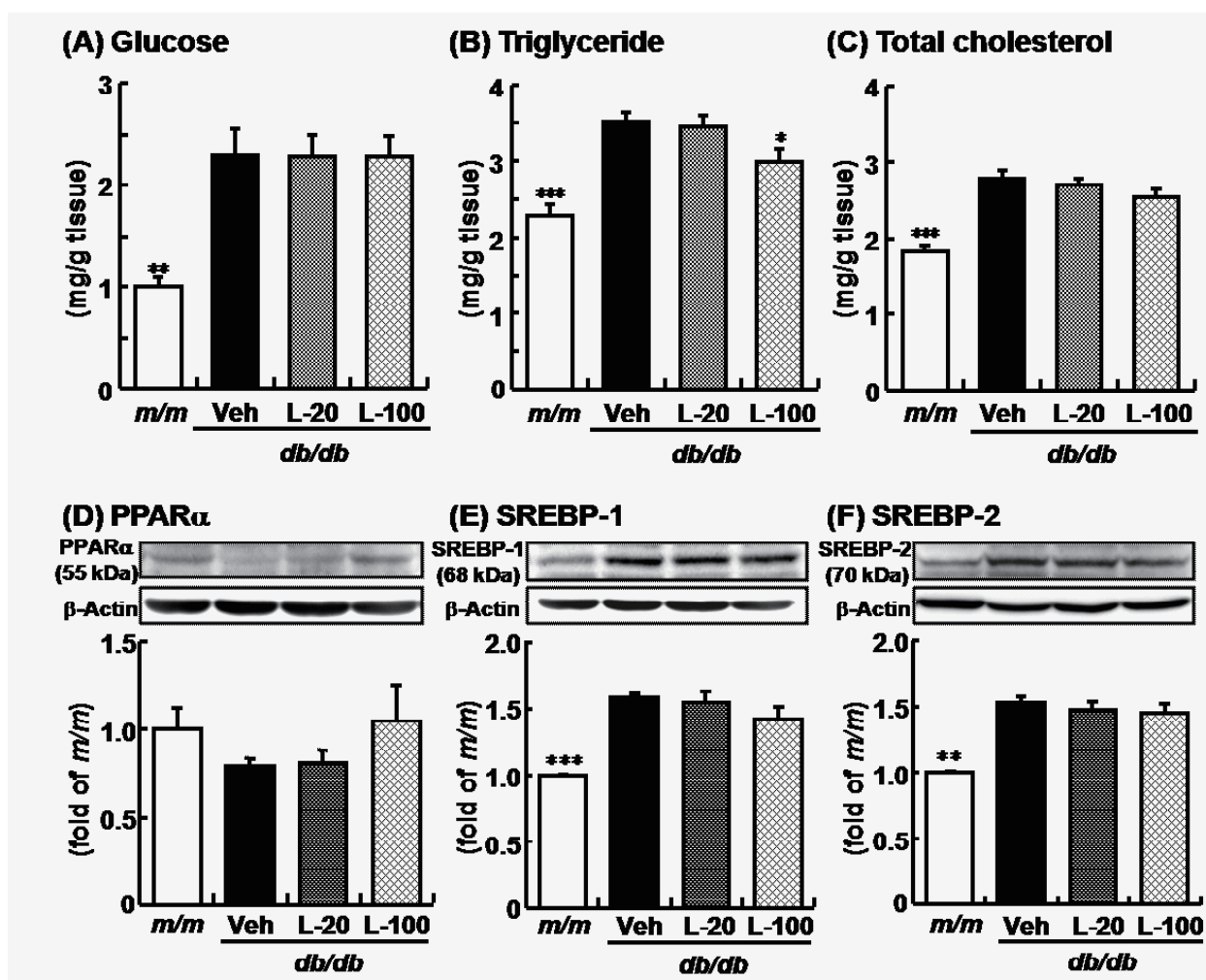


Figure 5. The glucose, triglyceride and total cholesterol contents and the protein expressions related to lipid metabolism in the kidney. (A) Glucose content, (B) triglyceride content, (C) total cholesterol content, (D) PPAR α expression, (E) SREBP-1 expression, (F) SREBP-2 expression. *m/m*, misty; Veh, vehicle-treated *db/db* mice; L-20, loganin 20 mg/kg body weight-treated *db/db* mice; L-100, loganin 100 mg/kg body weight-treated *db/db* mice. The results are presented as the means \pm S.E. ($n = 6$ or 10). * $p < 0.05$, ** $p < 0.01$, *** $p < 0.001$ vs. vehicle-treated *db/db* mice values.

Table 6. Biomarkers associated with oxidative stress in kidney

Item	<i>m/m</i>	<i>db/db</i>		
		Veh	L-20	L-100
TBARS (nmol/mg protein)	1.20 \pm 0.02***	1.37 \pm 0.01	1.29 \pm 0.05	1.27 \pm 0.03*
ROS (Fluorescence/min/mg protein)	2,056 \pm 34*	2,913 \pm 216	1,704 \pm 132***	1,745 \pm 142***
GSH (μ mol/mg protein)	8.45 \pm 0.18*	7.66 \pm 0.24	8.32 \pm 0.19*	8.62 \pm 0.18**
GSSG (μ mol/mg protein)	2.83 \pm 0.08*	3.22 \pm 0.11	2.73 \pm 0.16*	2.86 \pm 0.10*
GSH/GSSG	3.00 \pm 0.11***	2.39 \pm 0.09	3.13 \pm 0.17**	3.04 \pm 0.11***

m/m, misty; Veh, vehicle-treated *db/db* mice; L-20, loganin 20 mg/kg body weight-treated *db/db* mice; L-100, loganin 100 mg/kg body weight-treated *db/db* mice. * $p < 0.05$, ** $p < 0.01$, *** $p < 0.001$ vs. vehicle-treated *db/db* mice values.

However, the administration of loganin led to the suppression of hyperglycemia through the inhibition of food intake. The effect of loganin on type 2 diabetic renal damage was suggested to be mediated by hypoglycemic and antioxidant effects in the kidney, and also indirectly by the amelioration of metabolic disorders including dyslipidemia, oxidative stress, and the inflammatory response in other organs such as the liver.

4. Effect of 7-O-galloyl-D-sedoheptulose on renal damage in type 2 diabetic mice

To identify the effect of 7-O-galloyl-D-sedoheptulose on type 2 diabetic renal damage, *db/db* mice ($n = 10$ per group) were orally administered 7-O-galloyl-D-sedoheptulose at a dose of 20 or 100 mg per kg body weight per day for 8 weeks, respectively. The non-diabetic *m/m* mice ($n = 6$) as a normal group were

compared with the diabetic groups.

As shown in the results, the initial, final, and gain of body weights, and the levels of food and water intake in *db/db* mice were significantly higher than those in *m/m* mice (Table 7). Compared with the vehicle-treated *db/db* mice, the levels of body weight and food and water intake were not changed by 7-*O*-galloyl-D-sedoheptulose treatment throughout the experimental period. The oral administration of 7-*O*-galloyl-D-

sedoheptulose affected its favorable influences on the serum lipid profile and on renal glucose and triglyceride (Table 8, Figures 7A and 7B). The effect of 7-*O*-galloyl-D-sedoheptulose treatment on renal functional parameters (creatinine and urea nitrogen) are summarized in Table 9. The serum levels of creatinine and urea nitrogen in *db/db* mice were significantly higher than in *m/m* mice. However, these elevated renal dysfunction parameters in *db/db* mice were

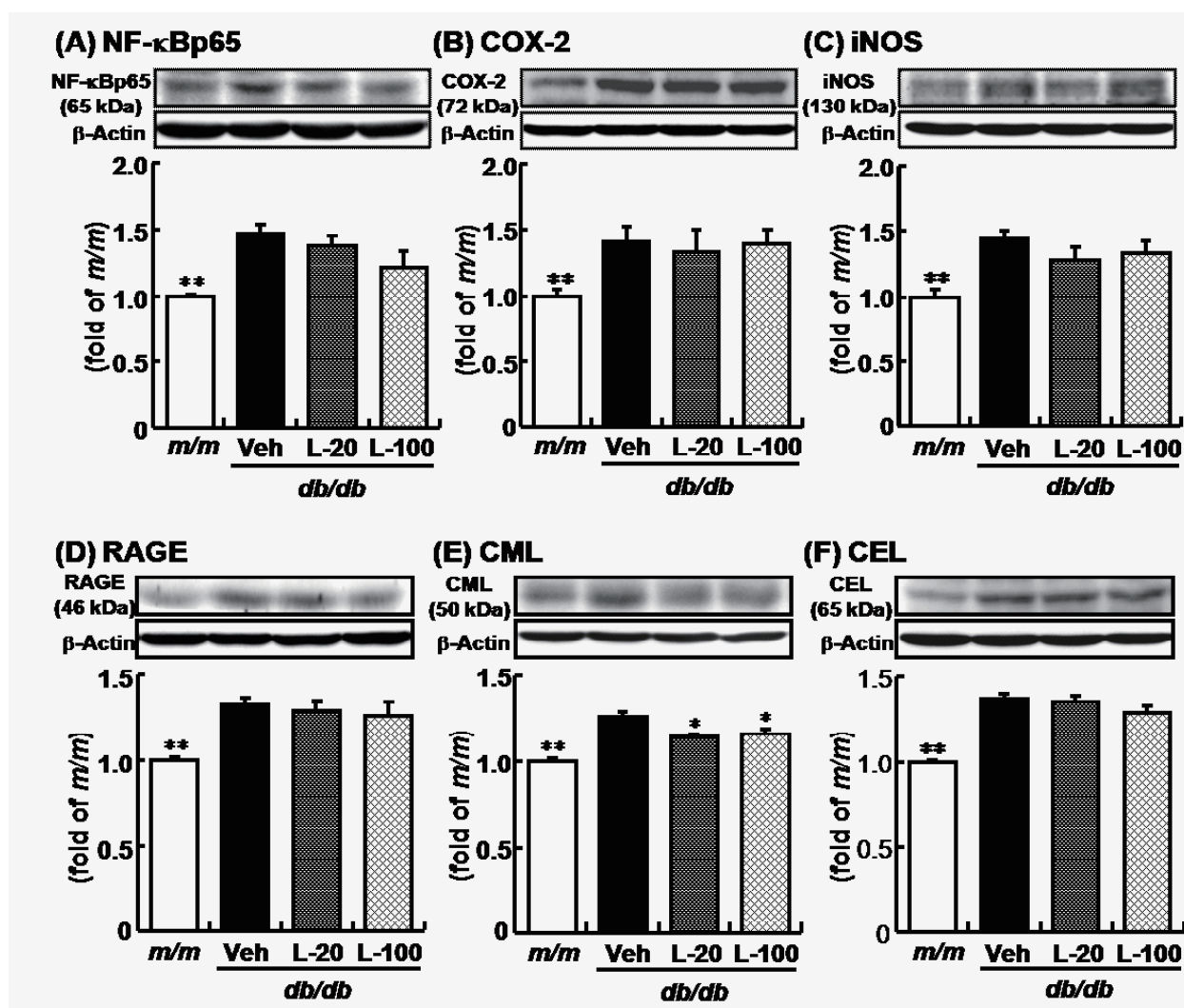


Figure 6. The protein expressions related inflammation and AGEs in the kidney. (A) NF-κBp65 expression, (B) COX-2 expression, (C) iNOS expression, (D) RAGE expression, (E) CML expression, (F) CEL expression. *m/m*, misty; Veh, vehicle-treated *db/db* mice; L-20, loganin 20 mg/kg body weight-treated *db/db* mice; L-100, loganin 100 mg/kg body weight-treated *db/db* mice. The results are presented as the means \pm S.E. ($n = 6$ or 10). * $p < 0.05$, ** $p < 0.01$ vs. vehicle-treated *db/db* mice values.

Table 7. Body weight, food intake and water intake

Group	Body weight			Food intake (g/day)	Water intake (mL/day)
	Initial (g)	Final (g)	Gain (g/8 weeks)		
<i>m/m</i>	22.1 \pm 0.5**	25.8 \pm 0.8**	3.7 \pm 0.3**	2.9 \pm 0.1**	3.9 \pm 0.3*
<i>db/db</i>					
Veh	40.0 \pm 0.8	49.2 \pm 1.3	9.2 \pm 0.5	5.6 \pm 0.2	13.2 \pm 0.8
GS-20	39.5 \pm 0.9	45.9 \pm 2.5	6.4 \pm 1.6	5.4 \pm 0.2	13.4 \pm 0.7
GS-100	40.2 \pm 0.8	49.7 \pm 1.8	9.6 \pm 1.1	5.5 \pm 0.1	12.8 \pm 0.8

m/m, misty; Veh, vehicle-treated *db/db* mice; GS-20, 7-*O*-galloyl-D-sedoheptulose 20 mg/kg body weight-treated *db/db* mice; GS-100, 7-*O*-galloyl-D-sedoheptulose 100 mg/kg body weight-treated *db/db* mice. * $p < 0.05$, ** $p < 0.01$ vs. vehicle-treated *db/db* mice values.

Table 8. Hematological analyses

Item	<i>m/m</i>	<i>db/db</i>		
		Veh	GS-20	GS-100
Glucose (mg/dL)	204.5 ± 13.3**	753.2 ± 33.9	722.9 ± 54.6	775.6 ± 35.0
Triglyceride (mg/dL)	56.8 ± 3.1**	242.6 ± 17.0	181.5 ± 14.7*	145.1 ± 13.6**
Total cholesterol (mg/dL)	115.9 ± 5.9**	183.2 ± 11.3	186.7 ± 14.2	171.0 ± 9.4*

m/m, misty; Veh, vehicle-treated *db/db* mice; GS-20, 7-*O*-galloyl-D-sedoheptulose 20 mg/kg body weight-treated *db/db* mice; GS-100, 7-*O*-galloyl-D-sedoheptulose 100 mg/kg body weight-treated *db/db* mice. * $p < 0.05$, ** $p < 0.001$ vs. vehicle-treated *db/db* mice values.

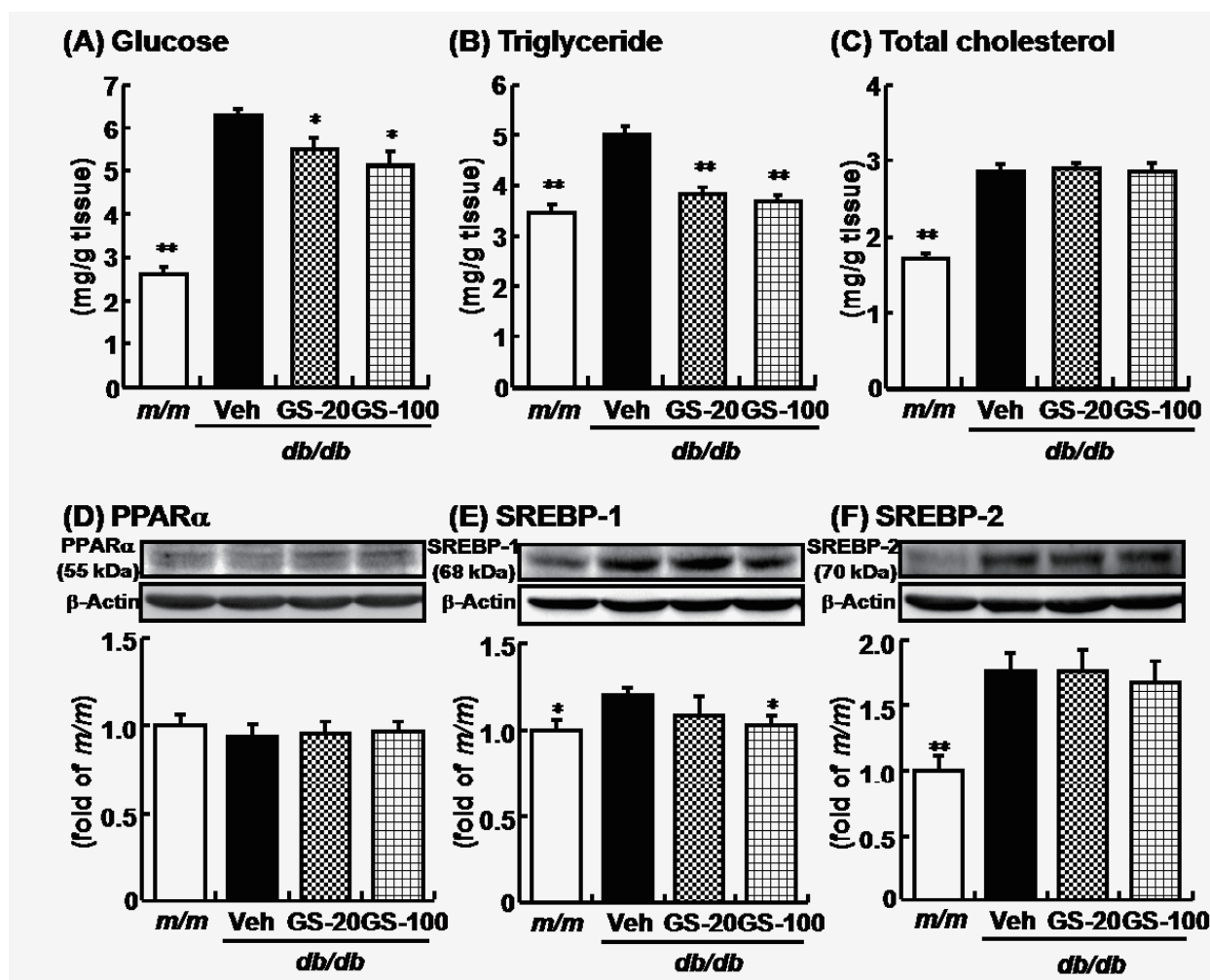


Figure 7. The glucose, triglyceride and total cholesterol contents and the protein expressions related to lipid metabolism in the kidney. (A) Glucose content, (B) triglyceride content, (C) total cholesterol content, (D) PPAR α expression, (E) SREBP-1 expression, (F) SREBP-2 expression. *m/m*, misty; Veh, vehicle-treated *db/db* mice; GS-20, 7-*O*-galloyl-D-sedoheptulose 20 mg/kg body weight-treated *db/db* mice; GS-100, 7-*O*-galloyl-D-sedoheptulose 100 mg/kg body weight-treated *db/db* mice. The results are presented as the means \pm S.E. ($n = 6$ or 10). * $p < 0.05$, ** $p < 0.01$ vs. vehicle-treated *db/db* mice values.

efficiently reduced by the 7-*O*-galloyl-D-sedoheptulose treatments. These results suggested the amelioration of renal dysfunction in *db/db* mice by 7-*O*-galloyl-D-sedoheptulose treatment. Compared with *db/db* vehicle-treated mice, no alteration in PPAR α expressions of renal tissue were shown in *m/m* and 7-*O*-galloyl-D-sedoheptulose-treated mice (Figure 7D). However, SREBP-1 and SREBP-2 protein expressions were markedly elevated in the kidney of vehicle-treated *db/db* compared with *m/m* mice (Figures 7E and 7F).

The administration of 7-*O*-galloyl-D-sedoheptulose of 100 mg/kg completely normalized the increased expressions of renal SREBP-1; however, SREBP-2 protein expressions remained unchanged in the kidney tissues (Figures 7E and 7F).

Besides the beneficial effects on lipid metabolism, 7-*O*-galloyl-D-sedoheptulose administration exerted an antioxidant effect. The elevated renal ROS and TBARS levels in *db/db* mice were lowered nearly to the level of *m/m* mice by 7-*O*-galloyl-D-sedoheptulose

Table 9. Renal functional parameters

Item	<i>m/m</i>	<i>db/db</i>		
		Veh	GS-20	GS-100
Creatinine (mg/dL)	0.31 ± 0.01*	0.46 ± 0.04	0.38 ± 0.02*	0.36 ± 0.02*
Urea-N (mg/dL)	27.5 ± 0.8**	40.3 ± 1.9	40.1 ± 1.6	38.5 ± 1.1*

m/m, misty; Veh, vehicle-treated *db/db* mice; GS-20, 7-*O*-galloyl-D-sedoheptulose 20 mg/kg body weight-treated *db/db* mice; GS-100, 7-*O*-galloyl-D-sedoheptulose 100 mg/kg body weight-treated *db/db* mice. * $p < 0.05$, ** $p < 0.001$ vs. vehicle-treated *db/db* mice values.

Table 10. Biomarkers associated with oxidative stress in kidney

Item	<i>m/m</i>	<i>db/db</i>		
		Veh	GS-20	GS-100
TBARS (nmol/mg protein)	1.03 ± 0.06***	1.62 ± 0.05	1.45 ± 0.04*	1.18 ± 0.08***
ROS (Fluorescence/min/mg protein)	1,798 ± 149***	3,338 ± 222	2,552 ± 124**	2,529 ± 105**
GSH (μmol/mg protein)	12.06 ± 0.72*	9.92 ± 0.36	10.69 ± 0.17	10.62 ± 0.35
GSSG (μmol/mg protein)	2.30 ± 0.15	2.58 ± 0.12	2.55 ± 0.02	2.40 ± 0.09
GSH/GSSG	5.01 ± 0.22**	4.07 ± 0.08	4.05 ± 0.09	4.28 ± 0.22

m/m, misty; Veh, vehicle-treated *db/db* mice; GS-20, 7-*O*-galloyl-D-sedoheptulose 20 mg/kg body weight-treated *db/db* mice; GS-100, 7-*O*-galloyl-D-sedoheptulose 100 mg/kg body weight-treated *db/db* mice. * $p < 0.05$, ** $p < 0.01$, *** $p < 0.001$ vs. vehicle-treated *db/db* mice values.

treatment at 100 mg/kg (Table 10). The *db/db* vehicle mice showed significantly decreased GSH/GSSG ratios compared with the *m/m* group, which resulted from the decreased GSH and increased GSSG in the kidney, but the reduction of the GSH/GSSG ratio in the kidney of *db/db* mice was not recovered on 7-*O*-galloyl-D-sedoheptulose treatment (Table 10). 7-*O*-galloyl-D-sedoheptulose administration showed inhibitory effects on the expression of an oxidative stress-induced transcriptional factor, NF-κB, in the kidney with the down-regulation of COX-2 and iNOS (Figures 8A-8C). These results showed that the anti-inflammatory effects of 7-*O*-galloyl-D-sedoheptulose may be associated with the down-regulation of COX-2 and iNOS followed by the inhibition of NF-κB transcription stimulated by oxidative stress in the kidney of type 2 diabetic mice.

The AGE-RAGE interaction activates transforming growth factor-beta1 signaling pathways and subsequently induces mesangial cell hypertrophy and glomerular sclerosis through fibronectin synthesis (41,42). Therefore, AGE accumulation in the kidney has been regarded as an index of progressive renal damage in diabetic complications. CML and CEL are well-characterized compounds that are commonly used as AGE markers (43). Particularly, CML is not only referred to as a glycoxidation product similar to pentosidine, but is also formed during the metal-catalyzed oxidation of polyunsaturated fatty acids in the presence of protein (44). In the present study, not only the over-expression of AGE (CML and CEL) but also the higher levels of NF-κB in the kidney of *db/db* mice were alleviated by 8-week treatment with 7-*O*-galloyl-D-sedoheptulose (Figures 8A, 8E, and 8F).

In summary, 7-*O*-galloyl-D-sedoheptulose treatment improved the impaired kidney function in

type 2 diabetic mice. The renoprotective effects of 7-*O*-galloyl-D-sedoheptulose in diabetes were mediated by the lipid-lowering and anti-inflammatory effects through the modulation of renal SREBP-1 and NF-κB expressions, respectively, and the inhibition of AGE accumulation.

5. Conclusion and Perspectives

The antidiabetic effects and mechanisms of morroniside, loganin, and 7-*O*-galloyl-D-sedoheptulose in *db/db* mice, as type 2 diabetic mice, were investigated, with a focus on the kidney damage caused by hyperglycemia, dyslipidemia, inflammation, RAGE activation, and AGE formation. Morroniside, loganin, and 7-*O*-galloyl-D-sedoheptulose showed the same lowering effects on elevated triglyceride, oxidative stress (TBARS and ROS) and AGE formation in the kidney of *db/db* mice. The effects of morroniside and 7-*O*-galloyl-D-sedoheptulose were mediated by the modulation of renal SREBP and NF-κB expressions, but the effect of loganin was presumably mediated by the hypoglycemic and antioxidant effects in the kidney, and also indirectly by the amelioration of metabolic disorders in other organs such as the liver.

In conclusion, two iridoid glycosides (morroniside and loganin) and one low-molecular-weight polyphenol (7-*O*-galloyl-D-sedoheptulose), the main active compounds of Corni Fructus, beneficially acted in type 2 diabetic model *db/db* mice through specified mechanisms, as summarized above. These findings allowed us to conclude that morroniside, loganin, and 7-*O*-galloyl-D-sedoheptulose would synergistically contribute to the inhibition of metabolic disorders (hyperglycemia and dyslipidemia), oxidative stress,

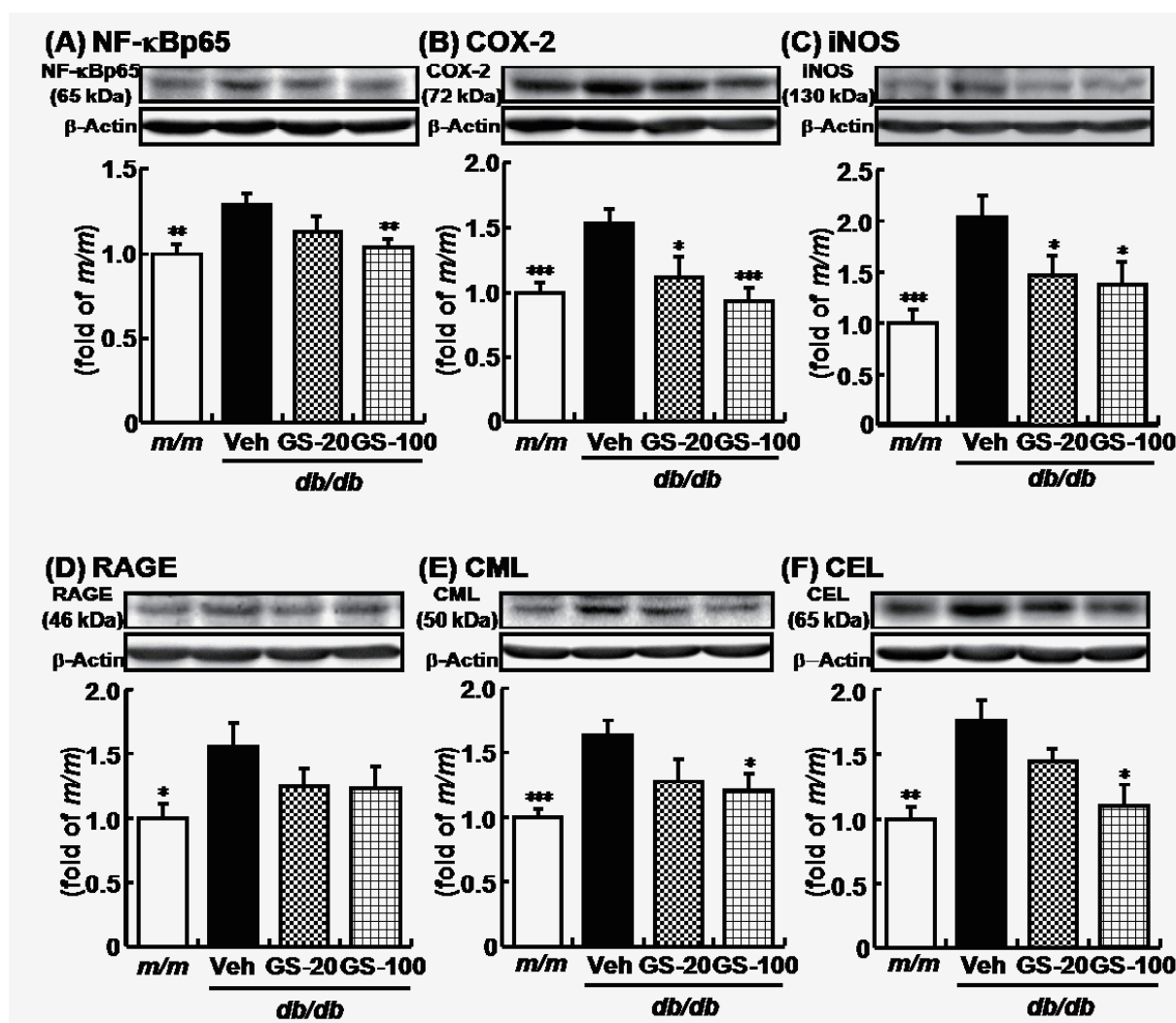


Figure 8. The protein expressions related inflammation and AGEs in the kidney. (A) NF-κBp65 expression, (B) COX-2 expression, (C) iNOS expression, (D) RAGE expression, (E) CML expression, (F) CEL expression. *m/m*, misty; Veh, vehicle-treated *db/db* mice; GS-20, 7-*O*-galloyl-D-sedoheptulose 20 mg/kg body weight-treated *db/db* mice; GS-100, 7-*O*-galloyl-D-sedoheptulose 100 mg/kg body weight-treated *db/db* mice. The results are presented as the means \pm S.E. ($n = 6$ or 10). * $p < 0.05$, ** $p < 0.01$, *** $p < 0.001$ vs. vehicle-treated *db/db* mice values.

inflammation, as well as AGE formation in the diabetic kidney. The present study advances knowledge on the beneficial effects of bioactive constituents of Corni Fructus, as well as the possible development of therapeutic or preventive agents for diabetic complications.

References

- Zimmet P. The burden of type 2 diabetes: Are we doing enough? *Diabetes Metab.* 2003; 29:6S9-6S18.
- Mokdad AH, Bowman BA, Ford ES, Vinicor F, Marks JS, Koplan JP. The continuing epidemics of obesity and diabetes in the United States. *JAMA.* 2001; 286:1195-1200.
- Kasuga M. Insulin resistance and pancreatic beta cell failure. *J Clin Invest.* 2006; 116:1756-1760.
- Brownlee M, Cerami A, Vlassara H. Advanced glycosylation end products in tissue and the biochemical basis of diabetic complications. *N Engl J Med.* 1988; 318:1315-1321.
- Singh R, Barden A, Mori T, Beilin L. Advanced glycation endproducts: A review. *Diabetologia.* 2001; 44:129-146.
- Inoguchi T, Battan R, Handler E, Sportsman JR, Heath W, King GL. Preferential elevation of protein kinase C isoform beta II and diacylglycerol levels in the aorta and heart of diabetic rats: Differential reversibility to glycemic control by islet cell transplantation. *Proc Natl Acad Sci U S A.* 1992; 89:11059-11063.
- Koya D, King GL. Protein kinase C activation and the development of diabetic complications. *Diabetes.* 1998; 47:859-866.
- Yabe-Nishimura C. Aldose reductase in glucose toxicity: a potential target for the prevention of diabetic complications. *Pharmacol Rev.* 1998; 50:21-33.
- Hunt JV, Dean RT, Wolff SP. Hydroxyl radical production and autoxidative glycosylation. Glucose autoxidation as the cause of protein damage in the experimental glycation model of diabetes mellitus and aging. *Biochem J.* 1988; 256:205-212.
- Nishikawa T, Edelstein D, Du XL, Yamagishi S, Matsumura T, Kaneda Y, Yorek MA, Beebe D, Oates

- PJ, Hammes HP, Giardino I, Brownlee M. Normalizing mitochondrial superoxide production blocks three pathways of hyperglycaemic damage. *Nature*. 2000; 404:787-790.
11. Bonnefont-Rousselot D, Bastard JP, Jaudon MC, Delattre J. Consequences of the diabetic status on the oxidant/antioxidant balance. *Diabetes Metab*. 2000; 26:163-176.
 12. Jakus V. The role of free radicals, oxidative stress and antioxidant systems in diabetic vascular disease. *Bratisl Lek Listy*. 2000; 101:541-551.
 13. West IC. Radicals and oxidative stress in diabetes. *Diabet Med*. 2000; 17:171-180.
 14. Miyata T. Alterations of non-enzymatic biochemistry in uremia, diabetes, and atherosclerosis ("carbonyl stress"). *Bull Mem Acad R Med Belg*. 2002; 157:189-198.
 15. Ceylan-Isik AF, Fliethman RM, Wold LE, Ren J. Herbal and traditional Chinese medicine for the treatment of cardiovascular complications in diabetes mellitus. *Curr Diabetes Rev*. 2008; 4:320-328.
 16. Li WL, Zheng HC, Bukuru J, De Kimpe N. Natural medicines used in the traditional Chinese medical system for therapy of diabetes mellitus. *J Ethnopharmacol*. 2004; 92:1-21.
 17. Chang JS, Chiang LC, Hsu FF, Lin CC. Chemoprevention against hepatocellular carcinoma of *Cornus officinalis* *in vitro*. *Am J Chin Med*. 2004; 32:717-725.
 18. Liou SS, Liu IM, Hsu SF, Cheng JT. Corni fructus as the major herb of Die-Huang-Wan for lowering plasma glucose in Wistar rats. *J Pharm Pharmacol*. 2004; 56:1443-1447.
 19. Vareed SK, Reddy MK, Schutzki RE, Nair MG. Anthocyanins in *Cornus alternifolia*, *Cornus controversa*, *Cornus kousa* and *Cornus florida* fruits with health benefits. *Life Sci*. 2006; 78:777-784.
 20. Yamabe N, Kang KS, Goto E, Tanaka T, Yokozawa T. Beneficial effect of Corni Fructus, a constituent of Hachimi-jio-gan, on advanced glycation end-product-mediated renal injury in streptozotocin-treated diabetic rats. *Biol Pharm Bull*. 2007; 30:520-526.
 21. Park CH, Cho EJ, Yokozawa T. Protection against hypercholesterolemia by Corni fructus extract and its related protective mechanism. *J Med Food*. 2009; 12:973-981.
 22. Hummel KP, Dickie MM, Coleman DL. Diabetes, a new mutation in the mouse. *Science*. 1966; 153:1127-1128.
 23. Kaku K, Province M, Permutt MA. Genetic analysis of obesity-induced diabetes associated with a limited capacity to synthesize insulin in C57BL/KS mice: Evidence for polygenic control. *Diabetologia*. 1989; 32:636-643.
 24. Münzberg H, Myers MG Jr. Molecular and anatomical determinants of central leptin resistance. *Nat Neurosci*. 2005; 8:566-570.
 25. Lee YA, Cho EJ, Yokozawa T. Effects of proanthocyanidin preparations on hyperlipidemia and other biomarkers in mouse model of type 2 diabetes. *J Agric Food Chem*. 2008; 56:7781-7789.
 26. Lee HS, Lee JS, Koh HI, Ko KW. Intraglomerular lipid deposition in routine biopsies. *Clin Nephrol*. 1991; 36:67-75.
 27. Meyer C, Stumvoll M, Nadkarni V, Dostou J, Mitrakou A, Gerich J. Abnormal renal and hepatic glucose metabolism in type 2 diabetes mellitus. *J Clin Invest*. 1998; 102:619-624.
 28. Sun L, Halaihel N, Zhang W, Rogers T, Levi M. Role of sterol regulatory element-binding protein 1 in regulation of renal lipid metabolism and glomerulosclerosis in diabetes mellitus. *J Biol Chem*. 2002; 277:18919-18927.
 29. Kim JB, Sarraf P, Wright M, Yao KM, Mueller E, Solanes G, Lowell BB, Spiegelman BM. Nutritional and insulin regulation of fatty acid synthetase and leptin gene expression through ADD1/SREBP1. *J Clin Invest*. 1998; 101:1-9.
 30. Robertson RP. Chronic oxidative stress as a central mechanism for glucose toxicity in pancreatic islet beta cells in diabetes. *J Biol Chem*. 2004; 279:42351-42354.
 31. Bashan N, Kovsan J, Kachko I, Ovadia H, Rudich A. Positive and negative regulation of insulin signaling by reactive oxygen and nitrogen species. *Physiol Rev*. 2009; 89:27-71.
 32. Bours V, Bonizzi G, Bentires-Alj M, Bureau F, Piette J, Lekeux P, Merville M. NF- κ B activation in response to toxic and therapeutic agents: Role in inflammation and cancer treatment. *Toxicology*. 2000; 153:27-38.
 33. Lawrence T, Gilroy DW, Colville-Nash PR, Willoughby DA. Possible new role for NF- κ B in the resolution of inflammation. *Nat Med*. 2001; 7:1291-1297.
 34. Barnes PJ, Karin M. Nuclear factor- κ B: A pivotal transcription factor in chronic inflammatory diseases. *N Engl J Med*. 1997; 336:1066-1071.
 35. Yamamoto Y, Gaynor RB. Therapeutic potential of inhibition of the NF- κ B pathway in the treatment of inflammation and cancer. *J Clin Invest*. 2001; 107:135-142.
 36. Zhang Z, Liong EC, Lau TY, Leung KM, Fung PC, Tipoe GL. Induction of apoptosis by hexamethylene bisacetamide is p53-dependent associated with telomerase activity but not with terminal differentiation. *Int J Oncol*. 2000; 16:887-892.
 37. Zhang G, Ghosh S. Toll-like receptor-mediated NF- κ B activation: A phylogenetically conserved paradigm in innate immunity. *J Clin Invest*. 2001; 107:13-19.
 38. Wing RR. Use of very-low-calorie diets in the treatment of obese persons with non-insulin-dependent diabetes mellitus. *J Am Diet Assoc*. 1995; 95:569-572.
 39. Heidland A, Sebekova K, Schinzel R. Advanced glycation end products and the progressive course of renal disease. *Am J Kidney Dis*. 2001; 38:S100-S106.
 40. Bierhaus A, Stern DM, Nawroth PP. RAGE in inflammation: A new therapeutic target? *Curr Opin Investig Drugs*. 2006; 7:985-991.
 41. Yamagishi S, Fukami K, Ueda S, Okuda S. Molecular mechanisms of diabetic nephropathy and its therapeutic intervention. *Curr Drug Targets*. 2007; 8:952-959.
 42. Hyogo H, Yamagishi S. Advanced glycation end products (AGE) and their involvement in liver disease. *Curr Pharm Des*. 2008; 14:969-972.
 43. Chappey O, Dosquet C, Wautier MP, Wautier JL. Advanced glycation end products, oxidant stress and vascular lesions. *Eur J Clin Invest*. 1997; 27:97-108.
 44. Fu MX, Requena JR, Jenkins AJ, Lyons TJ, Baynes JW, Thorpe SR. The advanced glycation end product, N^ε-(carboxymethyl)lysine, is a product of both lipid peroxidation and glycoxidation reactions. *J Biol Chem*. 1996; 271:9982-9986.

(Received March 17, 2010; Accepted May 18, 2010)

Brief Report

Stability of MALAT-1, a nuclear long non-coding RNA in mammalian cells, varies in various cancer cells

Hidenori Tani, Yo Nakamura, Kenichi Ijiri, Nobuyoshi Akimitsu*

Radioisotope Center, The University of Tokyo, Tokyo, Japan.

ABSTRACT: Recent large-scale transcriptome analyses have revealed a large number of transcripts with low protein-coding potential, known as non-coding RNAs (ncRNAs). Many studies revealed that several long ncRNAs are involved in the regulation of genome organization and gene expression, or in the structural components of functional domains in the nucleus. As regulation of mRNA decay in the cytoplasm is crucial for controlling the abundance of cellular transcripts and the levels of protein expression, so regulation of long non-coding RNA decay in the nucleus is considered to be important for biological function. Although enzymatic pathways involved in cytoplasmic mRNA decay have been studied extensively, far less is known about those in nuclear long ncRNA decay. Here, we have investigated decay of metastasis associated lung adenocarcinoma transcript 1 (MALAT-1), which is a long (~ 8 kb) ncRNA that is misregulated in many human cancers and was shown to be retained specifically in the nucleus in nuclear speckles, as a model of nuclear long ncRNA in mammalian cells. We have found that the half-life of MALAT-1 ranges from ~ 9 h to > 12 h in various cancer cells. Moreover, Xrn2, PM/ScI-75, PARN, and Mtr4, known nuclear RNases or RNA helicases, did not affect MALAT-1 degradation or single knockdown of these components did not change the MALAT-1 decay rate.

Keywords: Non-coding RNA, metastasis associated lung adenocarcinoma transcript 1 (MALAT-1), RNA degradation, cancer, nuclear speckle

1. Introduction

Most of the eukaryotic genome is transcribed, yielding

*Address correspondence to:

Dr. Nobuyoshi Akimitsu, Radioisotope Center, The University of Tokyo, 2-11-16 Yayoi, Bunkyo-ku, Tokyo 113-0032, Japan.

e-mail: akimitsu@ric.u-tokyo.ac.jp

a complex network of transcripts that include tens of thousands of long noncoding RNAs (ncRNAs) with little or no protein coding capacity. Recent studies revealed that several long ncRNAs in the nucleus are required for epigenetic silencing of multiple genes *in cis* within large chromosomal domains such as Xist, Air, and Kcnq1ot1 (1-3), or are essential structural/organizational components of paraspeckles such as MENε/β (4-6). As regulation of mRNA decay in the cytoplasm is important for controlling the abundance of cellular transcripts and the levels of protein expression, so regulation of long ncRNA decay in the nucleus is considered to be important for their biological function. Although the enzymatic pathways involved in cytoplasmic mRNA decay have been studied extensively (7-9), far less is known about those in nuclear long ncRNA decay.

Metastasis associated lung adenocarcinoma transcript 1 (MALAT-1), also known as NEAT2, is a long (~ 8 kb) ncRNA (10) which was shown to be retained specifically in the nucleus in nuclear speckles (11). It has domains that are thought to be involved in the assembly, modification, and/or storage of the pre-mRNA processing machinery. MALAT-1 was originally identified as a transcript showing significant expression in individuals exhibiting high risk for metastasis of non-small cell lung tumors (10), and subsequently showed broad expression in normal human and mouse tissues and is overexpressed in many human carcinomas, including those of the breast, pancreas, lung, colon, prostate, and liver (10-12). This implies that MALAT-1 misregulation may play a role in the development of numerous cancers. The nascent MALAT-1 transcript is processed to yield two ncRNAs that localize to different subcellular compartments (13). Recently, several studies revealed that MALAT-1 is associated with cell invasion (14,15).

In this study, we have investigated the decay of MALAT-1 as a model of nuclear long ncRNA in mammalian cells. We have found that the half-life of MALAT-1 ranges from ~ 9 h to > 12 h in various cancer cells. Moreover, we investigated whether nuclear nuclease components such as Xrn2, PM/ScI-75, PARN, and Mtr4 affect the decay rate of MALAT-1.

2. Materials and Methods

2.1. Cell culture

H1299 (human lung cancer cells), H1975 (human lung cancer cells), and HT1080 (human fibrosarcoma cells) cells were cultured at 37°C in the presence of 5% CO₂ in RPMI-1640 medium (Wako) supplemented with 10% fetal bovine serum and penicillin/streptomycin. A549 (human lung cancer cells) and HeLa Tet-off (TO) (human cervical cells) cells were cultured at 37°C in the presence of 5% CO₂ in Dulbecco's Modified Eagles Medium (D-MEM) supplemented with 10% fetal bovine serum and penicillin/streptomycin.

2.2. siRNA treatment

siRNAs were purchased from SIGMA, Gene Pharms, or NIPPON EGT. The sequences of the siRNAs for Xrn2, PM/ScI-75, PARN, and Mtr4 are 5'-AAGAGUACAGA UGAUCAUGUU-3', 5'-AACAUUCGAGAGAUUUGUA CUA-3', 5'-CCGCAACAAUAGUUUUACAGC-3', and 5'-GCCUAUGCACUUCAAAUGATT-3', respectively. These siRNAs were transfected into each HeLa TO cell using Lipofectamine RNAiMAX (Invitrogen) according to the manufacturer's instructions. As controls, cells were transfected with control siRNA (SIGMA). Quantitative real-time reverse transcriptase PCR was used to determine whether RNA interference achieved significant depletion of each target sequence.

2.3. RNA isolation and Northern blot analysis

Total RNA was isolated according to the method

of Chomczynski and Sacchi (16) at different times after the addition of 20 µg/mL of 5,6-dichloro-1-β-D-ribofuranosylbenzimidazole (DRB). Total RNA (4 µg) was resolved using 1% formaldehyde agarose gel electrophoresis under denaturing conditions and was transferred to a nylon membrane. RNA blots were stained with methylene blue to check for equal loading and transfer. Hybridization was performed using the ULTRAhyb (Ambion) with random primed [α -³²P]dCTP-labeled cDNA probes corresponding to MALAT-1 and 7SK. Hybridization signals were visualized and quantified with a FLA-9000 (FUJIFILM).

2.4. Quantitative real-time reverse transcriptase PCR

Total RNA was reverse transcribed into cDNA using the QuantiTect Reverse Transcription Kit (Qiagen). cDNA was amplified using the following primers: Xrn2 forward (5'-CTTTTCAGCAGCAAAGGTT-3') and reverse (5'-TGGAAGGCTGCATTCTGG-3'), PM/ScI-75 forward (5'-TCAGGATCTCATTTGGAA CAGA-3') and reverse (5'-CACAGGAAACCTGTCC AAGAA-3'), PARN forward (5'-GAAGGAAAAAG GCCAAGAAATTA-3') and reverse (5'-GGCTGTTC TTCGAGATGCTT-3'), Mtr4 forward (5'-GTTGAAG GGTGTACACATGAGG-3') and reverse (5'-TCCAA CTCGTGGTTTAAGTGG-3'), and GAPDH forward (5'-GCACCGTCAAGGCTGAGAAC-3') and reverse (5'-TGGTGAAGACGCCAGTGG-3'). GAPDH was used for normalization. The SYBR[®] Premix Ex Taq[™] II (Perfect Real Time) (TaKaRa) was used according to the manufacturer's instructions. Quantitative real-time reverse transcriptase PCR analysis was performed using a Thermal Cycler Dice Real Time System (TaKaRa).

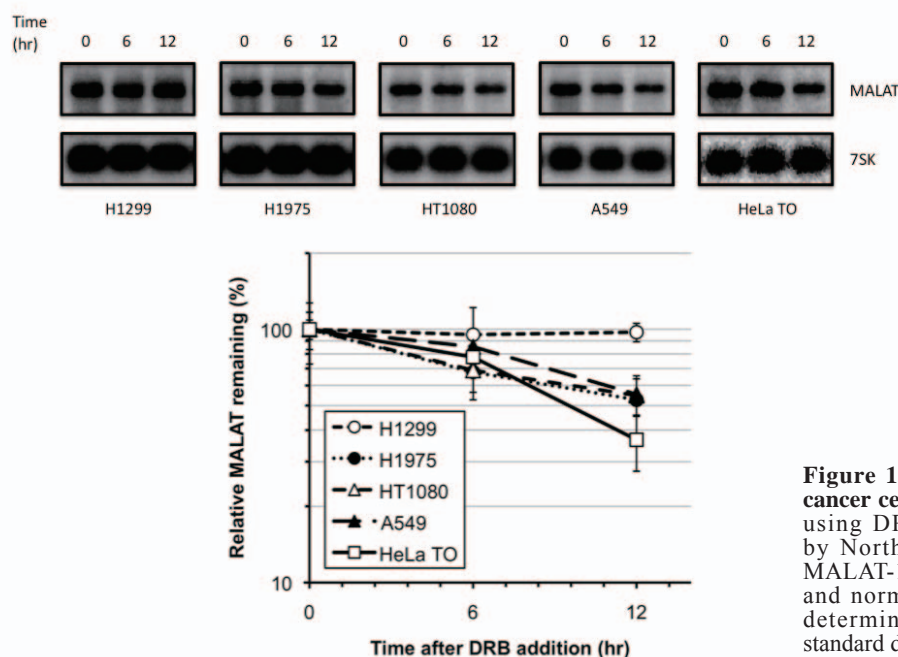


Figure 1. Decay of MALAT-1 in various cancer cells. MALAT-1 stability was assessed using DRB chase experiments, followed by Northern blot analysis. In the graph, MALAT-1 signal intensities were quantified and normalized to 7SK RNA in triplicate determinations. The error bars represent standard deviation.

3. Results and Discussion

3.1. MALAT-1 stability in various cancer cells

We first examined the decay of MALAT-1 in various cancer cells (H1299, H1975, A549, HT1080, and HeLa

TO cells) by DRB chase experiments using 7SK RNA as a control (Figure 1). Since DRB specifically inhibits transcription elongation by RNA Polymerase II, 7SK RNA, which is transcribed by RNA Polymerase III, is stably transcribed. Half-lives of MALAT-1 in H1299, H1975, A549, HT1080, and HeLa TO cells were >

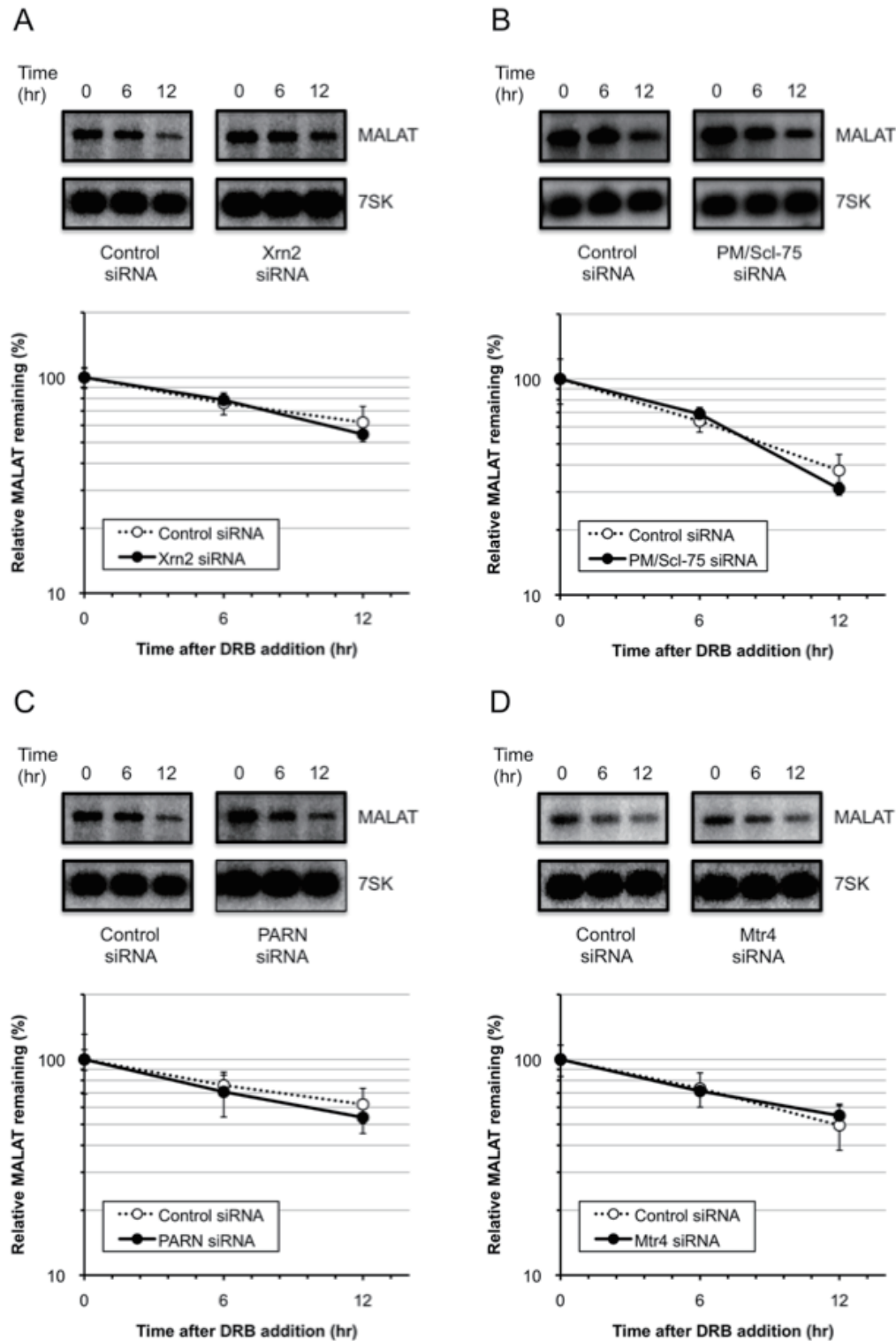


Figure 2. Decay of MALAT-1 after knockdown of several components by siRNA. HeLa TO cells were transfected with siRNA for (A) Xrn2, (B) Pm/Scf75, (C) PARN, or (D) Mtr4, and MALAT-1 stability was assessed using DRB chase experiments, followed by Northern blot analysis. In the graphs, MALAT-1 signal intensities were quantified and normalized to 7SK RNA in triplicate determinations. The error bars represent standard deviation.

12, ~ 12, ~ 12, ~ 12, and 9 h, respectively. MALAT-1 stabilities varied in various cancer cells. Interestingly, the half-life of MALAT-1 (~ 9 h) in HeLa TO cells is shorter than the median mRNA half-life (10 h) in human cells as described previously (17). This suggests that MALAT-1 may be actively degraded in HeLa TO cells. AU-rich elements (AREs) are present in the 3'-untranslated regions (3'-UTRs) of mRNA encoded in so-called early response genes, such as many proto-oncogenes, growth factors, and cytokines (18). AREs are recognized as the common RNA destabilizing element in mammalian cells. Interestingly, we found that MALAT-1 contains 21 AREs, and these are predominantly located in the 5'-untranslated regions (5'-UTRs). AREs encoded in MALAT-1 might be involved in fast degradation.

3.2. Knockdown of *Xrn2*, *PM/Scf-75*, *PARN*, and *Mtr4* in HeLa TO cells

To investigate the contributing components to degradation of MALAT-1 in HeLa TO cells, we targeted *Xrn2*, *PM/Scf-75/Rrp45*, Poly(A)-specific ribonuclease (*PARN*), and *Mtr4*. *Xrn2* is a nuclear 5'-to-3' exonuclease (19). *PM/Scf-75* is a core component of the exosome, which is a complex of 3'-to-5' exonucleases (20). *PARN* is a deadenylation nuclease that was found largely in the nuclear fraction (21). *Mtr4* is a putative RNA helicase, and is part of the recently identified TRAMP complex, which is required for the activation of the nuclear exosome *in vivo* by polyadenylation of target RNAs in yeast (22,23). Each siRNA for these components was introduced into HeLa TO cells, and the MALAT-1 decay rates in these cells were examined using Northern blot analysis. The siRNA of each target sequence was effective because knockdown of *Xrn2*, *PM/Scf-75*, *PARN*, or *Mtr4* reduced each transcript level to 17, 13, 9, and 24%, respectively. However, the depletions of these components did not change the MALAT-1 decay rate (Figure 2). These results suggest that *Xrn2*, *PM/Scf-75*, *PARN*, *Mtr4* did not affect MALAT-1 degradation or single knockdown of these components did not change the MALAT-1 decay rate.

Acknowledgements

This study was financially supported by a Research Fellowship of the Japan Society for the Promotion of Science.

References

1. Heard E, Chaumeil J, Masui O, Okamoto I. Mammalian X-chromosome inactivation: an epigenetics paradigm. *Cold Spring Harb Symp Quant Biol.* 2005; 69:89-102.
2. Braidotti G, Baubec T, Pauler F, Seidl C, Smrzka O, Stricker S, Yotova I, Barlow DP. The Air noncoding RNA: An imprinted *cis*-silencing transcript. *Cold Spring Harb Symp Quant Biol.* 2004; 69:55-66.
3. Pandey RR, Mondal T, Mohammad F, Enroth S, Redrup L, Komorowski J, Nagano T, Mancini-Dinardo D, Kanduri C. *Kcnq1ot1* antisense noncoding RNA mediates lineage-specific transcriptional silencing through chromatin-level regulation. *Mol Cell.* 2008; 32:232-246.
4. Sasaki YT, Ideue T, Sano M, Mituyama T, Hirose T. *MENε/β* noncoding RNAs are essential for structural integrity of nuclear paraspeckles. *Proc Natl Acad Sci U S A.* 2009; 106:2525-2530.
5. Sunwoo H, Dinger ME, Wilusz JE, Amaral PP, Mattick JS, Spector DL. *MEN ε/β* nuclear-retained non-coding RNAs are up-regulated upon muscle differentiation and are essential components of paraspeckles. *Genome Res.* 2009; 19:347-359.
6. Clemson CM, Hutchinson JN, Sara SA, Ensminger AW, Fox AH, Chess A, Lawrence JB. An architectural role for a nuclear noncoding RNA: *NEAT1* RNA is essential for the structure of paraspeckles. *Mol Cell.* 2009; 33:717-726.
7. Maquat LE. Nonsense-mediated mRNA decay: Splicing, translation and mRNP dynamics. *Nat Rev Mol Cell Biol.* 2004; 5:89-99.
8. Amrani N, Sachs MS, Jacobson A. Early nonsense: mRNA decay solves a translational problem. *Nat Rev Mol Cell Biol.* 2006; 7:415-425.
9. Behm-Ansmant I, Izaurralde E. Quality control of gene expression: A stepwise assembly pathway for the surveillance complex that triggers nonsense-mediated mRNA decay. *Genes Dev.* 2006; 20:391-398.
10. Ji P, Diederichs S, Wang W, Böing S, Metzger R, Schneider PM, Tidow N, Brandt B, Buerger H, Bulk E, Thomas M, Berdel WE, Serve H, Müller-Tidow C. *MALAT-1*, a novel noncoding RNA, and thymosin beta4 predict metastasis and survival in early-stage non-small cell lung cancer. *Oncogene.* 2003; 22:8031-8041.
11. Hutchinson JN, Ensminger AW, Clemson CM, Lynch CR, Lawrence JB, Chess A. A screen for nuclear transcripts identifies two linked noncoding RNAs associated with SC35 splicing domains. *BMC Genomics.* 2007; 8:39.
12. Lin R, Maeda S, Liu C, Karin M, Edgington TS. A large noncoding RNA is a marker for murine hepatocellular carcinomas and a spectrum of human carcinomas. *Oncogene.* 2006; 26:851-858.
13. Wilusz JE, Freier SM, Spector DL. 3' end processing of a long nuclear-retained noncoding RNA yields a tRNA-like cytoplasmic RNA. *Cell.* 2008; 135:919-932.
14. Guo F, Li Y, Liu Y, Wang J, Li Y, Li G. Inhibition of metastasis-associated lung adenocarcinoma transcript 1 in CaSki human cervical cancer cells suppresses cell proliferation and invasion. *Acta Biochim Biophys Sin (Shanghai).* 2010; 42:224-229.
15. Tseng JJ, Hsieh YT, Hsu SL, Chou MM. Metastasis associated lung adenocarcinoma transcript 1 is up-regulated in placenta previa increta/percreta and strongly associated with trophoblast-like cell invasion *in vitro*. *Mol Hum Reprod.* 2010; 15:725-731.
16. Chomczynski P, Sacchi N. Single-step method of RNA isolation by acid guanidinium thiocyanate-phenol-chloroform extraction. *Anal Biochem.* 1987; 162:156-159.
17. Yang E, van Nimwegen E, Zavolan M, Rajewsky N, Schroeder M, Magnasco M, Darnell JE. Decay

- rates of human mRNAs: Correlation with functional characteristics and sequence attributes. *Genome Res.* 2003; 13:1863-1872.
18. Chen CY, Shyu AB. AU-rich elements: Characterization and importance in mRNA degradation. *Trends Biochem Sci.* 1995; 20:465-470.
 19. West S, Gromak N, Proudfoot NJ. Human 5' → 3' exonuclease Xrn2 promotes transcription termination at co-transcriptional cleavage sites. *Nature.* 2004; 432:522-525.
 20. Vanacova S, Stefl R. The exosome and RNA quality control in the nucleus. *EMBO Rep.* 2007; 8:651-657.
 21. Yamashita A, Chang TC, Yamashita Y, Zhu W, Zhong Z, Chen CY, Shyu AB. Concerted action of poly(A) nucleases and decapping enzyme in mammalian mRNA turnover. *Nat Struct Mol Biol.* 2005; 12:1054-1063.
 22. Vanáčová S, Wolf J, Martin G, Blank D, Dettwiler S, Friedlein A, Langen H, Keith G, Keller W. A new yeast poly(A) polymerase complex involved in RNA quality control. *PLoS Biol.* 2005; 3:e189.
 23. LaCava J, Houseley J, Saveanu C, Petfalski E, Thompson E, Jacquier A, Tollervey D. RNA degradation by the exosome is promoted by a nuclear polyadenylation complex. *Cell.* 2005; 121:713-724.

(Received May 7, 2010; Revised June 6, 2010; Accepted June 16, 2010)

Brief Report

Alkyne- and 1,6-elimination-succinimidyl carbonate-terminated heterobifunctional poly(ethylene glycol) for reversible "Click" PEGylation

Yumei Xie, Shaofeng Duan, M. Laird Forrest*

Department of Pharmaceutical Chemistry, University of Kansas, Lawrence, Kansas, USA.

ABSTRACT: A new heterobifunctional (succinimidyl carbonate, SC)-activated poly(ethylene glycol) (PEG) with a reversible 1,6-elimination linker and a terminal alkyne for "click" chemistry was synthesized with high efficiency and low polydispersity. The α -alkyne- ω -hydroxyl PEG was first prepared using trimethylsilyl-2-propargyl alcohol as an initiator for ring-opening polymerization of ethylene oxide followed by mild deprotection with tetrabutylammonium fluoride. The hydroxy end was then modified with diglycolic anhydride to generate α -alkyne- ω -carboxylic acid PEG. The reversible 1,6-elimination linker was introduced by conjugation of a hydroxymethyl phenol followed by activation with *N,N'*-disuccinimidyl carbonate to generate the heterobifunctional α -alkyne- ω -SC PEG. The terminal alkyne is available for "click" conjugation to azido ligands *via* 1,3-dipolar cycloaddition, and the succinimidyl carbonate will form a reversible conjugate to amines (*e.g.* in proteins) that can release the unaltered amine after base or enzyme catalyzed cleavage of the 1,6-linker.

Keywords: PEGylation, heterobifunctional PEG

1. Introduction

Poly(ethylene glycol) (PEG) is often employed as a solubilizer for poorly water soluble drugs. The conjugation of PEG, or PEGylation, is known to increase *in vivo* blood circulatory time, reduce immunogenicity, and improve stability and pharmacological properties of both small molecule and large biological drugs, including peptides, proteins, viruses, enzymes, and DNAs. The

majority of these systems utilize monofunctional PEG with only one reactive terminal group, such as a hydroxy, amine, thiol, aldehyde, carboxylic acid, or activated variants. Targeted drug delivery systems using PEGylated therapeutics require two reactive termini on the PEG, *i.e.*, α,ω -heterobifunctional PEG; one bound to the therapeutic and the other available for conjugation to targeting ligands, such as peptides, antibodies, or proteins. Unfortunately, most commercially available PEGs are not suitable for high extents of PEGylation because they form irreversibly conjugates that may hinder activity of the therapeutic cargo. Furthermore, delicate targeting antibodies must be conjugated under aqueous conditions, and most available linkers are not suitable for heterogeneous conjugation in aqueous milieu.

The 1,3-dipolar cycloaddition reaction (termed "click" chemistry) between alkyne and organic azides, which yields the corresponding 1,2,3-triazoles, is highly chemoselective and can be performed under mild reaction conditions in aqueous buffers within a wide pH range. Several publications have reported the application of click chemistry to label proteins (1-3), modify viruses (4), synthesize a "clickable" PEG-dendrimer (5), and introduce biological ligands onto the surface of liposomes (6) and Au nanoparticles (7). Recently Kataoka and coworkers reported an azide-terminated PEG that could be used in click reactions with alkyne-bearing ligands (8).

A reversible 1,6-elimination PEG linker was reported by Greenwald *et al.* (9,10), and lysozyme was conjugated onto the PEG *via* the ϵ -amino group of lysine residues. Under physiological conditions, the unaltered lysozyme was released after enzymatic or hydrolytic cleavage of the 1,6-linker.

Heterobifunctional PEGs combining a "clickable" termini and reversible amine conjugation offer novel possibilities for the PEGylation and targeting of both small molecule and large bimolecular drugs.

2. Materials and Methods

All chemicals were obtained from Fisher Scientific

*Address correspondence to:

Dr. M. Laird Forrest, Department of Pharmaceutical Chemistry, University of Kansas, 2095 Contant Avenue, Lawrence, Kansas 66047, USA.
e-mail: mforrest@ku.edu

(Pittsburgh, PA, USA) or Sigma-aldrich (St. Louis, MO, USA) and used as received unless stated otherwise. Ethylene oxide was purchased from Balchem Corporation (New Hampton, NY, USA), refrigerated, and used within 3 months of receipt. Dichloromethane (DCM) and tetrahydrofuran (THF) were distilled under argon immediately before use. All reactions were conducted under an atmosphere of dry argon in flamed glassware. NMR spectra were taken on a 400-MHz Bruker and chemical shifts δ are reference to TMS in ppm.

Synthesis of α -alkyne- ω -hydroxyl PEG (1).

The following procedure is for 4,500 Da PEG; other lengths were synthesized similarly. Freshly sublimated naphthalene (3 mmol), potassium (3 mmol), and THF (20 mL) were mixed in a dry 250-mL two-neck flask. After 24 h, the solution turned to dark green and was then diluted with THF (40 mL). The 3-trimethylsilyl-2-propargyl alcohol (TMSP, 3 mmol) was dried overnight over calcium hydride, vacuum distilled, and added into the flask. The solution was stirred for 24 h and transitioned to lime green as the initiator was formed. Ethylene oxide was freshly distilled over calcium hydride and added *via* a cold syringe. The reaction proceeded for 72 h at 20°C. The produced α -trimethylsilyl-propargyl- ω -hydroxyl PEG was precipitated from THF in cold diethyl ether three times and dried under vacuum. The alkyne termini was deprotected by addition of tetrabutylammonium fluoride ($\text{Bu}_4\text{NF}\cdot 3\text{H}_2\text{O}$ or TBAF, 1.6 mmol) to a solution of α -trimethylsilyl-propargyl- ω -hydroxyl PEG (1.5 mmol) in 35 mL of THF with stirring for 3 h at 20°C (11). The solution was concentrated under reduced pressure and filtered through a short silica pad to remove TBAF. The yield of polymer **1** after purification was 48% (3.4 g).

Synthesis of α -alkyne- ω -carboxylic acid PEG (2). Diglycolic anhydride (5.6 mmol) and 4-dimethylaminopyridine (DMAP, 5.6 mmol) were added to a solution of **1** (0.70 mmol) in DCM (32 mL) and stirred at 20°C for 24 h. The solution was concentrated under reduced pressure, and polymer **2** was precipitated in cold diethyl ether, filtered, and crystallized from DCM (ca. 2 mL) with isopropyl alcohol (IPA) (ca. 10 mL). The yield after purification was 95%. $^1\text{H NMR}$ (CDCl_3): δ 3.48 (t, $J = 2.5$ Hz, CHCCH_2-), 3.60-3.77 (br s, $-\text{CH}_2\text{CH}_2-$), 3.83 (d, $J = 3.5$ Hz, CHCCH_2-), 4.22 (t, $J = 3.2$ Hz, $-\text{CH}_2\text{CH}_2\text{OOC}-$), 4.23 (s, $-\text{OCH}_2\text{COOH}$), 4.32 (s, $-\text{OOCCH}_2\text{O}-$).

Synthesis of α -alkyne- ω -thiazolidine-2-thione PEG (3). The carboxyl terminal of **2** was activated with a thiazolidine-2-thione by addition of 2-mercaptothiazoline (2-MT, 2.1 mmol) and DMAP (2.1 mmol) to a solution of **2** (0.68 mmol) in DCM (31 mL), chilling on ice to 0°C, and then adding 1-[3-(dimethylamino) propyl]-3-ethylcarbodiimide hydrochloride (EDC, 2.1 mmol). After 20 min, the solution was warmed to 20°C and stirred for 24 h. The polymer **3** was precipitated from DCM with ice cold

diethyl ether, filtered, and crystallized from IPA. The yield of **3** was 87%. $^1\text{H NMR}$ (CDCl_3): δ 3.42 (t, $J = 7.7$ Hz, $-\text{NCH}_2\text{CH}_2\text{S}-$), 3.46 (t, CHCCH_2-), 3.58-3.76 (br s, $-\text{CH}_2\text{CH}_2-$), 3.82 (d, $J = 3.5$ Hz, CHCCH_2-), 4.22 (t, $J = 3.2$ Hz, $-\text{CH}_2\text{CH}_2\text{OOC}-$), 4.28 (s, $-\text{OCH}_2\text{CON}-$), 4.31 (s, $-\text{OOCCH}_2\text{O}-$), 4.63 (t, $J = 7.3$ Hz, $-\text{NCH}_2\text{CH}_2\text{S}-$).

Synthesis of 4-hydroxymethyl-2,6-dimethylphenol (4). A solution of 2,6-xyleneol (70 mmol), 37% formaline (140 mmol), and NaOH (70 mmol) was mixed at 20°C for 18 h, forming a crystalline mass. Acetic acid (100 mmol) in 50 mL water was added into the mixture, and the orange/yellow solids were removed by filtration. The filtrate was extracted four times with 25 mL of DCM giving the colorless crystalline **4** (1.5 g, 18% yield) after vacuum drying (12). $^1\text{H NMR}$ (acetone- d_6): δ 2.19 (s, 6H, ArCH_3), 3.81 (s, 1H, ArCH_2OH), 4.44 (s, 2H, ArCH_2OH), 6.90 (s, 2H, Ar protons), 7.09 (s, 1H, ArOH).

Synthesis of α -alkyne- ω -dimethylphenyl alcohol PEG (5). To a solution of polymer **3** (0.55 mmol) in 25 mL of DCM was added **4** (3.3 mmol) and DMAP (3.3 mmol). After stirring at 20°C for 24 h, the solution was concentrated under reduced pressure and precipitated in ice cold diethyl ether, filtered, and crystallized from IPA. The yield of polymer **5** after purification was 87%. $^1\text{H NMR}$ (CDCl_3): δ 2.13 (s, 6H, ArCH_3), 3.48 (t, $J = 2.5$ Hz, CHCCH_2-), 3.60-3.77 (br s, $-\text{CH}_2\text{CH}_2-$), 3.83 (d, $J = 3.5$ Hz, CHCCH_2-), 4.19 (t, $J = 3.2$ Hz, $-\text{CH}_2\text{CH}_2\text{OOC}-$), 4.25 (s, $-\text{OCH}_2\text{COOH}$), 4.27 (s, $-\text{OOCCH}_2\text{O}-$), 4.64 (s, ArCH_2OH), 7.07 (s, Ar protons).

Synthesis of α -alkyne- ω -(succinimidyl carbonate, SC) PEG (6). Pyridine (PyD, 1.9 mmol) and disuccinimidyl carbonate (DSC, 1.9 mmol) were added to a solution of polymer **5** (0.47 mmol) in 21 mL of DCM and 8.9 mL of DMF, and mixed at 20°C for 24 h. The mixture was concentrated under reduced pressure and precipitated in ice cold diethyl ether three times, filtered, and crystallized from IPA to yield 2 g of polymer **6** (94 % yield). $^1\text{H NMR}$ (CDCl_3): δ 2.15 (s, ArCH_3), 2.81 (s, $-\text{CH}_2\text{CH}_2-$ of NHS), 3.48 (t, $J = 2.5$ Hz, CHCCH_2-), 3.60-3.77 (br s, $-\text{CH}_2\text{CH}_2-$ of PEG), 3.83 (d, $J = 3.5$ Hz, CHCCH_2-), 4.19 (t, $J = 3.2$ Hz, $-\text{CH}_2\text{CH}_2\text{OOC}-$), 4.25 (s, $-\text{OCH}_2\text{COOH}$), 4.27 (s, $-\text{OOCCH}_2\text{O}-$), 5.33 (s, $\text{ArCH}_2\text{OCO}-$), 7.07 (s, Ar protons).

Synthesis of azidoacetic acid. Azidoacetic acid was synthesized according to a reported procedure (13). In a 100-mL round-bottom flask, a solution of 0.5 mol NaN_3 (1.43 g, 22 mmol) in freshly distilled DMSO (44 mL) was stirred for 24 h at 20°C under argon. Bromoacetic acid (2.78 g, 20 mmol) was added into the above NaN_3/DMSO solution, and the reaction was monitored by a Fourier transform infrared spectroscopy (Nicolet 510P FT-IR Spectrometer, Waltham, MA). The reaction mixture was quenched with 100 mL of H_2O and extracted three times with diethyl ether (60 mL);

the organic layer was then washed with H₂O (2 × 100 mL) and brine (100 mL), dried over MgSO₄, filtered, and rotavaped to yield a light yellow liquid. ¹H NMR (CDCl₃): δ 3.97 (s, -COCH₂-), 10.82 (s, HOCO-). The characteristic absorption was found at 2,117 cm⁻¹, which was a vibration of the N₃ group in the FTIR spectra.

Synthesis of α-IR820-ω-SC PEG conjugates (8).

The IR820 diamine was produced by mixing IR 820 (85 mg, green solid, 0.1 mmol) and 1,3-diaminopropane (0.89 g, 12 mmol) in anhydrous DMF (5 mL). The reaction was monitored by thin layer chromatography (TLC) and the product was purified on silica gel (EtOAc:MeOH, 1:1). The IR820 diamine (13 mg, 14.65 nmol) in 0.5 mL of anhydrous DMF was reacted with azidoacetic acid (1.4 mg, 13.95 nmol) in the presence of DMAP (0.85 mg, 6.98 nmol) and *N,N'*-dicyclohexylcarbodiimide (3.45 mg, 16.74 nmol) at 20°C under argon. The product IR820 azide **7** was dried under vacuum and used without further purification. According to the "click" method of Rostovtsev *et al.* (14), the Huisgen 1,3-dipolar cycloaddition of IR820 azide **7** (13 mg, 13.40 nmol) and alkyne-terminal PEG **6** (M_n 5,000, 59 mg, 12.18 nmol) proceeded in the presence of 1 mol% copper (II) sulfate and 5 mol% sodium ascorbate in a mixture of water and *tert*-butyl alcohol (2:1, v/v) at room temperature overnight. The reaction mixture was dialyzed against H₂O (1,000 MWCO; Pierce, Rockford, IL) until no color was present in the dialysate. The resulting α-IR820-ω-SC PEG conjugate (compound **8**) was lyophilized and stored at -20°C in a desiccator.

Polymer analysis. Molecular weights and distributions were determined using a Shimadzu 2010HCT system with a Shimadzu RID-10A refractive index detector and the Shimadzu EZStart 7.4 software. Samples (100 μL) were applied to a Shodex GPC LF804 column using *N,N*-dimethylformamide with 10 mM LiCl as the mobile phase (0.8 mL/min, 40°C). The calibration curve was generated with PEG standards from Scientific Polymer Products (Ontario, NY).

Analysis of α-IR820-ω-SC PEG conjugates. The excitation and emission wavelengths of α-IR820-ω-SC PEG conjugates (1 mg/mL in MeOH) were determined on a Shimadzu RF-5301PC spectrofluorophotometer. A Shimadzu 2010HCT system coupled with a Shimadzu RID-10A refractive index detector and a Waters 2475 multi wavelength fluorescence detector along with a Shodex GPC LF804 column was used to confirm the successful conjugation of the IR820 azide and alkyne-terminal PEG.

3. Results and Discussion

The alkyne PEG was synthesized by the anionic ring-opening polymerization of ethylene oxide initiated by potassium trimethylsilyl-propynyl-olate, which was formed *in situ* by the reaction between 3-trimethylsilyl-

2-propargyl alcohol and potassium naphthalene. The trimethylsilyl terminal of the PEG chain can be deprotected with tetrabutylammonium fluoride, leaving alkyne exposed as one terminal, which can undergo 1,3-dipolar cycloaddition to azides (Figure 1). The gel permeation chromatography (GPC) analysis revealed that the resulting α-alkyne-ω-hydroxyl PEG had a number average molecular weight (M_n) of 4,546, and a polydispersity index (PI, M_w/M_n) of 1.045 (Table 1).

In order to modify polymer **1**, the hydroxyl end was conjugated with diglycolic anhydride to generate α-alkyne-ω-carboxylic acid PEG (polymer **2**). The single peak at δ 4.23 (s, -OCH₂COOH) on the NMR spectra demonstrated the successful conversion of hydroxyl end to carboxylic acid terminal. In order to introduce the 1,6-elimination moiety into the PEG, the carboxyl terminal of **2** was first converted into a thiazolidine-2-thione followed by the acylation of the phenolic hydroxyl group on 4-hydroxymethyl-2,6-dimethylphenol (compound **4**). The acylation reaction selectively occurred at the phenolic -OH because under basic conditions, the phenolate anion was more nucleophilic compared to the primary benzyl alcohol (**15**). The PEG benzyl alcohol (compound **5**) was activated by disuccinimidyl carbonate in the presence of pyridine as base. The activated α-alkyne-ω-SC PEG (compound **6**) can easily couple to amino-containing ligands such as proteins *via* a carbamate bond under mild reaction conditions (**16**).

Physical characterizations of the produced α-alkyne-ω-SC PEGs are given in Table 1. Three different molecular weights of 5, 16 and 80 kDa were synthesized with narrow polydispersities (PI < 1.25). As the molecular weight of the PEG linker increased, the PI slightly increased. This was most likely due to side reactions during ring-opening polymerization and chain breakage during repeated precipitation and crystallization steps.

The reported PEG linker has functional termini of alkyne and succinimidyl carbonate. The SC terminus can form carbamate conjugates with the primary amines of proteins, *i.e.*, amine or lysine or the N-terminus, while the alkyne terminus can undergo 1,3-dipolar cycloaddition, *i.e.*, "click" reaction, with azido ligands to form 1,2,3-triazoles, such as modified targeting proteins, antibodies, or peptides. The model fluorescent dye IR820 azide (compound **7**) was "click" conjugated to α-alkyne-ω-SC PEG (M_n 5,000) in aqueous solution using an *in situ* formed copper (I) salt as the catalyst. The α-IR820-ω-SC PEG conjugate (compound **8**) had excitation and emission wavelengths at 585 nm and 605 nm, respectively, indicating the successful conjugation of IR820 azide and α-alkyne-ω-SC PEG since the free IR820 had a maxima excitation of 710 nm and emission of 820 nm. GPC analysis of α-IR820-ω-SC PEG conjugates (Figure 2) showed conjugation of IR820 azide to alkyne-terminal PEG as indicated

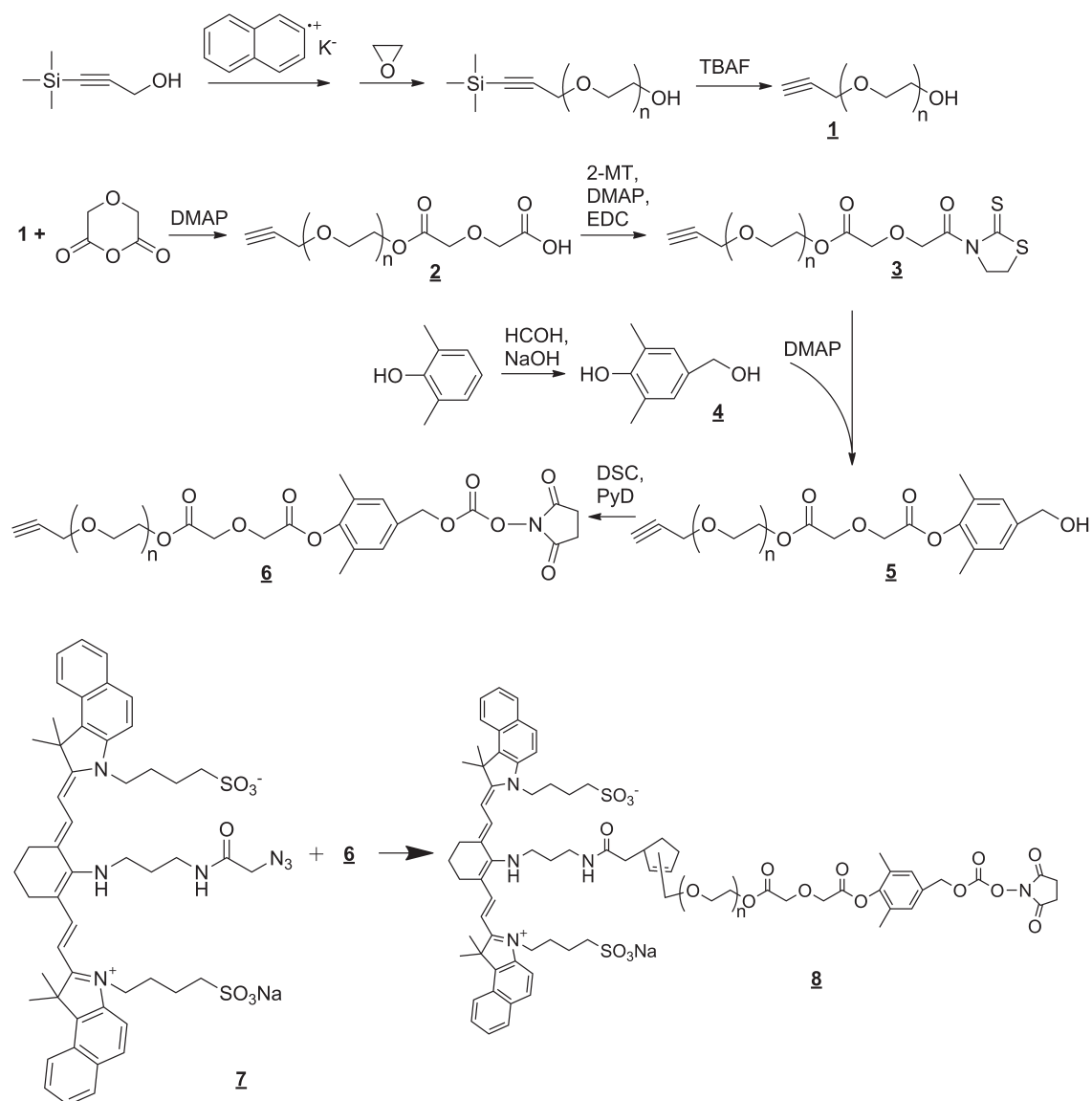


Figure 1. Synthesis of reversible "click" PEG and IR820 conjugates.

Table 1. Molecular weight and polydispersities of α -alkyne- ω -SC PEG by gel permeation chromatography

	5 kDa		16 kDa		80 kDa	
	M_n	PI	M_n	PI	M_n	PI
α -alkyne- ω -SC PEG	4,853	1.124	16,113	1.206	80,105	1.231

by the fluorescent peak coeluting with the polymer (RI detection) at around 11.5 min; by contrast, no fluorescent peak was observed for the unconjugated α -alkyne- ω -SC PEG (data not shown).

In vivo, the reversible PEG linker system is known to cleave at a predictable rate by enzymatic cleavage, followed by a rapid 1,6-benzyl elimination reaction to release intact proteins or drugs (9,10,15,17). The hydrolytic rate of the PEG reversible linker can be regulated by modifying the chemistry of the phenol ring, for example, the introduction of the steric hindrance *via* the 2,6-dimethyl substitution on the phenol ring resulted in a longer plasma $t_{1/2}$ of PEG-

amphotericin B and PEG-Daunorubicin, compared with no substitution on the phenol ring (15,18). In addition, the release rate of the conjugated proteins and drugs was closely related with the number of PEG strands used. It was reported that in the PEG-lysozyme system, intact lysozyme was released more rapidly from the single PEG strand conjugates than the multistrand conjugates (9,10).

Biopharmaceuticals such as proteins, antibodies, and peptides had a 24% market share in 2007, with 18 drugs reaching "blockbuster" status with \$1 billion-plus sales (19). PEGylation has become an important tool to improve residence time and stability of biotech drugs

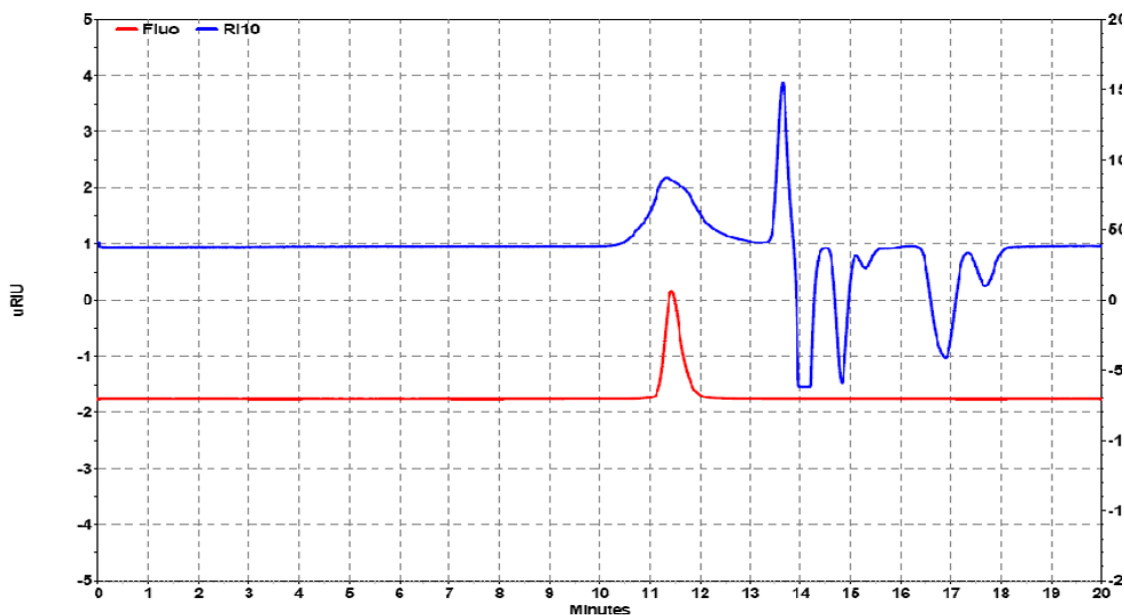


Figure 2. Gel chromatography analysis of α -IR820- ω -SC PEG conjugates. The 5 K PEG conjugate RI peak (top, 11.5 min) corresponds to the fluorescence peak (bottom, 11.5 min) indicating "click" conjugation of the dye and polymer.

in the body (20); however, the site of PEG conjugation cannot be controlled if multiple sites are available, which may negatively impact drug efficacy. Reversible linkers can overcome this limitation by restoring the native molecule after cleavage. In addition, most biologicals require relatively high concentrations since they are competing for binding sites with endogenous ligands, so the addition of targeting ligands to diseased tissues may further improve efficacy. The reported heterobifunctional, reversible "click" poly(ethylene glycol) may be useful as a single agent for both protection and targeting of biologicals.

Acknowledgements

This work was supported by awards from the National Institutes of Health (R21 CA132033 and P20 RR015563) and the American Cancer Society (Research Scholar Grant RSG-08-133-01-CDD). In addition, partial support for this project and its authors was provided by the University of Kansas Cancer Center (Research Pilot Award) and the University of Kansas (General Research Fund Award).

References

- Deiters A, Cropp TA, Mukherji M, Chin JW, Anderson JC, Schultz PG. Adding amino acids with novel reactivity to the genetic code of *Saccharomyces cerevisiae*. *J Am Chem Soc.* 2003; 125:11782-11783.
- Deiters A, Cropp TA, Summerer D, Mukherji M, Schultz PG. Site-specific PEGylation of proteins containing unnatural amino acids. *Bioorg Med Chem Lett.* 2004; 14:5743-5745.
- Link AJ, Tirrell DA. Cell surface labeling of *Escherichia coli* via copper(I)-catalyzed [3+2] cycloaddition. *J Am Chem Soc.* 2003; 125:11164-11165.
- Wang Q, Chan TR, Hilgraf R, Fokin VV, Sharpless KB, Finn MG. Bioconjugation by copper(I)-catalyzed azide-alkyne [3+2] cycloaddition. *J Am Chem Soc.* 2003; 125:3192-3193.
- Fernandez-Megia E, Correa J, Riguera R. "Clickable" PEG-dendritic block copolymers. *Biomacromolecules.* 2006; 7:3104-3111.
- Hassane FS, Frisch B, Schuber F. Targeted liposomes: Convenient coupling of ligands to preformed vesicles using "click chemistry". *Bioconjug Chem.* 2006; 17:849-854.
- Brennan JL, Hatzakis NS, Tshikhudo TR, Dirvianskyte N, Razumas V, Patkar S, Vind J, Svendsen A, Nolte RJ, Rowan AE, Brust M. Bionanoconjugation via click chemistry: The creation of functional hybrids of lipases and gold nanoparticles. *Bioconjug Chem.* 2006; 17:1373-1375.
- Hiki S, Kataoka K. A facile synthesis of azido-terminated heterobifunctional poly(ethylene glycol)s for "click" conjugation. *Bioconjug Chem.* 2007; 18:2191-2196.
- Lee S, Greenwald RB, McGuire J, Yang K, Shi C. Drug delivery systems employing 1,6-elimination: Releasable poly(ethylene glycol) conjugates of proteins. *Bioconjug Chem.* 2001; 12:163-169.
- Greenwald RB, Yang J, Zhao H, Conover CD, Lee S, Filpula D. Controlled release of proteins from their poly(ethylene glycol) conjugates: Drug delivery systems employing 1,6-elimination. *Bioconjug Chem.* 2003; 14:395-403.
- Cai CZ, Vasella A. Oligosaccharide analogs of polysaccharides. Part 3. A new protecting group for alkynes: orthogonally protected dialkynes. *Helv Chim Acta.* 1995; 78:732-757.
- Massy DJR, McKillop A. Carboxyalkylthiomethylation of phenols. *Synthesis.* 1989; 1989:253-255.
- Alvarez SG, Alvarez MT. A practical procedure for the synthesis of alkyl azides at ambient temperature in

- dimethyl sulfoxide in high purity and yield. *Synthesis*. 1997; 1997:413-414.
14. Rostovtsev VV, Green LG, Fokin VV, Sharpless KB. A stepwise Huisgen cycloaddition process: Copper(I)-catalyzed regioselective "ligation" of azides and terminal alkynes. *Angew Chem Int Ed Engl*. 2002; 41:2596-2599.
 15. Greenwald RB, Pendri A, Conover CD, Zhao H, Choe YH, Martinez A, Shum K, Guan S. Drug delivery systems employing 1,4- or 1,6-elimination: Poly(ethylene glycol) prodrugs of amine-containing compounds. *J Med Chem*. 1999; 42:3657-3667.
 16. Miron T, Wilchek M. A simplified method for the preparation of succinimidyl carbonate polyethylene-glycol for coupling to proteins. *Bioconjug Chem*. 1993; 4:568-569.
 17. Greenwald RB, Pendri A, Conover CD, Lee C, Choe YH, Gilbert C, Martinez A, Xia J, Wu DC, Hsue M. Camptothecin-20-PEG ester transport forms: The effect of spacer groups on antitumor activity. *Bioorg Med Chem*. 1998; 6:551-562.
 18. Conover CD, Zhao H, Longley CB, Shum KL, Greenwald RB. Utility of poly(ethylene glycol) conjugation to create prodrugs of amphotericin B. *Bioconjug Chem*. 2003; 14:661-666.
 19. Lawrence S. Billion dollar babies – biotech drugs as blockbusters. *Nat Biotechnol*. 2007; 25:380-382.
 20. Veronese FM, Pasut G. PEGylation, successful approach to drug delivery. *Drug Discov Today*. 2005; 10:1451-1458.

(Received April 10, 2010; Revised May 19, 2010; Accepted May 21, 2010)

Original Article**Di(hetero)arylamines in the benzo[*b*]thiophene series as novel potent antioxidants**João P. Silva¹, Vera A. Machado¹, Ricardo C. Calhella², Maria-João R. P. Queiroz², Olga P. Coutinho^{1,*}¹ CBMA – Molecular and Environmental Biology Centre, Department of Biology, University of Minho, Braga, Portugal;² Centre of Chemistry, University of Minho, Braga, Portugal.

ABSTRACT: The damaging consequences of oxidative stress are known to be involved in several pathologies. So, the development of new drugs that can aid cells to cope with excessive levels of free radicals still assumes great relevance. Here, we investigated the antioxidant properties of four novel di(hetero)arylamines (named MJQ1, MJQ3, MJQ4 and MJQ5), sharing a common benzo[*b*]thiophene nucleus (an indole analogue), against oxidative damage induced to H9c2 myoblasts. Cell proliferation, evaluated by the sulforhodamine B assay, was not compromised by the presence of any of these compounds for concentrations below 50 μ M (at 24 h) and 1 μ M (72 h). Moreover, all of them showed a dose-dependent protective effect against *tert*-butylhydroperoxide (*t*-BHP)-induced cell death for concentrations in the nanomolar range. Their ability to scavenge free radicals seems to account for their protective effects, as they were able to prevent almost completely, at 25 nM, *t*-BHP-induced intracellular ROS formation, assessed by DCF fluorescence. Furthermore, their relatively high partition coefficient values are indicative of their ability to easily permeate lipid membranes and act intracellularly. Additionally, these novel diarylamines led to a reduction, between 60-70%, of the amount of DNA strand breaks induced by *t*-BHP, evaluated by the Comet assay, and lipid peroxidation (TBARS assay) induced by the oxidant pair ascorbate/iron. In all these parameters, which show their ability to prevent the oxidation of the main biomolecules, their protective role was superior to the traditional antioxidant Trolox. Although the mechanisms underlying the action of these diarylamines are currently under investigation, the data obtained so far reveals their high pharmacological potential as antioxidant molecules.

Keywords: Di(hetero)arylamines, benzo[*b*]thiophene derivatives, antioxidants, cardiac oxidative stress, H9c2 myoblasts

1. Introduction

Reactive oxygen (ROS) and nitrogen (RNS) species can accumulate intracellularly as a result of both exogenous and/or endogenous factors (1). In normal physiological conditions, these species are maintained in equilibrium by the cells' antioxidant defence systems and are known to play important roles in the regulation of physiological functions (2,3). However, an imbalance in the equilibrium, favouring the oxidants, can result in a situation defined as oxidative stress (4,5), which causes damage to all biomolecules, including DNA, lipids and proteins, and is ultimately involved in the regulation of mechanisms leading to cell death (5). In addition, it is often implicated in the etiology of several pathologies, such as atherosclerosis (6), neurodegenerative diseases (7,8) and ischemia-reperfusion injury (9).

Cells possess effective enzymatic (*e.g.* superoxide dismutase, catalase, glutathione peroxidase) and non-enzymatic (*e.g.* glutathione, thioredoxin, coenzyme Q) antioxidant systems to help them cope with oxidative stress (10). Also, several compounds present in plants and vegetables (*e.g.* vitamins C and E, polyphenols) have been suggested to have the ability to react with free radicals (11), protecting cells from damage. However, there are some drawbacks associated to these natural compounds, as some reports describe pro-oxidant effects for many of them, which may eventually result in cell death too (12-14). In this regard, the undergoing development of novel synthetic compounds with antioxidant activity that may help the endogenous defence system, assumes special relevance (15).

Secondary amines, in particular diarylamines, are regarded as important molecules that can aid in the antioxidant protection, since their reducing properties

*Address correspondence to:

Dr. Olga P. Coutinho, Biology Department, University of Minho, Campus de Gualtar, Braga 4710-057, Portugal.
e-mail: olgapc@bio.uminho.pt

make them suitable as good radical scavengers, able to react either with O-centered or C-centered radicals (16,17).

Esteves and collaborators (16) evaluated the redox properties and free radical scavenging activity of some diarylamines by cyclic voltammetry and the DPPH radical reduction assay, respectively. They observed that the compounds with a *p*-methoxyphenyl moiety in their structures presented lower oxidation potentials and higher radical scavenging activity. In another study (18), a high antioxidant activity was also demonstrated for diarylamines in the benzo[*b*]thiophene series, which proved to be even better antioxidant molecules than the well-known synthetic standards butylated hydroxyanisole (BHA) and butylated hydroxytoluene (BHT). These results were the first indication of the potential of diarylamines in the benzo[*b*]thiophene series to be used as antioxidants in biological systems.

Later on, Queiroz and co-workers (19) reported the synthesis and evaluation of the antioxidant properties of 7-aryl or 7-heteroaryl-amino-2,3-dimethylbenzo[*b*]thiophenes, by assessing their free radical scavenging activity and reducing power, establishing some structure-activity relationships based on the presence and position of different substituents (1 or 2 OMe and a nitrile group) on the phenyl ring, or on the presence of a pyridine ring and on the position of its nitrogen atom relative to the N-H bond. In a more recent study (20), cyclic voltammetry was used to evaluate the antioxidant activity of those molecules (7-aryl or 7-heteroaryl-amino-2,3-dimethylbenzo[*b*]thiophenes), while comparing their oxidation potentials with those of the classical antioxidants BHA and BHT, showing the importance of the presence of the methoxylated arylamine moiety to the antioxidant properties of the molecule compared with the presence of a pyridine ring. By its turn, it was also shown that the presence of electron-donating groups (*e.g.* methoxy) on the arylamine moiety showed lower oxidation potential than compounds with electron-withdrawing groups. The position of the methoxy group on the arylamine moiety also seemed to affect the oxidation potential, being that a methoxy group in the *para* position relative to the NH group, or two methoxy groups, one in the *para* and other in *meta* position, increased the antioxidant activity in comparison with molecules containing a single methoxy group in the *meta* position.

In this study, we evaluated the antioxidant potential of four di(hetero)arylamines in the benzo[*b*]thiophene series (named MJQ1, MJQ3, MJQ4 and MJQ5), which differ in the number of methoxy (OCH₃) and methyl (CH₃) groups present within their structures (Figure 1). Three of them are entirely new synthetic molecules not tested in biological systems. For MJQ1 we have previously reported good antioxidant properties, particularly at mitochondria level (21). In the same study we have tested another benzo[*b*]thiophene

derivative, aminated in the thiophene ring with a pyridine (MJQ2), which did not show to be as good as antioxidant.

So in the present work we focused on the MJQ1 analogues. We intended to address their protective role against oxidative injury induced by pro-oxidant stimuli on a cardiomyocyte model, the H9c2 cell line, since cardiac cells are recognized to be highly susceptible to this kind of damage (22).

2. Materials and Methods

2.1. Chemistry

The compounds in study, named MJQ1, MJQ3, MJQ4 and MJQ5 were synthesized by palladium-catalyzed C-N Buchwald-Hartwig coupling of 6-bromotri or tetra methylbenzo[*b*]thiophenes with methoxylated anilines (23) in the Center of Chemistry of the University of Minho (Braga, Portugal). They all share a common benzo[*b*]thiophene nucleus and differ mainly in the number of methoxy (OCH₃) and methyl (CH₃) groups present within their structures. The synthesis and chemical characterization of the compounds MJQ1 and MJQ5 have been previously published (21,23). For the other two compounds (MJQ3 and MJQ4) the synthesis procedure is described below. The dry powders obtained were reconstituted in DMSO, aliquoted and maintained at -20°C, protected from light. After thawed each aliquot was used only once.

2.2. General methods of synthesis

Melting points (°C) were determined in a Stuart SMP3 apparatus and are uncorrected. ¹H and ¹³C NMR spectra were recorded on a Varian Unity Plus (300 and 75.4 MHz, respectively) or an Avance III Bruker (400 MHz and 100.6 MHz, respectively). Chemical shifts are given in ppm and coupling constants in Hz. The mass spectra were obtained by electronic impact

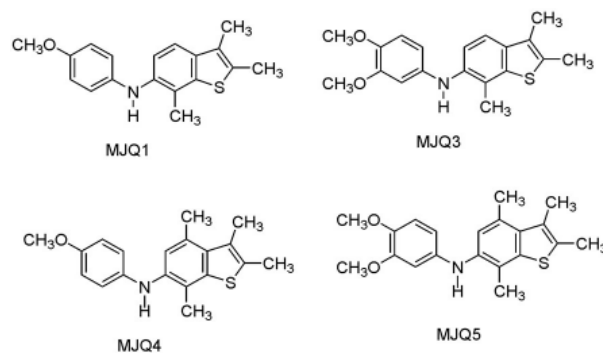


Figure 1. Schematic structure of the di(hetero)arylamines studied MJQ1, MJQ3, MJQ4, and MJQ5. They all possess a tri or tetramethylated benzo[*b*]thiophene moiety and differ mainly in the number of methoxy (OCH₃) and methyl (CH₃) groups present within their structures.

unless stated in the mass spectrometry external service of the University of Vigo (Spain). Elemental analysis was performed on a LECO CHNS 932 elemental analyser. The reactions were monitored by thin layer chromatography (TLC). Column chromatography was performed on Macherey-Nagel silica gel 230-400 mesh. Petroleum ether refers to the boiling range 40-60°C. Ether refers to diethylether. When solvent gradient was used, the increase of polarity was made gradually from petroleum ether to mixtures of ether/petroleum ether increasing 10% of ether until the isolation of the product.

A dry Schlenk tube was charged, under Argon, with dry toluene (3-4 mL), the benzo[*b*]thiophene, Pd(OAc)₂ (3 mol%), *rac*-BINAP (4 mol%), Cs₂CO₃ (1.4 equiv.), the methoxyaniline, and the mixture was heated at 100°C for several hours. After cooling, ether was added and the mixture was filtered under vacuum. The filtrate was evaporated under reduced pressure to give a residue which was submitted to column chromatography using solvent gradient from neat petroleum ether to mixtures of diethyl ether/petroleum ether, increasing 10% of ether till the isolation of the product, unless stated otherwise.

2.2.1. 6-(3,4-Dimethoxyanilino)-2,3,7-trimethylbenzo[*b*]thiophene (**MJQ3**)

From 6-bromo-2,3,7-trimethylbenzo[*b*]thiophene (150 mg, 0.590 mmol), 3,4-dimethoxyaniline (95.0 mg, 0.649 mmol), heating for 7 h, and using solvent gradient from neat petroleum ether to 20% ether/petroleum ether in the column chromatography, compound **MJQ3** was obtained as a white solid (150 mg, 78%), m.p. 119-121°C. ¹H NMR (400 MHz, DMSO-*d*₆): δ 2.21 (3H, s, Me), 2.29 (3H, s, Me), 2.41 (3H, s, Me), 2.56 (3H, s, Me), 3.66 (3H, s, OMe), 3.67 (3H, s, OMe), 6.33 (1H, dd, *J* = 8.6 and 2.4 Hz, 6'-H), 6.56 (1H, d, *J* = 2.4 Hz, 2'-H), 6.77 (1H, d, *J* = 8.4 Hz, 5'-H), 7.15 (1H, *J* = 8.4 Hz, Ar-H), 7.27 (1H, s, N-H), 7.35 (1H, d, *J* = 8.4 Hz, Ar-H) ppm. ¹³C NMR (100.6 MHz, DMSO-*d*₆): δ 11.17 (Me), 13.41 (Me), 15.98 (Me), 55.24 (OMe), 56.23 (OMe), 102.37 (CH), 107.51 (CH), 113.60 (CH), 117.60 (CH), 119.10 (CH), 121.28 (C), 127.47 (C), 130.43 (C), 135.19 (C), 138.00 (C), 139.23 (C), 139.76 (C), 142.23 (C), 149.59 (C). MS (EI) *m/z* (%) 327 (M⁺, 82), 312 (100). HRMS M⁺ calct. for C₁₉H₂₁NO₂S 327.1293, found 327.1297.

2.2.2. 6-(4-Methoxyanilino)-2,3,4,7-tetramethylbenzo[*b*]thiophene (**MJQ4**)

From 6-bromo-2,3,4,7-tetramethylbenzo[*b*]thiophene (150 mg, 0.730 mmol), 4-methoxyaniline (99 mg, 0.803 mmol), heating for 7 h, and using solvent gradient from neat petroleum ether to 20% ether/petroleum ether in the column chromatography, compound **2a** was obtained as a white solid (102 mg, 45%), m.p.

136-138°C. ¹H NMR (300 MHz, DMSO-*d*₆): δ 2.20 (3H, s, Me), 2.36 (3H, s, Me), 2.40 (3H, s, Me), 2.56 (3H, s, Me), 3.36 (3H, s, OMe), 6.79 (coalesced ABq, 2', 3', 5' and 6'-H), 6.80 (1H, s, 5-H), 7.18 (1H, s, N-H) ppm. ¹³C NMR (75.4 MHz, DMSO-*d*₆): δ 13.70 (Me), 14.95 (Me), 15.56 (Me), 21.10 (Me), 55.29 (OMe), 114.54 (CH), 118.09 (CH), 118.38 (C), 120.13 (CH), 129.04 (C), 129.53 (C), 130.44 (C), 133.30 (C), 137.62 (C), 138.98 (C), 140.02 (C), 152.81 (C). Anal. Calcd for C₁₉H₂₁NOS: C 73.28, H 6.80, N 4.50, S 10.29; found: C 73.27, H 6.89, N 5.53, S 10.14.

2.3. Other chemicals

Fetal bovine serum (FBS) was obtained from BioChrom KG (Berlin, Germany); 6-hydroxi-2,5,7,8-tetrametilcromano-2-carboxylic acid 97% (Trolox), Dulbecco's Modified Eagle's Medium (DMEM) cell culture medium, dimethyl sulfoxide (DMSO), EDTA, trypsin, *tert*-butylhydroperoxide and sulforhodamine B were purchased from Sigma-Aldrich (St. Louis, MO, USA). 2',7'-Dichlorodihydrofluorescein diacetate (DCFH₂-DA) was obtained from Invitrogen (Eugene, OR, USA).

2.4. H9c2 cell culture

H9c2 cell line was originally derived from embryonic rat heart tissue using selective serial passages (24). It was originally purchased from America Tissue Type Collection (Manassas, VA, USA). This cell line has been used extensively in the literature as a model for cardiomyoblasts and has also been considered as a proper model to study molecular responses of the cardiomyocyte to oxidative damage (25,26). Cells were grown in Dulbecco's Modified Eagle's Medium (DMEM) supplemented with 1.5 g/L sodium bicarbonate, 10% foetal bovine serum, 100 U/mL of penicillin and 100 µg/mL of streptomycin in 75 cm² tissue culture flasks, and maintained at 37°C, in a humidified incubator containing 5% CO₂. To prevent loss of differentiation potential, cells were not allowed to become confluent. So, they were fed every 2-3 days, and sub-cultured once they reached 70-80% confluence, by treatment with a 0.05% trypsin/EDTA solution. Cells were seeded at a density of 35,000 cells/mL, either in 24-well plates (final volume of 1 mL/well) for sulforhodamine B assays, or 6-well plates (final volume of 2 mL medium/well) for other assays. To detect intracellular ROS, cells were seeded in coverslips placed in the bottom of 6-well plates.

2.5. Sulforhodamine B (SRB) assay

The effects of the nitrogen compounds on cell proliferation *per se* and on the protection against *t*-BHP-induced cell death was evaluated by the sulforhodamine

B assay, as previously described (27). Briefly, H9c2 cells were seeded in 24-well plates and incubated with the diarylamines for different time points, in the presence or absence of *tert*-butylhydroperoxide (*t*-BHP). Following this treatment, cells were fixed in ice cold methanol, containing 1% acetic acid, for at least 1 h, and then incubated with 0.5% (w/v) sulforhodamine B dissolved in 1% acetic acid for 1 h at 37°C. Unbound dye was removed by washing several times with 1% acetic acid. Bound SRB was then solubilised with 10 mM Tris base solution, pH 10. After dissolving the SRB through agitation of the plates, 200 μ L from each well were transferred to 96-well plates and the absorbance read at 540 nm, against a blank containing 10 mM Tris alone. Results were expressed relatively to $t = 0$ h, in the presence of the vehicle alone (DMSO), which was considered as 100% of cell proliferation/cell viability.

2.6. Detection of intracellular reactive oxygen species

Intracellular ROS formation was assessed by measuring the fluorescence of DCF, the oxidation product of the non-fluorescent probe 2',7'-dichlorodihydrofluorescein diacetate (DCFH₂-DA), according to a method previously described (27), with slight modifications.

Briefly, cells plated in coverslips placed in the bottom of 6-well plates were treated with *t*-BHP and the diarylamines for 3 h and then incubated with 10 μ M DCFH₂-DA for 30 min, at 37°C, in the dark. Cells were then observed by fluorescence microscopy using a fluorescein filter in a Leica DM 5000B microscope. The intracellular mean fluorescence intensity was quantified using the ImageJ 1.40g software (National Institutes of Health, USA).

2.7. Single cell gel electrophoresis (Comet assay)

Protection against oxidative damage to DNA was assessed by the Comet assay, as previously described (28). In brief, cells plated at a density of 5×10^5 cells/well were treated with 50 μ M *t*-BHP and the diarylamines (at 10 and 25 nM) for 3 h to induce the formation of strand breaks. After treatment with the compounds, cells were trypsinised, spread on agarose-coated slides and lysed. The DNA that remained embedded in the agarose was subjected to an electrophoresis in alkaline conditions, for 20 min at 1 V/cm. The electric field makes the broken DNA loops, if they exist, to extend towards the anode, yielding an image that looks like a comet. Finally, slides were neutralised with 0.4 M Tris, pH 7.5 and fixed with absolute ethanol. Comets were stained with ethidium bromide and analysed under a fluorescence microscope. Comet quantification was performed by visual scoring. This method, which correlates well with computer-assisted image analysis of the % of DNA in the comets' tail (28), is based in the classification of comets into

one of five classes of damage (from 0 to 4) in 100 nucleoids, giving a score range between 0 and 400.

2.8. Measurement of lipid peroxidation – TBARS assay

The extent of lipid peroxidation was determined by measuring the levels of Thiobarbituric Acid-Reactive Substances (TBARS), as described in a previous publication (29). Cells were plated at a density of 1.7×10^6 cells/well in 6-well plates and TBARS formation was induced by the oxidant pair 2 mM ascorbate/100 μ M iron (II) for 1 h, at 37°C. The amount of TBARS produced was calculated using the molar absorption coefficient of 1.56×10^5 M \cdot cm⁻¹, normalized for the total protein content and expressed as nmol TBARS/mg protein. The protection of the diarylamines against lipid peroxidation was determined according to the following formula:

$$\% \text{ Protection} = 1 - [(D - C)/OP] \times 100$$

where *D* is the amount of TBARS in the presence of the diarylamines, *C* is the basal lipid peroxidation (negative control) and *OP* is the amount of TBARS in the presence of the oxidant pair.

2.9. Partition coefficients

The diarylamines degree of hydrophobicity was determined by measuring the partition coefficients (PC) in an *n*-octanol/HEPES system, as previously described (29). The diarylamines were dissolved in *n*-octanol at a concentration of 20 μ M and 1 mL of each solution was shaken with 20 mL HEPES (20 mM, pH 7.4), for 10 min, at room temperature. The two different phases formed were then separated by centrifugation. The absorbance peaks of each compound, required to assess their concentrations in each solution, were determined at 305 nm for MJQ1, 307 nm for MJQ3 and 308 nm for both MJQ4 and MJQ5. PC values were then calculated using the formula:

$$PC = \log (C_o/C_H)$$

where *C_o* and *C_H* are the concentrations of the diarylamines in *n*-octanol and HEPES, respectively. The *C_H* values were indirectly determined by calculating the difference between the initial and the final concentrations of the compound in the octanol phase.

2.10. Statistical analysis

Data are expressed as the mean \pm S.E.M., of the indicated number of experiments. The significance of the differences between the means observed was evaluated using the unpaired two-tailed Student's *t*-test or the one-way ANOVA followed by the Student-

Newman-Keuls post-hoc test. A difference of $p < 0.05$ was considered significant.

3. Results

3.1. Effects on toxicity and cell proliferation

The effects of the diarylamines on toxicity and cell proliferation were assessed by the sulforhodamine B assay. The compounds were tested at a range of concentrations between 1 and 50 μM , during a period of 72 h.

In Figure 2, it is possible to observe that none of the compounds is toxic to H9c2 cells at any of the concentrations tested, since the percentage of proliferation does not decrease below the levels measured at time zero (0 h). However, some effects on cell proliferation could be observed, which varied according to the compound tested. In this way, MJQ5 was the one that less affected this parameter, since that only after 48 h, and for the highest concentration (50 μM), cell proliferation was reduced. By its turn at 72 h incubation with this diarylamine, only concentrations of 10 μM and above affected cell proliferation. At that same concentration a decrease in cell proliferation could be observed earlier (at 24 h), for all other compounds. At 48 h, MJQ4 showed some deleterious effects for a 25

μM concentration, while MJQ1 and MJQ3 revealed to affect proliferation in a statistically significant way for lower concentrations, namely 1 and 5 μM , respectively. After 72 h of cell incubation in the presence of MJQ1, MJQ3, and MJQ4, proliferation was also significantly affected for the lower concentrations tested (1 μM for MJQ1 and MJQ4, and 5 μM for MJQ3).

To determine if the diarylamines were able to afford protection against cell death induced by an oxidant stimulus, H9c2 cells were incubated for 6 h in the presence of 50 μM *t*-BHP and different concentrations of the diarylamines. Cell viability was then evaluated by the SRB assay. The thiol-oxidizing agent *t*-BHP is metabolized intracellularly, leading to the formation of *tert*-butoxyl radicals, being commonly used as an inducer of oxidative stress in several cell models (30,31).

As shown in Figure 3, *t*-BHP induces a decrease of 55.7% in cell viability, which is prevented by all the diarylamines, in a dose-dependent manner, for concentrations at the nanomolar range. This protection was statistically significant at 10 nM and above for MJQ3, MJQ4, and MJQ5. For MJQ1 the protective effect was only significant for concentrations equal or superior to 25 nM. At this concentration (25 nM) all the compounds showed about 100% protection. It should be noted that the concentrations at which the compounds

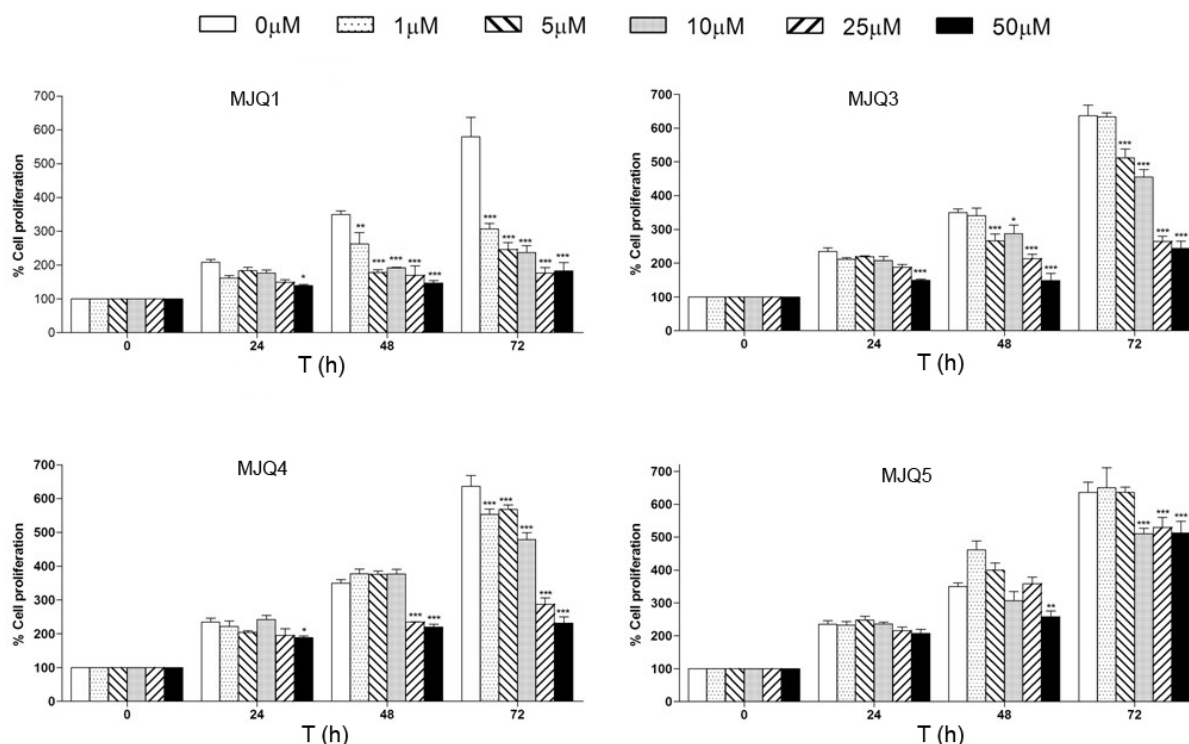


Figure 2. Cellular proliferation assessed with the sulforhodamine B assay. H9c2 cells proliferation was followed up to 72 h, in the presence of different compounds concentrations, as indicated. The percentage of cellular proliferation was calculated relatively to $t = 0$ h. Proliferation in control cells (no test compounds) was assessed in the presence of 0.1% DMSO. For each concentration the mean \pm S.D. for at least three independent experiments is represented. No statistically significant differences were found between the different concentrations shown and the respective controls for each time point. * $p < 0.05$, ** $p < 0.01$, *** $p < 0.001$, relatively to control cells (white bars) at respective time period.

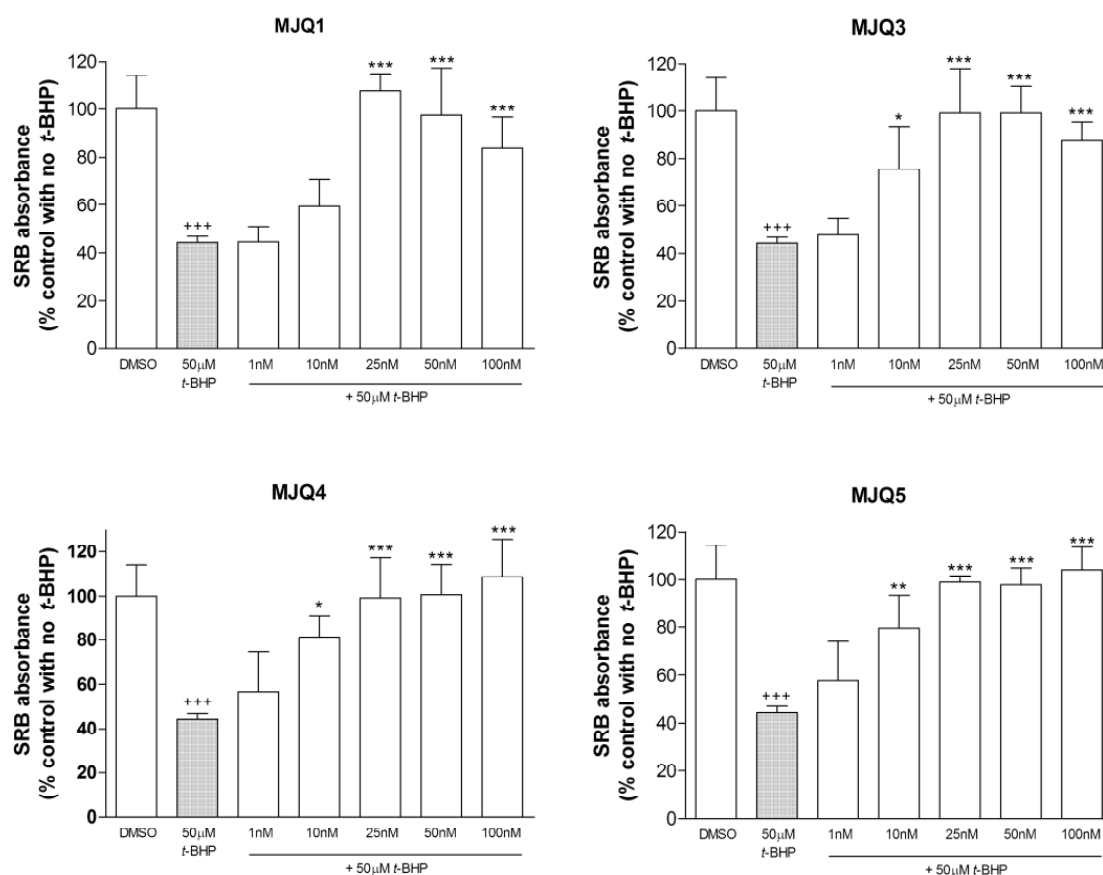


Figure 3. Effects of the diarylamines on the reduction of cell viability evaluated by the sulforhodamine B assay. H9c2 cells were incubated for 6 h in the presence of the compounds and 50 μM *t*-BHP. Results are presented in terms of percentage of cell viability, determined relatively to the control containing only 0.1% DMSO, which was considered as representing 100% of viability. For each bar, the mean ± S.E.M. for at least three independent experiments is represented. *** $p < 0.001$, compared to control cells (DMSO); * $p < 0.05$, ** $p < 0.01$, *** $p < 0.001$, as compared to 50 μM *t*-BHP.

showed to protect against cell death were far below the ones that affected cell proliferation.

These results show the elevated potential of these novel diarylamines to protect cells against oxidative stress-induced cell death.

3.2. Scavenging of intracellular reactive oxygen species

The effect of the compounds on the intracellular formation of reactive oxygen species was determined by fluorescence microscopy, through the detection of the oxidized form (DCF) of dichlorofluorescein probe. Oxidative stress was induced by incubating cells with 50 μM *t*-BHP for 3 h, and the diarylamines (at 10 and 25 nM) added simultaneously with the pro-oxidant.

Incubation with the pro-oxidant alone evidenced an increase in the cell mean fluorescence (Figure 4) corresponding to ROS formation. However, in the presence of all the compounds tested, the amount of those reactive species was greatly decreased, to values approximate to the control. Both concentrations assayed (10 and 25 nM) showed the same levels of protection. In addition, the novel compounds proved to have a higher

protective effect than the classical antioxidant Trolox, regardless of the concentration used.

In this way, these results indicate that the protective role of the new diarylamines against *t*-BHP-induced cell death may be somehow related with their ROS scavenging activity.

3.3. Protection against oxidative DNA damage

Once formed, reactive oxygen species may interact with biomolecules, resulting in damaging consequences to all of them (32). In particular, the attack of ROS to DNA may lead to several oxidative modifications, including strand breaks formation. This appearance of strand breaks was evaluated by the Comet assay, after treating cells in the same conditions used to assess the compounds' protection against intracellular ROS formation.

As depicted in Figure 5, cells treated with the pro-oxidant stimulus showed an increase in the levels of strand breaks formation. However, a significant reduction of about 60-70% in the extent of DNA damage was observed in the presence of

all the diarylamines, when added to cells at 25 nM concentration. This protective effect was also noticed for a lower concentration (10 nM), although in this case the reduction in the amount of damage was slightly lower. Nevertheless, at both concentrations, the protection of diarylamines against this kind of oxidative damage was higher than the one observed in

cells treated with Trolox. Moreover, it should be noted that the compounds, by themselves, do not induce the formation of strand breaks, as observed in cells treated with the compounds alone.

Therefore, these results indicate the elevated potential of the novel molecules in study to protect cardiomyocytes against oxidative DNA damage.

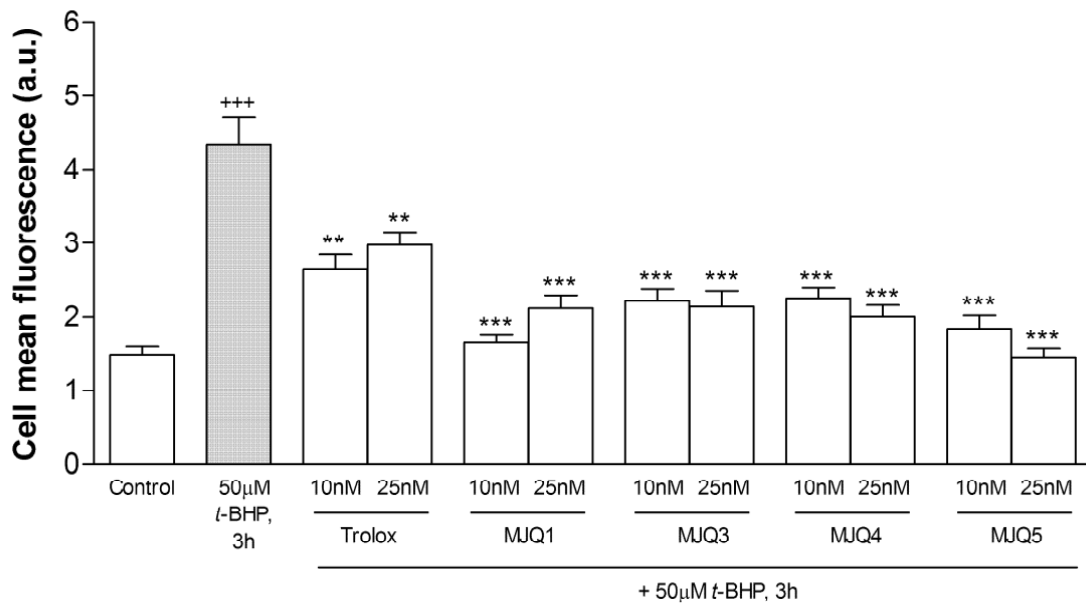


Figure 4. Effects of the compounds on *t*-BHP-induced intracellular ROS formation. H9c2 cells were incubated in the presence of *t*-BHP and the diarylamines for 3 h. Increase in intracellular oxidative stress was detected by oxidation of the fluorescent probe dichlorofluorescein (DCF) by fluorescence microscopy. At least five fields per sample were analyzed in each experiment. For each bar is represented the mean \pm S.E.M. for five independent experiments. +++ $p < 0.001$, compared with control; ** $p < 0.01$, *** $p < 0.001$, relatively to *t*-BHP.

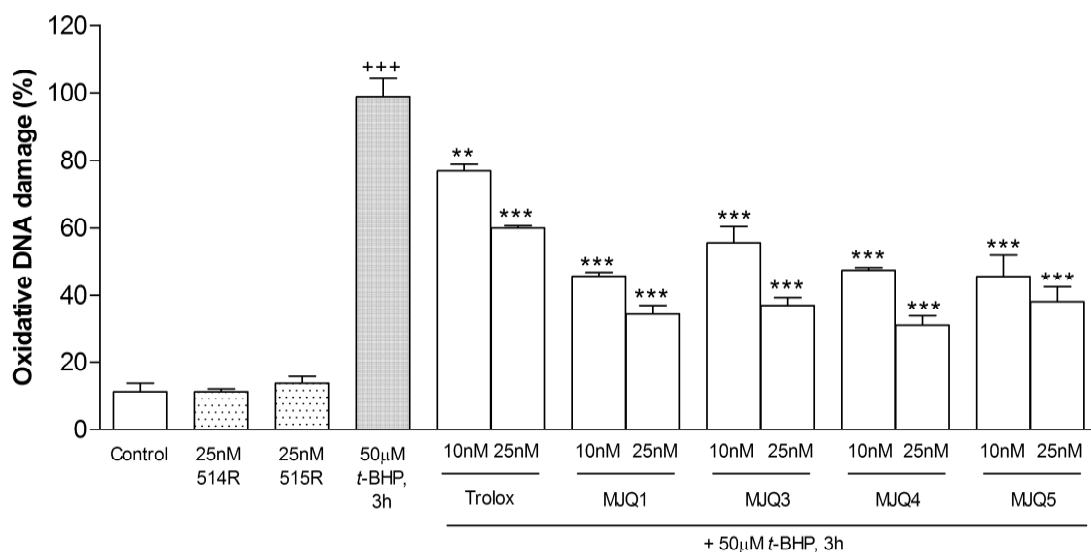


Figure 5. Diarylamines' protection against *t*-BHP-induced formation of DNA strand breaks, evaluated by the Comet assay. Oxidative DNA damage was induced by incubating H9c2 cells for 3 h in the presence of 50 μ M *t*-BHP. The compounds were added to the cells simultaneously with the pro-oxidant stimulus. Each bar represents the mean \pm S.E.M. for at least three independent experiments. +++ $p < 0.001$, compared to control cells; ** $p < 0.01$, *** $p < 0.001$, compared to 50 μ M *t*-BHP.

3.4. Effects of the compounds on lipid peroxidation

Membrane lipid peroxidation can also occur as a consequence of oxidative stress. In fact, polyunsaturated fatty acids, because of their multiple double bonds, are extremely sensitive to oxidation by free radicals (33).

The oxidant pair ascorbate/iron(II), which has been previously shown to induce high levels of lipid peroxidation in other cell models (34,35) was chosen to induce this kind of damage in this cardiomyocyte cell model. Ascorbate acts as a pro-oxidant agent, by reducing Fe^{3+} to Fe^{2+} , which then leads to the formation of hydroxyl radicals *via* the Fenton reaction, thereby causing the oxidation of membrane lipids (3,36).

Therefore, after incubating cells with the oxidant pair for 1 h, we observed an increase in lipid peroxidation, indicated by 4-fold increase in the levels of TBARS (Figure 6). These high levels were significantly reduced by simultaneous treatment with the diarylamines at 25 nM, which is indicative of their ability to prevent the oxidation of membrane lipids, once again for a low concentration. In particular, MJQ3 presented a slightly higher percentage of protection ($86.95 \pm 8.23\%$) when compared with the other three diarylamines (Figure 6, **Insert**). The high protection observed for MJQ1 is in agreement with the one previously observed in

a neuronal cell model and in isolated mitochondria by using a similar deleterious agent (21). Again the protective effects observed revealed to be quite superior to the one observed for Trolox.

3.5. Determination of the compounds' liposolubility

The partition coefficient (PC) is a measure of the relative lipophilic/hydrophobic behaviour of a chemical and has been commonly associated to a drug's biological activity (37). Therefore, the degree of hydrophobicity of the diarylamines was measured by determining this parameter in an *n*-octanol/HEPES system.

As shown in Table 1, all the diarylamines show high partition coefficient values, which is indicative of their high ability to cross lipid membranes and act intracellularly. Among the tested diarylamines, MJQ3 showed the highest affinity for the octanol phase (highest PC values), followed by MJQ4 and MJQ5, with similar values, and finally by MJQ1. In general, the values here obtained were higher than the ones presented by other compounds tested in our lab (34) and were similar (and, in the case of MJQ3, even higher) to some natural compounds tested by others in the same octanol/HEPES system (38), thus confirming a superior

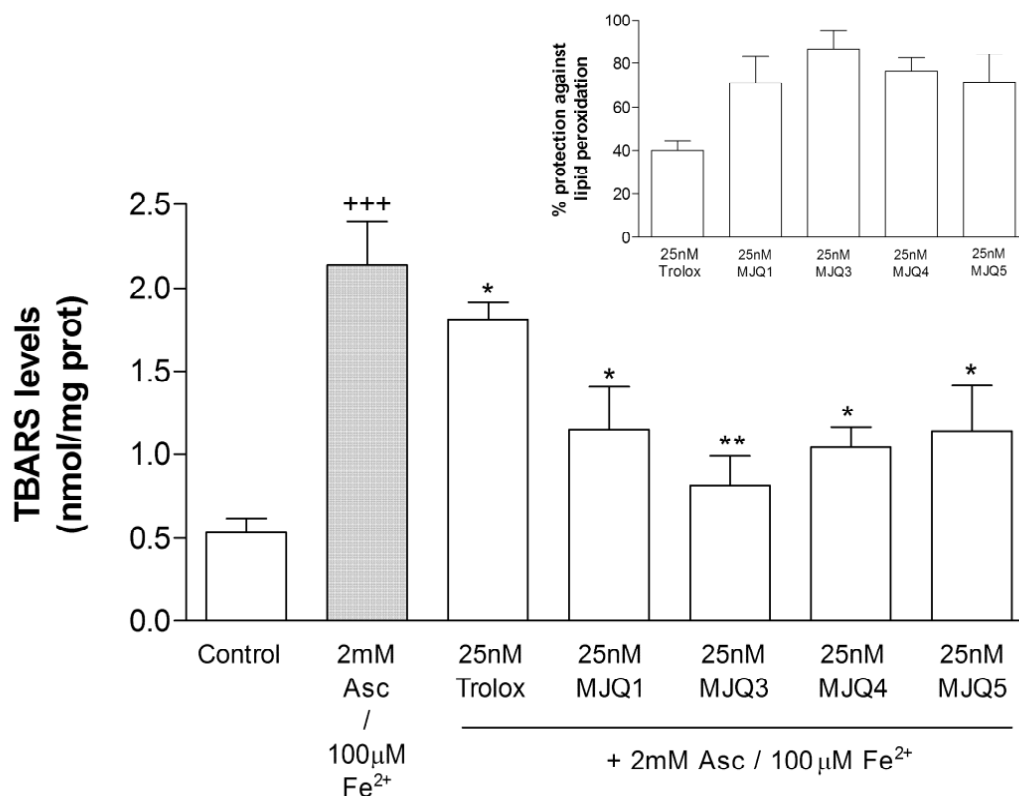


Figure 6. Relative drug protection against lipid peroxidation. Cells were incubated for 1 h with the oxidant pair 2 mM ascorbate/100 μM Fe^{2+} . The diarylamines were added to the cells at the same time as the oxidant pair. Each column represents the mean \pm S.E.M., considering the results obtained for at least three different experiments. +++ $p < 0.001$, compared to control cells; * $p < 0.05$, ** $p < 0.01$, compared to the oxidant stimulus. **Insert:** Percentage of protection relatively to the controls as described in "Material and Methods".

Table 1. Partition coefficients (PC) of the diarylamines

Compound	PC values
MJQ1	1.87 ± 0.06
MJQ3	2.95 ± 0.40
MJQ4	2.14 ± 0.32
MJQ5	2.10 ± 0.23

PC values were measured in an *n*-octanol/HEPES system as described in "Materials and Methods". A higher PC value means higher liposoluble profile. Results represent the mean ± S.E.M. for at least three independent experiments.

ability of diarylamines to cross the lipid bilayer and to act inside cells.

4. Discussion

A redox imbalance in the cell can cause oxidative damage to all types of biomolecules and even lead to cell death as an ultimate consequence. In this way, oxidative stress is commonly associated to the etiology of several pathological conditions (2).

This work comprises a small part of a broader project aiming the development and/or improvement of new synthetic molecules with the ability to scavenge free radicals, acting as antioxidants, and thus preventing oxidative stress. Although the four diarylamines herein tested share the same benzo[*b*]thiophene nucleus, they exhibit some structural differences. In particular, they differ in the number of methoxy (one in MJQ1 and MJQ4, and two in MJQ3 and MJQ5, in the same positions) and methyl groups (three in MJQ1 and MJQ3, and four in MJQ4 and MJQ5, in the same positions). It should be noted that besides being able to scavenge a free radical by donating one H[•], an antioxidant should also be able of stabilizing the unpaired electron that is formed in its own molecule as a consequence of the radical scavenging activity. With the introduction of these groups, namely the methoxy ones, it was expected a greater stabilization of the radical formed after scavenging of the free radical.

In this study, we evaluated the antioxidant potential of these four diarylamines, by addressing their protective role against oxidative injury on a cardiomyocyte model, the H9c2 cell line, since cardiac cells have for long been recognized to be highly susceptible to this kind of damage.

As a first approach, we observed that none of the diarylamines was toxic to the cells. However, for high concentrations (in the micromolar range), they interfered with the process of cell proliferation to some extent, especially after a 48 h incubation period. Nevertheless, it should be taken into account that they present protection at concentrations far below the ones that affected cell proliferation, and for shorter incubation time periods. In fact, they were able to revert cell death induced by *t*-BHP at concentrations in the nanomolar range, in a dose-dependent manner.

The thiol-oxidizing agent *t*-BHP is known to be

metabolized intracellularly, where it generates *tert*-butoxyl radicals (31). In this way, *t*-BHP-induced cell death is associated to an increase in the levels of oxidative stress, as it has also been reported in H9c2 cells (27). Therefore, we determined the protective role of the diarylamines against the intracellular increase of reactive oxygen species, induced by that agent, by analysing the changes in DCF fluorescence. We observed that all the diarylamines led to a reduction in the levels of intracellular ROS formation at very low concentrations (10 and 25 nM), an effect that seems to correlate well with the protection observed against *t*-BHP-induced cell death. Therefore, these results confirm the diarylamines' elevated antioxidant activity and suggest that their ROS scavenging ability may indeed result in a decrease in cell death induced by high levels of oxidative stress.

As previously stated, the presence of excessive levels of reactive oxygen species inside the cells is known to also cause damage to all main biomolecules. In this way, we determined if the diarylamines were able to prevent ROS-induced oxidative modifications to both DNA and membrane lipids. Indeed, the amount of DNA strand breaks induced by the pro-oxidant *t*-BHP was significantly reduced in the presence of the compounds. Since cardiac cells are post-replicative, oxidative damage to these cells' DNA could result in the deterioration of cardiac function (39). Therefore, the protection observed for the diarylamines on oxidative DNA damage in this myoblast cell line is of great relevance.

In addition, the incubation of the cells with the diarylamines led to a reduction in the levels of lipid peroxidation induced by the oxidant pair ascorbate/iron(II). This oxidant pair, which generates free radicals *via* the Fenton reaction, was chosen since it has been commonly used in other cell models, like PC12 (34) and retinal (35) cells, and because it induced higher levels of TBARS levels, in comparison with *t*-BHP (data not shown). It should be noted that, although all the diarylamines show similar protective effects at this level, MJQ3 percentage of protection was slightly higher than the ones observed for the other related compounds. This may be explained, at least partly, by its higher partition coefficient value, which confers a more liposoluble profile to this compound, in comparison with the other ones, thus allowing it to better cross lipid membranes and act on this kind of damage.

In fact, the partition coefficients obtained for the diarylamines are indicative of their high liposolubility, which enables them to permeate cells, contributing to their intracellular action. In terms of liposolubility, these diarylamines resembled or even performed better than some common natural antioxidant compounds (40). However, the correlation between the diarylamines structures and their liposolubility profiles is not

straightforward. As expected, the presence of two non-polar methoxy group increases the liposolubility, as is observed by comparing the diarylamines containing three methyl groups in their structures (MJQ3 > MJQ1). The presence of four methyl groups was also expected to increase the liposolubility of the compounds, which is observed through comparison of MJQ4 and MJQ5 with MJQ1. However, the expected increase in liposolubility observed by the presence of more methoxy groups is not observed when we put MJQ4 side by side with MJQ5, indicating that the methoxy non-polar effect disappears when four methyl groups are present in the diarylamines' structures.

Overall, no significant differences in terms of the antioxidant protection profile could be observed when comparing all the diarylamines tested. This suggests that the modifications introduced to the molecules, namely the presence of one or two methoxy and three or four methyl groups, may not in fact be the main responsible for the scavenging activity of the diarylamines, though may alter their liposolubility. Nevertheless, the importance of those functional groups in these molecules seems to be relevant, as they aid in the stabilization of the radical formed upon scavenging of a free H radical.

It should also be taken into consideration that in all parameters, namely intracellular ROS formation, oxidative DNA damage and lipid peroxidation, the diarylamines evoked protection profiles higher than the ones observed with the classical antioxidant and hydrosoluble vitamin E analogue, Trolox. This adds further value to the compounds in study, as they show an increased ability to prevent oxidative injury when compared to some existing molecules that are commonly used for its antioxidant activity.

In conclusion, we present evidence for the elevated antioxidant potential of novel molecules that demonstrated a high protective role against intracellular ROS formation and oxidative injury to biomolecules like lipids and DNA, resulting in an overall protection against oxidative stress-induced cell death. These effects were attained at a nanomolar range and even at a so low concentration they were superior to the classical antioxidant Trolox. Nevertheless, this work should be regarded as a first approach in the evaluation of the effects of the diarylamines as antioxidants in cells, and further studies are being conducted in order to address other potential intracellular action targets for these molecules. The results described allow us to introduce modifications to the structures of these molecules, in order to ameliorate them and thus increase their antioxidant activity and possibly direct them to specific molecular targets. In this regard, a recently proposed quantitative structure-activity relationship (QSAR) model (41) can be used to predict the antioxidant activity, and thus guide the synthesis, of derivatives of compounds used in this work.

Altogether, the data herein obtained encourage us to continue to study the potential of these promising diarylamines as molecules with a possible pharmacological application against pathological situations in which oxidative stress-mediated injury occurs.

Acknowledgements

We wish to thank Dr. Paulo Oliveira (CNC, University of Coimbra, Portugal) for gently providing the H9c2 cell line. This work was supported by FCT research project PTDC/QUI/68382/2006 and R. Calhella's PhD grant (SFRH/BD/29274/2006).

References

1. Stadtman ER. Role of oxidant species in aging. *Curr Med Chem.* 2004; 11:1105-1112.
2. Valko M, Leibfritz D, Moncol J, Cronin MT, Mazur M, Telser J. Free radicals and antioxidants in normal physiological functions and human disease. *Int J Biochem Cell Biol.* 2007; 39:44-84.
3. Halliwell B, Gutteridge JMC. *Free Radicals in Biology and Medicine.* 3rd ed., Oxford University Press, New York, NY, USA, 1999.
4. Sies H. Oxidative stress: oxidants and antioxidants. *Exp Physiol.* 1997; 82:291-295.
5. Nordberg J, Arnér ES. Reactive oxygen species, antioxidants, and the mammalian thioredoxin system. *Free Radic Biol Med.* 2001; 31:1287-1312.
6. Uemura M, Manabe H, Yoshida N, Fujita N, Ochiai J, Matsumoto N, Takagi T, Naito Y, Yoshikawa T. Alpha-tocopherol prevents apoptosis of vascular endothelial cells *via* a mechanism exceeding that of mere antioxidant. *Eur J Pharmacol.* 2002; 456:29-37.
7. Halliwell B. Role of free radicals in the neurodegenerative diseases – Therapeutic implications for antioxidant treatment. *Drugs Aging.* 2001; 18:685-716.
8. Jang JH, Aruoma OI, Jen LS, Chung HY, Surh YJ. Ergothioneine rescues PC12 cells from beta-amyloid-induced apoptotic death. *Free Radic Biol Med.* 2004; 36:288-299.
9. He A, Wang JA, Gui C, Jiang Y, Sun Y, Chen T. Changes of mitochondrial pathway in hypoxia/reoxygenation induced cardiomyocytes apoptosis. *Folia Histochem Cytobiol.* 2007; 45:397-400.
10. Behl C, Moosmann B. Antioxidant neuroprotection in Alzheimer's disease as preventive and therapeutic approach. *Free Radic Biol Med.* 2002; 33:182-191.
11. Masella R, Di Benedetto R, Vari R, Filesi C, Giovannini C. Novel mechanisms of natural antioxidant compounds in biological systems: Involvement of glutathione and glutathione-related enzymes. *J Nutr Biochem.* 2005; 16:577-586.
12. Elbling L, Weiss RM, Teufelhofer O, Uhl M, Knasmueller S, Schulte-Hermann R, Berger W, Micksche M. Green tea extract and (-)-epigallocatechin-3-gallate, the major tea catechin, exert oxidant but lack antioxidant activities. *FASEB J.* 2005; 19:807-809.
13. Lambert JD, Hong J, Yang GY, Liao J, Yang CS. Inhibition of carcinogenesis by polyphenols: Evidence

- from laboratory investigations. *Am J Clin Nutr.* 2005; 81:284S-291S.
14. Boots AW, Li H, Schins RP, Duffin R, Heemskerk JW, Bast A, Haenen GR. The quercetin paradox. *Toxicol Appl Pharmacol.* 2007; 222:89-96.
 15. Cemeli E, Baumgartner A, Anderson D. Antioxidants and the Comet assay. *Mutat Res.* 2009; 681:51-67.
 16. Esteves MA, Narender N, Marcelo-Curto MJ, Gigante B. Synthetic derivatives of abiestic acid with radical scavenging activity. *J Nat Prod.* 2001; 64:761-766.
 17. Scott G. Antioxidants. *Bull Chem Soc Jpn.* 1988; 61:165-170.
 18. Ferreira IC, Queiroz MJ, Vilas-Boas M, Estevinho LM, Begouin A, Kirsch G. Evaluation of the antioxidant properties of diarylamines in the benzo[*b*]thiophene series by free radical scavenging activity and reducing power. *Bioorg Med Chem Lett.* 2006; 16:1384-1387.
 19. Queiroz MJ, Ferreira IC, Calhelha RC, Estevinho LM. Synthesis and antioxidant activity evaluation of new 7-aryl or 7-heteroarylamino-2,3-dimethylbenzo[*b*]thiophenes obtained by Buchwald-Hartwig C-N cross-coupling. *Bioorg Med Chem Lett.* 2007; 15:1788-1794.
 20. Abreu R, Falcão S, Calhelha RC, Ferreira IC, Queiroz MJ, Vilas-Boas M. Insights in the antioxidant activity of diarylamines from the 2,3-dimethylbenzo[*b*]thiophene through the redox profile. *J Electroanal Chem.* 2009; 628:43-47.
 21. Pinto-Basto D, Silva JP, Queiroz MJ, Moreno AJ, Coutinho OP. Antioxidant activity of synthetic diarylamines: A mitochondrial and cellular approach. *Mitochondrion.* 2009; 9:17-26.
 22. Sardão VA, Oliveira PJ, Holy J, Oliveira CR, Wallace KB. Vital imaging of H9c2 myoblasts exposed to *tert*-butylhydroperoxide – characterization of morphological features of cell death. *BMC Cell Biol.* 2007; 8:11-27.
 23. Ferreira IC, Queiroz MJ, Kirsch G. Synthesis of diarylamines in the benzo[*b*]thiophene series bearing electron donating or withdrawing groups by Buchwald-Hartwig C-N coupling. *Tetrahedron.* 2003; 59:975-981.
 24. Kimes BW, Brandt BL. Properties of a clonal muscle cell line from rat heart. *Exp Cell Res.* 1976; 98:367-381.
 25. L'Ecuyer T, Horenstein MS, Thomas R, Heide RV. Anthracycline-induced cardiac injury using a cardiac cell line: potential for gene therapy studies. *Mol Gen Metabol.* 2001; 74:370-379.
 26. Dangel V, Giray J, Ratge D, Wisser H. Regulation of beta-adrenoceptor density and mRNA levels in the rat heart cell-line H9c2. *Biochem J.* 1996; 317:925-931.
 27. Silva JP, Sardão VA, Coutinho OP, Oliveira PJ. Nitrogen compounds prevent H9c2 myoblast oxidative stress-induced mitochondrial dysfunction and cell death. *Cardiovasc Toxicol.* 2010; 10:51-65.
 28. Silva JP, Gomes AC, Coutinho OP. Oxidative DNA damage protection and repair by polyphenolic compounds in PC12 cells. *Eur J Pharmacol.* 2008; 601:50-60.
 29. Silva JP, Areias FM, Proença MF, Coutinho OP. Oxidative stress protection by newly synthesized nitrogen compounds with pharmacological potential. *Life Sci.* 2006; 78:1256-1267.
 30. Pias EK, Aw TY. Early redox imbalance mediates hydroperoxide-induced apoptosis in mitotic competent undifferentiated PC-12 cells. *Cell Death Differ.* 2002; 9:1007-1016.
 31. Alia M, Ramos S, Mateos R, Bravo L, Goya L. Response of the antioxidant defense system to *tert*-butyl hydroperoxide and hydrogen peroxide in a human hepatoma cell line (HepG2). *J Biochem Mol Toxicol.* 2005; 19:119-128.
 32. Kohen R, Nyska A. Oxidation of biological systems: Oxidative stress phenomena, antioxidants, redox reactions, and methods for their quantification. *Toxicol Pathol.* 2002; 30:620-650.
 33. Niki E, Yoshida Y, Saito Y, Noguchi N. Lipid peroxidation: Mechanisms, inhibition, and biological effects. *Biochem Biophys Res Commun.* 2005; 338:668-676.
 34. Silva JP, Proença F, Coutinho OP. Protective role of new nitrogen compounds on ROS/RNS-mediated damage to PC12 cells. *Free Radic Res.* 2008; 42:57-69.
 35. Rego AC, Santos MS, Proença MT, Oliveira CR. Influence of vitamin E succinate on retinal cell survival. *Toxicology.* 1998; 128:113-124.
 36. Hiroi M, Ogihara T, Hirano K, Hasegawa M, Morinobu T, Tamai H, Niki E. Regulation of apoptosis by glutathione redox state in PC12 cells exposed simultaneously to iron and ascorbic acid. *Free Radic Biol Med.* 2005; 38:1057-1072.
 37. Bhat KL, Garg A, Bock CW. Calculated values of the octanol-water partition coefficient and aqueous solubility for aminoazobenzenedyes and related structures. *Dyes Pigm.* 2002; 52:145-159.
 38. Areias FM, Rego AC, Oliveira CR, Seabra RM. Antioxidant effect of flavonoids after ascorbate/Fe²⁺-induced oxidative stress in cultured retinal cells. *Biochem Pharmacol.* 2001; 62:111-118.
 39. L'Ecuyer T, Sanjeev S, Thomas R, Novak R, Das L, Campbell W, Heide RV. DNA damage is an early event in doxorubicin-induced cardiac myocyte death. *Am J Physiol Heart Circ Physiol.* 2006; 291:H1273-H1280.
 40. Kitagawa S, Nabekura T, Takahashi T, Nakamura Y, Sakamoto H, Tano H, Hirai M, Tsukahara G. Structure-activity relationships of the inhibitory effects of flavonoids on P-glycoprotein-mediated transport in KB-C2 cells. *Biol Pharm Bull.* 2005; 28:2274-2278.
 41. Abreu RM, Ferreira IC, Queiroz MJ. QSAR model for predicting radical scavenging activity of di(hetero)arylamines derivatives of benzo[*b*]thiophenes. *Eur J Med Chem.* 2009; 44:1952-1958.

(Received March 9, 2010; Accepted May 30, 2010)

Original Article**Development of a microemulsion-based formulation to improve the availability of poorly water-soluble drug**

Fathy I. Abd-Allah, Hamdy M. Dawaba*, Ahmed M. S. Ahmed

Department of Pharmaceutics & Industrial Pharmacy, Faculty of Pharmacy, Al-Azhar University, Nasr City, Cairo, Egypt.

ABSTRACT: The objective of our investigation was to design a thermo-dynamically stable microemulsion formulation of the model drug piroxicam with minimum surfactant concentration in order to improve its solubility. The solubility of piroxicam in different oils was examined. Effects of the co-surfactant:surfactant ratio and water content on microemulsion formulation were evaluated. Phase studies were performed for systems composed of oleic acid as the oil phase, Tween-80 as surfactant, and propylene glycol as co-surfactant at a constant percentage of water to elucidate the effect of microemulsion components on the area of microemulsion formulation. The viscosity and conductivity of certain microemulsion formulations were examined as a function of water dilution. The results showed that oleic acid, Tween-80, and propylene glycol resulted in the highest solubilization of piroxicam. The amount of water that was successfully incorporated into a microemulsion system was directly proportional to the co-surfactant:surfactant ratio and inversely proportional to the percentage amount of the oil phase present in the system. Microemulsion systems displayed changes in their viscosity and conductivity upon water dilution. The pre-microemulsion systems could be used as solvents to provide enhanced solubilizing capacity and stabilization for the solubilized drug. These systems could be loaded with the drug and stored in their original form in order to produce a microemulsion containing the drug *in situ* upon aqueous dilution. The incorporation of piroxicam in microemulsion formulations led to enhancement of the piroxicam release profile by allowing constant and regular *in vitro* release as well as reducing piroxicam's particle size to that suited to a microemulsion. Thus, the usage of a microemulsion technique led to improvement in

piroxicam availability, suggesting the potential for technique's use as a topical vehicle for piroxicam delivery.

Keywords: Microemulsion, availability, solubility, poorly water soluble, model drug, piroxicam

1. Introduction

Microemulsions, which are optically isotropic and thermodynamically stable systems of water, oil, surfactant, and co-surfactant, have been studied as drug delivery systems because of their capacity to solubilize poorly water-soluble drugs as well as their enhancement of topical and systemic availability. For example, oral microemulsion formulations have been successfully developed for cyclosporine, a highly lipophilic and poorly aqueous soluble drug, in order to improve its oral absorption and reduce variations in its absorption (1,2). A study also reported that the microemulsion formulation *N*-4472(*N*-[2-(3,5-di-*tert*-butyl-4-hydroxyphenethyl)-4,6-difluorophenyl]-*N'*-[4-(*N*-benzylpiperidyl)]urea), a poor water-soluble drug, significantly improved oral absorption, irrespective of whether the subject was fed (3). The improved absorption from a microemulsion is presumably due to incorporation of the drug into microemulsion droplets. Smaller microemulsion droplets result in an increased specific surface area and increased membrane permeability of the drug *via* solubilization of certain membrane components and pore formation. All these factors lead to enhanced contact with the gastro-intestinal tract. Another important factor is the inner polarity of droplets, which is governed by the hydrophilic-lipophilic balance of surfactant used. A change in droplet polarity may affect the arrangement of the drug and surfactant on the droplet interface and alter drug release (4). Microemulsions have also been considered as topical (5), transdermal (6), and parenteral drug delivery systems (7), and several studies have reported the use of a microemulsion as a nasal drug delivery system (8). In the present

*Address correspondence to:

Dr. Hamdy M. Dawaba, Department of Pharmaceutics & Industrial Pharmacy, Faculty of Pharmacy, Al-Azhar University, Nasr City, Cairo, Egypt.
e-mail: hamdydr2010@yahoo.com

work, different pre-microemulsion and microemulsion formulations was prepared in order to improve piroxicam availability. This was done by selection of the most suitable microemulsion components that led to the highest solubilization of piroxicam. Then, the selected microemulsion formulations were characterized to help in selecting the most suitable formulation.

2. Materials and Methods

2.1. Materials

Piroxicam was purchased from El-Nasr Pharmaceutical Chemicals Co., Cairo, Egypt (Batch No. 20030202). Castor oil and dimethylsulfoxide (DMSO) were from El-Gomheria Pharmaceutical Co., Cairo, Egypt. Olive oil was from El-Fayrouz Pharmaceutical Co., Cairo, Egypt. Linseed oil, coconut oil, turpentine oil, oleic acid, and propylene glycol were from Morgan Pharmaceutical Co., Cairo, Egypt. Paraffin oil was from SMGO Pharmaceutical Co., Cairo, Egypt. Peanut oil was from Sigma-Aldrich, St Louis, MO, USA. Tween-80, Tween-60, Tween-40, Span-80, and *n*-butanol were from ADWIC Pharmaceutical Co., Cairo, Egypt. Tween-20 was from Merck KGaA, Darmstadt, Germany.

2.2. Solubility studies of piroxicam in different oils, surfactants, and co-surfactants

The solubility of piroxicam was examined in different oils, *i.e.*, castor oil, olive oil, linseed oil, paraffin oil, coconut oil, turpentine oil, oleic acid, and peanut oil; surfactants, *i.e.*, Tween-20, Tween-40, Tween-60, Tween-80, and span-80; and co-surfactants, *i.e.*, *n*-butanol and propylene glycol. The equilibrium solubility method was performed as follows. Briefly, an excess amount of piroxicam was added to 10 mL of each solvent (the aforementioned oils, surfactants, and co-surfactants) in 30 mL screw-capped vials and the whole mixture was mixed by vortexing. The vials were then shaken at 37°C for 72 h at 100 rpm in a thermostatically controlled water bath shaker (Weiss Gallenkamp, Loughborough, UK). Then, the supernatant layer was separated and subjected to centrifugation at 3,000 rpm for 5 min in order to remove the undissolved drug. Samples of these solutions were then collected and the drug concentration was determined spectrophotometrically at 350 nm against a suitable blank of DMSO using an ultraviolet spectrophotometer SP6-550 (Pye Unicam, Cambridge, England). All experiments were performed in triplicate.

2.3. Microemulsion formulation and phase diagram preparation

The selected oil, surfactant, and co-surfactant from the aforementioned solubility studies were used to

formulate microemulsions and prepare phase diagrams. The microemulsion domains were distinguished by the corresponding phase diagrams. The microemulsion phases were identified as the area in the phase diagram where a clear and transparent formulation was produced based on visual inspection of numerous samples. No attempts were made to distinguish among the true solutions, micelles, bicontinuous structures, w/o (water dispersed in oil) and o/w (oil dispersed in water) microemulsions, *etc.* The domains of existing transparent, isotropic systems were considered to correspond to the microemulsion phases. Phase diagrams were determined at room temperature (approximately 25°C) as outlined by Li *et al.* (8) with slight modifications. The ternary phase diagrams of surfactant, co-surfactant, and oil were prepared at a constant percentage of water from 0 to 400% of total initial weight of surfactant, co-surfactant, and oil mixtures, with mixtures containing 0% water referring to pre-microemulsion. For initial determination of microemulsion phase areas within the entire phase diagram, about 36 sample mixtures (based on 10% change in weight) of oil, surfactant, and co-surfactant were carefully weighed, mixed with the aid of a vortex, and visually inspected for phase clarity and flowability. For more exact determination of the areas corresponding to pre-microemulsions, additional mixtures of surfactant, co-surfactant, and oil were prepared with a concentration change rate of 5% for each component at the boundary obtained from the previous step. Samples were then titrated with water in a drop-wise manner and mixed thoroughly by vortexing until clear and transparent microemulsion phase regions could be identified. Once the microemulsion phase was identified, additional samples were prepared to determine the boundary regions. No heating was used during the preparation. The clear areas corresponding to either pre-microemulsions or diluted microemulsions were depicted in a triangular phase diagram using AutoCAD 2000 from Microsoft.

2.4. Preparation of microemulsions containing piroxicam

Piroxicam was accurately weighed and simply added to the selected pre-microemulsion bases from the prepared phase diagrams. Vortexing was required to dissolve piroxicam completely in microemulsion systems. The final piroxicam concentration was adjusted to 0.5% w/v.

2.5. Characterization of the selected microemulsions

The following methods were used to characterize microemulsions.

2.5.1. Determination of the particle size of microemulsions

The particle size was determined for both pre-microemulsion formulations (*i.e.*, piroxicam-free

formulations) and microemulsions containing piroxicam using a JEOL Transmission Electron Microscope (JTEM) model 1010 (JEOL, Tokyo, Japan).

2.5.2. Drug solubility in microemulsion components

An excess amount of piroxicam was added to each oil, Tween-80, propylene glycol, and water in 30 mL screw-capped vials and the whole mixture was mixed by vortexing. The vials then were shaken at 37°C for 72 h at 100 rpm in a thermostatically controlled water bath shaker. Then, the supernatant layer was separated and subjected to centrifugation at 3,000 rpm for 5 min in order to remove the undissolved drug. Samples of these solutions were then collected and the drug concentration was determined spectrophotometrically at 350 nm against a suitable blank of DMSO. Samples with the same composition (without the drug) were treated similarly and used as a control.

In order to examine the effect of the co-surfactant: surfactant ratio on the solubility of piroxicam, an excess amount of the drug was added to pre-microemulsion concentrate with weight ratios of co-surfactant (propylene glycol) to surfactant (Tween-80) ranging from 0.29:1 to 2:1. After equilibration of 72 h at ambient temperature, the equilibrated samples were centrifuged at 3,000 rpm for 5 min to remove the undissolved drug. Drug free samples with the same composition were treated similarly and used as a control.

To examine the effect of water content in microemulsion formulations on the solubility of the drug, an excess amount of the drug was added to each ample containing different percentages of water ranging from 0 to 200% of total pre-microemulsion weight and the procedure for drug separation and analysis was repeated as mentioned above.

2.5.3. Viscosity of microemulsions

The effect of water dilution on microemulsion viscosity was studied using a Brookfield DV viscometer (model DV-II+; Brookfield Engineering Laboratories, Inc., Middleboro, MA, USA) with a number 0 spindle at 50 rpm at room temperature (25°C). Samples of pre-microemulsion and microemulsion formulations were prepared and viscosity measurements were carried out at different concentrations of water (from 0 to 200% of total pre-microemulsion weight) in order to determine the effect of water dilution on the microemulsion structure.

2.5.4. Electrical conductivity

Conductivity measurements were carried out to demonstrate the effect of water dilution on microemulsion structure. Microemulsion formulations were chosen at different percentages of water (from about 10 to 400% of total microemulsion weight).

Measurements were done at 25°C. The adherence of surfactant on the electrode and the cell inner wall was avoided by pre-washing the cell twice with the sample to be measured before each measurement.

2.5.5. Thermodynamic stability of microemulsions

Thermodynamic stability was examined for both pre-microemulsion formulations (*i.e.*, piroxicam-free formulations) and microemulsions containing piroxicam through the following procedures: (i) *Heating-cooling cycle* – Six cycles were carried out between refrigerator temperature (4°C) and 45°C with storage at each temperature of no less than 48 h. The formulations that were stable at these temperatures were subjected to a centrifugation test. (ii) *Centrifugation test* – Passing formulations were centrifuged at 3,500 rpm for 30 min. Those formulations that had no phase separation were used in a freeze-thaw stress test. (iii) *Freeze-thaw cycle* – Three freeze-thaw cycles were carried out between –21°C and 25°C with storage of formulations at each temperature for no less than 48 h (9,10).

2.5.6. Physical stability of microemulsions

Pre-microemulsions and microemulsions with different water concentrations were visually inspected over 6 months for any signs of drug precipitation, phase separation and/or color change. Viscosity measurements and repeated centrifugation of the system were carried out for 30 min at 13,000 rpm at specified time intervals to ensure the stability of the system formed (11).

2.5.7. In vitro release studies for piroxicam

In vitro release studies of piroxicam from the microemulsion bases were carried out using PWIT11 USP dissolution test apparatus (Pharma Test, Hainburg, Germany) with the temperature of the water bath kept at $37 \pm 2^\circ\text{C}$ according to the manufacturer's instructions. The dissolution apparatus was adapted for semi-solid pharmaceutical drug dosage forms and was set up as follows: the dissolution medium, 300 mL phosphate buffer, pH 7.4; diffusion system with static cell, 120 rpm. A synthetic cellulose acetate membrane (7.54 cm, Fischer Scientific Co., London, UK) previously treated with distilled water at 100°C for 5 min and maintained at 4°C was fixed at the end of a glass tube of a diffusion cell that was manufactured at the Faculty of Science, Ain-Shams University, Cairo, Egypt. The experimental procedure was carried out using 2 mL of either pre-microemulsion or microemulsion. The analysis was performed with 2 mL samples taken from the dissolution medium at 15 min intervals. The removed samples were replaced by equal volumes of phosphate buffer of the same pH to maintain a constant volume for the receiving medium. Control samples with the

same composition of oil, surfactant, and co-surfactant were treated as before in order to eliminate the effect of microemulsion components on the UV absorption of piroxicam. The amount of the drug released from the formulations was determined spectrophotometrically at 350 nm by measuring the test samples against blank samples. Experiments were performed in triplicate and mean results were reported (12).

3. Results and Discussion

3.1. Solubility studies of piroxicam in various solvents including water, different oils, surfactants, and co-surfactants

Identifying an appropriate solvent to dissolve piroxicam and then formulating microemulsion formulations is crucial because only the dissolved drug can penetrate the skin. In order to screen appropriate solvents for the preparation of microemulsions, the solubility of piroxicam in various solvents including oils, surfactants, and co-surfactants was measured and the obtained results were summarized in Table 1. The solubility of piroxicam in oleic acid was found to be 12.6 mg/mL. This value was the best among all the investigated oils, but it was still much lower than that of Tween-80, which dissolved piroxicam of up to 17.8 mg/mL (Table 1). In addition, propylene glycol had better piroxicam solubility than *n*-butanol (Table 1).

As mentioned above, piroxicam is known to be water-insoluble. This fact has been proven by the experimental work in this study as water had the lowest solubility with respect to piroxicam among the investigated solvents. Piroxicam solubility in water was 0.0836 mg/mL (Table 1), which equals 0.66%, 0.47%, and 1.3% of piroxicam solubility in oleic acid, Tween-80, and propylene glycol, respectively.

These results revealed that the solubility of piroxicam in oleic acid, Tween-80, and propylene

glycol was 150.8, 212.4, and 76.78 times the aqueous solubility of piroxicam. Therefore, oleic acid was selected as the oil phase, Tween-80 as the surfactant, and propylene glycol as the co-surfactant in this study.

3.2. Microemulsion formulation and phase diagram preparation

The method used to prepare the phase diagrams of microemulsions was slightly modified, as described before (8). All possible regions for microemulsion formation at all possible ratios of surfactant:co-surfactant:oil were represented. The microemulsion phases were identified as the area in the phase diagram where a clear and transparent formulation was produced based on visual inspection of numerous samples. No attempts were made to distinguish among the true solutions, micelles, bicontinuous structures, w/o and o/w microemulsions, *etc.* The domains of existing transparent, isotropic systems were considered to correspond to the microemulsion phases. The ternary phase diagrams of surfactant, co-surfactant, and oil were determined at a constant percentage of water from 0 to 200% of total initial weight of surfactant, co-surfactant, and oil mixtures, with mixtures containing 0% water referring to a pre-microemulsion (Figure 1). Based on visual identification, regions corresponding to clear isotropic systems were considered microemulsion areas (gray shaded areas in Figure 1) while clear, highly viscous systems were considered gel areas (black-shaded area in Figure 1). The rest of the phase diagrams consisted of regions corresponding to turbid and conventional emulsion systems. The effect of water concentration on the areas of isotropic regions was evident in the given phase diagrams.

3.2.1. Effect of water dilution on the area of microemulsions

Based on visual observations, there was a complete separation of the phases or turbidity for the formulations that did not contain either surfactant or co-surfactant, respectively, regardless of the percent of water added. As the percent of water added increased, the clear isotropic area decreased until the percent of water added was from 60% to 400% of the total initial weight. The clear isotropic area disappeared in all the formulations investigated (Figure 1). Upon addition of 50% water, an oleic acid/Tween-80/propylene glycol system started to form a translucent gel phase (Figure 1), the area of which decreased in size with further dilution and which completely disappeared at 100% dilution of the system. Whether or not the observed transformation of the clear pre-microemulsion areas to turbid phases was preceded by translucent gel phases upon dilution may be due to a conversion to macroemulsion phases (13). Upon dilution with small portions of water, the pre-microemulsion system may be converted into w/o

Table 1. Solubility of piroxicam in microemulsions with different components

Components of microemulsion	Piroxicam solubility (mg/mL)
Water	0.0836
Castor oil	2.72
Linseed oil	4.65
Coconut oil	4.37
Oleic oil	12.6
Olive oil	3.78
Paraffin oil	0.133
Turpentine oil	1.52
Peanut oil	2.98
Tween-80	17.8
Tween-60	17.2
Tween-40	13.6
Tween-20	17.6
Span-80	2.68
Propylene glycol	6.42
<i>n</i> -Butanol	4.33

microemulsions, particularly at higher ratios of the oil phase. However, upon dilution with excess aqueous phase w/o microemulsions are inverted into o/w emulsions, microemulsions, and/or w/o/w emulsions; a number of liquid crystalline phases are considered to be possible intermediates during this phase inversion process (14). Systems that remained clear and fluid at higher dilutions with the aqueous phase are expected to be of the o/w type where the oil phase ratio is lower.

3.2.2. Effect of oil properties on the area of microemulsions

An oil's properties can affect the production of microemulsions. The formation of a microemulsion is favored when small molecular weight oils are present. Unfortunately, pharmaceutically acceptable oils tend to be of large molecular weight and semi-polar in nature. This fact, together with the oil's properties and concentration, is important in determining the drug loading capacity of any microemulsion. Thus, examining the effect of the oil on microemulsion formation is essential (15).

Oleic acid is an oil with a relatively large molecular volume (15). In an oleic acid system, the pre-microemulsion had a large, clear isotropic area at the beginning of phase determination. However, upon addition of 10% water a great reduction in the isotropic clear area was observed (Figure 1). The oleic acid system started to develop a clear viscous gel area at 50% dilution with water. This viscous gel area appeared at only 50% dilution with water and promptly disappeared when this dilution limit was exceeded. These results agreed with

those of Mokhtar *et al.* (16), who studied the effect of different oils on the microemulsion area formed. An explanation of oleic acid behavior, the miscibility of oleic acid with propylene glycol, and the lipophilicity of oleic acid must be taken into consideration. Oleic acid is miscible with propylene glycol. This could account for the difference in the area of the pre-microemulsion systems when comparing the behavior of oleic acid to that of different oils (16). The formation of the gel area during dilution with an increasing amount of water (50%) could be due to conversion from a w/o to an o/w microemulsion system (13). The roughly constant clear isotropic region at dilutions from 10 to 30% in an oleic acid system is an indication of a solubilized system where the incorporated water is miscible with propylene glycol and can solubilize Tween-80 while propylene glycol could be considered a co-solvent for oleic acid. The system in this area could be considered to be saturated with respect to both oleic acid and water. Upon further dilution, a gel phase was generated at 50%, followed by a sharp reduction in the clear isotropic area at 100% dilution due to system conversion. This may be due to the dilution of the surfactant Tween-80 to levels below effective oil solubilization (16,17).

Thus, the most suitable formulations for preparation of microemulsion bases containing piroxicam were selected based on the data in Table 1 and the corresponding phase diagrams (Figure 1). These formulations were then studied to further characterize their microemulsion properties. Table 2 summarizes the composition of the selected microemulsion formulations that were chosen for further investigation.

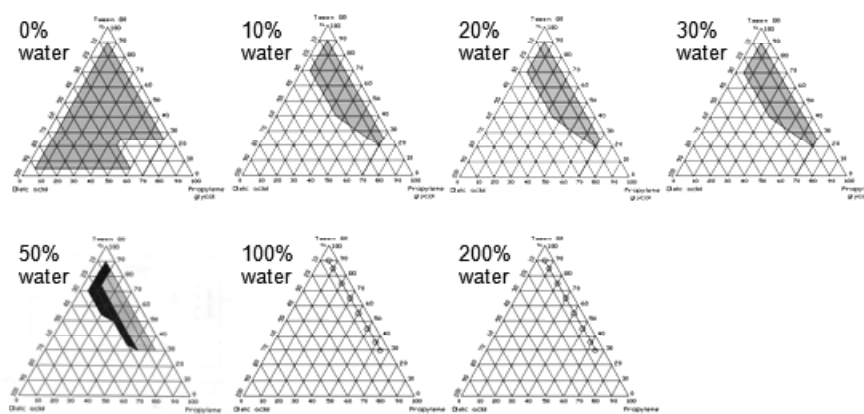


Figure 1. Triangular phase diagrams of different systems with varied water content. Grey and black shaded areas represent clear isotropic microemulsion and clear gel areas, respectively.

Table 2. Composition of the microemulsion formulations selected for further investigation

No.	Oil (%)	Surfactant (%)	Co-surfactant (%)	Water (%)	Drug (%)
F1	10	70	20	50	0.5
F2	10	60	30	50	0.5
F3	10	50	40	50	0.5
F4	10	40	50	50	0.5
F5	10	30	60	50	0.5

3.3. Particle size of microemulsions

Transmission electron microscopy is one of several techniques used to measure the size of microemulsion droplets. In this study, all the selected microemulsion samples, regardless of whether or not they contained piroxicam, had a particle size ranging from 100 nm to 500 nm. This falls within the range for the particle size of a microemulsion preparation (data not shown). Transmission electron microscopy revealed that pre-microemulsion formulation No. 2 and the corresponding formulation with the drug produced the best images among the investigated formulations (Figures 2 and 3).

Figure 2 shows TEM photos of the formulation No. 2 pre-microemulsion. In photos 2A and 2B (magnification, $\times 40,000$ and $\times 50,000$, respectively), the spherical shape of microemulsion droplets with a particle size of 500 nm is apparent.

Figure 3 shows TEM photos of formulation No. 2 microemulsion containing piroxicam. As is apparent from photos 3A and 3C (magnification, $\times 30,000$ and $\times 40,000$, respectively), piroxicam was incorporated in the spherical shape of the microemulsion droplets while retaining a particle size of 500 nm. This suggests that piroxicam's particle size was reduced to a size suited to a microemulsion in order for piroxicam to be incorporated in the microemulsion droplets. There was no change in the microemulsion particle size upon incorporation of piroxicam inside the microemulsion droplets since the photos indicate that the particle size remained 500 nm.

3.4. Drug solubility in microemulsion components

The development of a microemulsion system for the pharmaceutical delivery of both poorly soluble and slightly water-soluble drugs requires selection of a suitable surfactant, co-surfactant, and oil. The solubility of piroxicam was determined in each component of the microemulsion system. The solubility of piroxicam in the microemulsion components was determined by the equilibrium solubility method as described in the "Materials and Methods", and the results obtained are shown in Table 1.

3.5. Effect of the co-surfactant:surfactant ratio on the solubility of piroxicam

Since the pre-microemulsion system was used as a solvent to provide a better solubilization capacity and stabilization for the solubilized drug, the effect of the formulation parameters on drug solubility in such systems must be studied. These systems could be loaded with drugs and stored as-is in order to produce a microemulsion *in situ* upon aqueous dilution. As Figure 4 clearly shows, the solubility of piroxicam decreased from 5.874 to 3.294 mg/mL as the PG/T80 ratio increased from 0.29:1 to 1:1 when using a constant OA concentration (10%). This was followed by an increase to 3.7 mg/mL as the ratio increased to 1.25:1 and then again by a decrease to 3.1 mg/mL when the ratio reached 2:1. These results indicate that the highest solubility of piroxicam was found to occur at co-

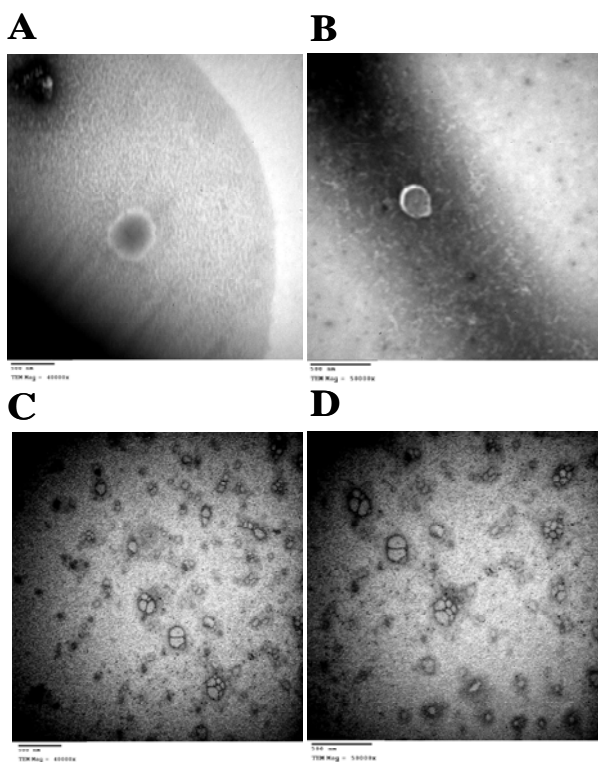


Figure 2. TEM photos of pre-microemulsion formulation 2.

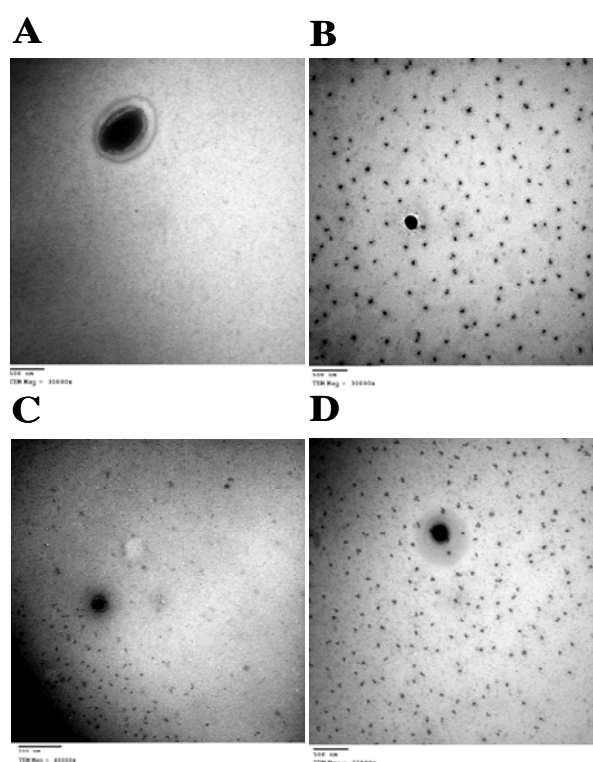


Figure 3. TEM photos of microemulsion formulation 2.

surfactant/surfactant ratios between 0.29:1 to 0.8:1 for all the systems studied

3.6. Effect of water content in microemulsion formulations on the solubility of piroxicam

Dilution of a microemulsion is very common both during mixing with other aqueous systems for reconstitution or in biological fluid after administration. Decreased drug solubility in microemulsion systems on dilution could be ascribed to the decreased concentrations mainly responsible for enhanced solubility (oil, surfactant, and co-surfactant).

Since orientation of microemulsion components is dependent on the enhanced solubility of drugs to a great extent, addition of components that can disturb this orientation (for example, addition of water to a microemulsion containing somewhat highly hydrophobic components such as oleic acid) could lead to decreased solubilizing capacity or even instability of the system itself (16).

In this study, water dilution of the microemulsion formulations greatly affected piroxicam solubility in all tested formulations. Solubility profiles are shown in Figure 5. The obtained results revealed a strange pattern of piroxicam solubility in each microemulsion formulation. To be more specific,

Microemulsion formulation 1 (ME F1): After 10% water was added, there was a decrease in solubility followed by an increase in solubility when the percent of water added reached 25%. A decrease in solubility occurred when the percent of water added reached 50%, followed by an increase in solubility when the percent of water added reached 100%. Then, a sharp decrease in solubility occurred when the percent of water added reached 200%.

Microemulsion formulation 2 (ME F2): There was a sharp decrease in solubility as the percent of water added increased from 0% to 25%. This was followed by an increase in solubility when the percent of water

added reached from 50% to 100%. A decrease in solubility occurred again when the percent of water added reached 200%.

Microemulsion formulation 3 (ME F3): After 10% water was added, there was an increase in solubility followed by a sharp decrease in solubility when the percent of water added reached 25% to 50%. This was followed by an increase in solubility when the percent of water added reached 100%. A decrease in solubility occurred when the percent of water added reached 200%.

Microemulsion formulation 4 (ME F4): After 10% water was added, there was an increase in solubility followed by a small decrease in solubility when the percent of water added reached 25% to 50%. This was followed by a sharp decrease in solubility when the percent of water added reached 100%. A small increase in solubility occurred when the percent of water added reached 200%.

Microemulsion formulation 5 (ME F5): After 10% water was added, there was an increase in solubility followed by a decrease in solubility as the percent of water added reached 25%. This was followed by an increase in solubility as the percent of water added reached 50%. Then, there was a slight decrease in solubility as the percent water added reached 100%. A sharp decrease in solubility then occurred as the percent of water added reached 200%.

3.7. Viscosity of microemulsions

Interpretation of the viscosity of microemulsions is problematic not because of uncertainties about the role of the interfacial region but due to the difficulty in obtaining meaningful measurements. When microemulsion particles are spherical, they follow a Newtonian dispersion, and when the system undergoes a transition from spheres to cylinders or lamellae the viscosity changes abruptly and the flow is described as non-Newtonian (14). The extent of dilution could have

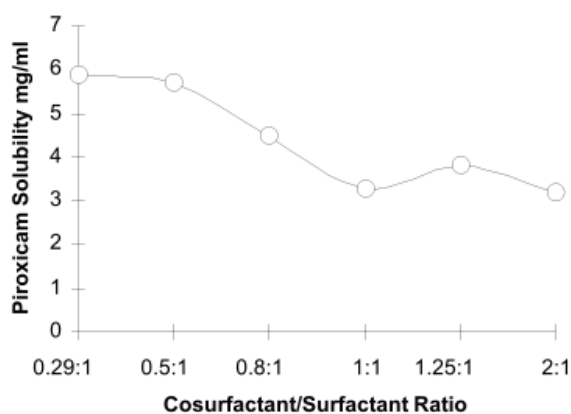


Figure 4. Effect of the co-surfactant-to-surfactant ratio on the solubility of piroxicam.

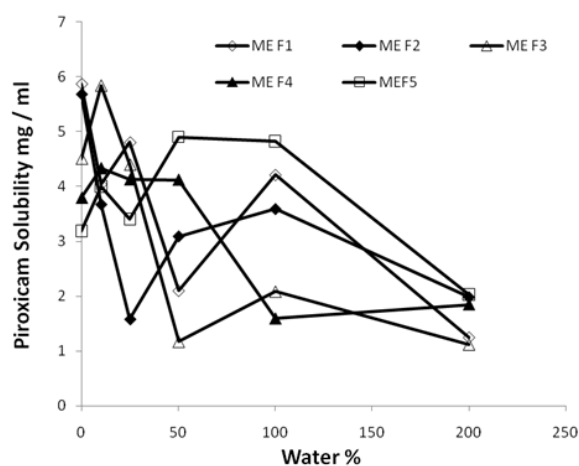


Figure 5. Summary of the effect of water content on the solubility of piroxicam.

a dramatic effect on the viscosity of a microemulsion. The viscosity of the tested microemulsion samples initially increased but then decreased upon dilution with water. The maximum increase in viscosity was observed at 50% aqueous dilution followed by a sharp decrease in viscosity afterwards. The increase in viscosity upon water dilution may be attributed to (i) an increase in the degree of hydration of the very hydrophilic polyoxyethylene oxide head groups of the surfactant and also to (ii) the presence of propylene glycol, which increases the hydrophilicity of the surfactant (18). The results obtained are shown in Figure 6.

3.8. Electrical conductivity of microemulsions

Electrical conductivity measurements can be used to analyze the microstructure of a microemulsion. An o/w microemulsion has a conductance in the same range as the conductance in the neat aqueous phase, and the conductance in a w/o microemulsion is typically four to five orders of magnitude lower. In a bicontinuous case, both water and oil self-diffusion coefficients are of the same order of magnitude as in the neat liquid (16-19).

The great changes in conductivity with water dilution can be attributed to phase inversion from reverse swollen micelles (w/o) to direct micelles (o/w). A constant correlation could exist between the specific structure and the electrical conductivity of the microemulsion, providing support for the use of electroconductivity measurements to localize bicontinuous media on the diagrams (6).

The concept of percolation transition proposed by de Gennes and Taupin (20) was used to interpret the conductivity of disordered media such as microemulsions (21). In such systems (microemulsions), conductivity is governed by a universal law independent of the physical properties of the medium such that

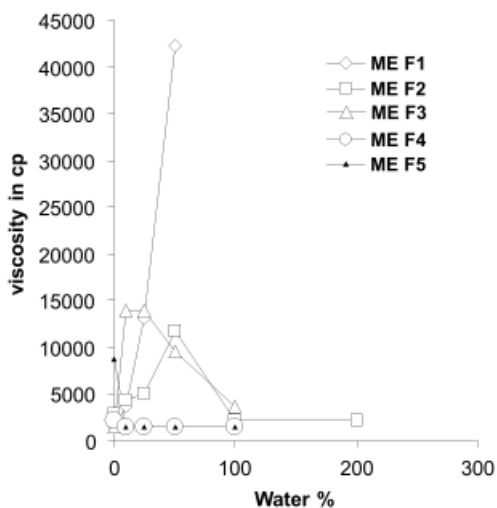


Figure 6. Effect of water content on the viscosity of microemulsion formulations.

$$K = (Q_w - Q_p)t$$

where K is the conductivity in millivolts (mV), Q_w is the water volume fraction (dispersed volume fraction), Q_p is the dispersed volume fraction at the percolation threshold, and t depends on the system dimensionality ($t = 1.5-1.6$ for a three-dimensional system).

In the present work, the conductance values (K) in the selected microemulsions were examined to see if they followed this law or not (the data is shown in Figure 7). In order to determine Q_p (the percolation threshold), $K_{1/t}$ was plotted versus Q_w . Figure 8 represents the percolation threshold of the five formulations investigated. For $t = 1.5$, a linear correlation between $K_{1/t}$ and Q_w was noted. Similar results were obtained by Thevenin *et al.* (6), who posited that the intrinsic Q_p value depends on the droplet size and the interaction between them. Thevenin *et al.* also indicated that the low value of the threshold is the consequence of the attractive interactions of the conductive species in the system. An interesting finding from the current study is that the highest threshold

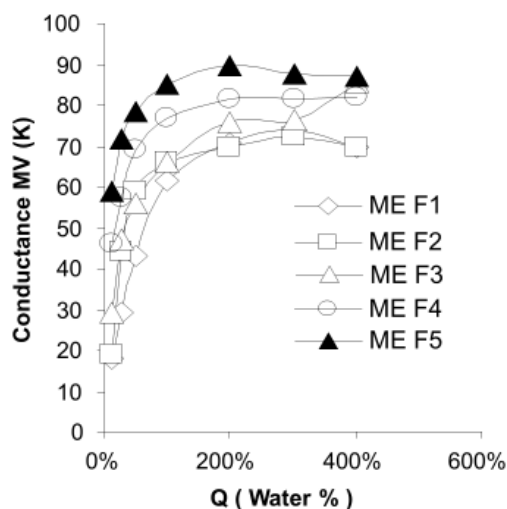


Figure 7. Electro-conductivity of selected microemulsion formulations with different water content.

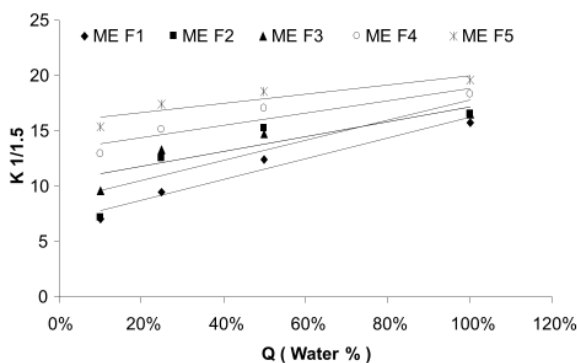


Figure 8. Percolation threshold determination.

value was obtained with a more lipophilic co-surfactant, which should require more dilution before transition to a bicontinuous system.

3.9. Thermodynamic stability of microemulsions

Thermo stability differentiates nano- or microemulsions from emulsions that have kinetic stability and will eventually display phase separation (9,10). All tested formulations succeeded in passing thermodynamic stability tests such as a heating-cooling cycle test, centrifugation test, and a freeze-thaw stress cycle test.

3.10. Physical stability of microemulsions

Pre-microemulsion and microemulsion formulations with different levels of water dilution were stored at 25°C and protected from light for about six months. The tested pre-microemulsion formulations remained in a single phase, were clear, and had no changes in color or viscosity (data not shown). In addition, the microemulsion formulations containing piroxicam were exposed to the same test conditions and the results clearly revealed that there was no drug precipitation and no color or viscosity changes (data not shown).

3.11. In vitro release studies with piroxicam

In vitro release of piroxicam was performed as described in the "Materials and Methods". The release profiles of piroxicam from each formulation were determined by plotting the percentage of piroxicam released over time in minutes (Figure 9). The results of piroxicam release were compared to those of a piroxicam solution in phosphate buffer, pH 7.4.

As shown in Figure 9, after 5 h about 74.2%, 62.4%, 52.2%, 44.9%, and 40.6% of piroxicam was released from ME F2, ME F1, ME F4, ME F3, and ME F5, respectively, whereas about 100% of the drug was released from the aqueous buffer solution of the drug over the same period of time. This suggests that free piroxicam is released very quickly from the buffer solution. Since the microemulsion formulations have higher viscosity than the reference solution, piroxicam was quickly released from this solution. The data clearly revealed that the release rates of piroxicam depended on the viscosity of the system. This agrees with data from Attwood and Florence (14), who stated that the rate of drug release from microemulsion formulations depended on the vehicle used, the viscosity of the system, and the existence of surfactant micelles. This conclusion also agrees with the results obtained by El-Badry (22).

The effect of vehicle viscosity on the amount of drug released was studied, and the amount of drug released was found to be inversely proportional to the viscosity of the vehicle used but independent of the

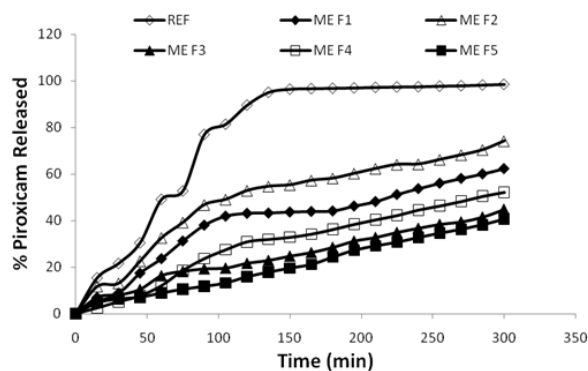


Figure 9. Percent release of piroxicam from microemulsion formulations as compared to a piroxicam solution in phosphate buffer, pH 7.4.

nature of viscolizer used. This conclusion agrees with the data from Mokhtar *et al.* (16), who studied the *in vitro* release of atenolol from different microemulsion bases. Mokhtar *et al.* found that the release rates of atenolol depended substantially on the vehicle used, the viscosity of the system, and the existence of surfactant micelles. The present results also agree with data from Dalmora *et al.* (12), who studied the effect of incorporation of piroxicam in positively charged microemulsions on the release profile. Dalmora *et al.* found that this incorporation resulted in a maximum release level about 3.6-fold lower than that of the control solution (the same concentration of piroxicam in a phosphate buffer, pH 5.5). Therefore, the previous data imply that the incorporation of piroxicam in the microemulsion formulations may result in less release than from the reference solution (*i.e.*, an aqueous buffer solution of piroxicam) over the same period of time. Another more important characteristic observed in the systems containing a microemulsion is the capacity for the internal phase (the oil) of the microemulsion to retain piroxicam. This allowed a constant and regular release over time in comparison to the reference solution.

4. Conclusion

Solubility studies showed that oleic acid, Tween-80, and propylene glycol resulted in the highest solubilization of piroxicam, and thus a triangular phase diagram was prepared using these components. In accordance with the prepared triangular phase diagrams, the most suitable microemulsion formulations were selected for further investigation. The selected microemulsion formulations were then characterized. Particle size measurement proved that all the investigated formulations, regardless of whether they had only microemulsion bases (*i.e.*, piroxicam-free formulations) or contained piroxicam, had a particle size of 500 nm, which falls within the range for the particle size of a microemulsion. Both physical and thermodynamic

stability tests proved that all the selected microemulsion formulations were physically and thermodynamically stable. Finally, an *in vitro* study of piroxicam release from these formulations allowed the selection of the most suitable microemulsion formulations with the greatest *in vitro* release of piroxicam. The most suitable microemulsion formulation in this study was microemulsion formulation 2, which consisted of 10% oleic acid, 60% Tween-80, 30% propylene glycol, 50% water of the total pre-microemulsion weight, and 0.5% piroxicam. This formulation had the best particle size as well as good physical and thermodynamic stability in addition to the best and the greatest *in vitro* release among all of the investigated formulations. The incorporation of piroxicam in microemulsion formulations led to enhancement of the piroxicam release profile by allowing constant and regular *in vitro* release as well as reducing piroxicam's particle size to that suited to a microemulsion. Thus, the usage of a microemulsion technique led to improvement in piroxicam availability, suggesting the potential for the technique's use as topical vehicle for piroxicam delivery.

References

1. Coony GF, Jeevanadam V, Choudhury S, Feutren G, Mueller EA, Eisen HJ. Comparative bioavailability of neoral and sandimmune in cardiac transplantation recipients over 1 year. *Transplant Proc.* 1998; 30:1892-1894.
2. Kim CK, Ryu SA, Park KM, Lim SJ, Hwang SJ. Preparation and physicochemical characterization of phase inverted water/oil microemulsion containing cyclosporine A. *Int J Pharm.* 1997; 147:131-134.
3. Itoh K, Tozuka Y, Oguchi T, Yamamoto K. Improvement of physicochemical properties of N-4472. Part I: formulation design by using self microemulsifying system. *Int J Pharm.* 2002; 238:153-160.
4. Shah NH, Carvajal MT, Patel CI, Infeld MH, Malick AW. Self-emulsifying drug delivery systems (SEDDS) with polyglycolizedglycerides for improving *in vitro* dissolution and oral absorption of lipophilic drugs. *Int J Pharm.* 1994; 106:15-23.
5. García-Celma MJ, Azemar N, Pes MA, Solans C. Solubilization of anti-fungal drugs in water/POE(20) sorbitan monoleate/oil systems. *Int J Pharm.* 1994; 105:77-81.
6. Thevenin MA, Grossiord JL, Poelman MC. Sucrose esters/cosurfactant microemulsion systems for transdermal delivery: assessment of bicontinuous structures. *Int J Pharm.* 1996; 137:177-186.
7. Corsawant CV, Thoren P, Engstrom S. Triglyceride based microemulsion for intravenous administration of sparingly soluble substances. *J Pharm Sci.* 1998; 87:200-208.
8. Li L, Nandi I, Kim KH. Development of an ethyl laurate-based microemulsion for rapid-onset intranasal delivery of diazepam. *Int J Pharm.* 2002; 237:77-85.
9. Lawrence MJ, Rees GD. Microemulsion-based media as novel drug delivery systems. *Adv Drug Deliv Rev.* 2000; 45:89-121.
10. Shafiq S, Shakeel F, Talegaonkar S, Ahmad FJ, Khar RK, Ali M. Development and bioavailability assessment of ramipril nanoemulsion formulation. *Eur J Pharm Biopharm.* 2007; 66:227-243.
11. Gasco MR, Gallarate M, Trotta M, Buchiero L, Gremmo E, Chiappero O. Microemulsion as topical delivery vehicles: Ocular administration of timolol. *J Pharm Biomed Anal.* 1989; 7:433-439.
12. Dalmora ME, Dalmora SL, Oliveria AG. Inclusion complex of piroxicam with β -cyclodextrin and incorporation in cationic microemulsion. *In vitro* drug release and *in vivo* topical anti-inflammatory effect. *Int J Pharm.* 2001; 222:45-55.
13. Constantinides PP, Yiv SH. Particle size determination of phase-inverted water-in-oil microemulsions under different dilution and storage conditions. *Int J Pharm.* 1995; 115:225-234.
14. Attwood D, Florence AT. *Surfactant systems: Their Chemistry, Pharmacy and Biology.* Chapman and Hall, London, UK, 1983.
15. Aboofazeli R, Lawrence CB, Wicks SR, Lawrence MJ. Investigation into the formation and characterization of phospholipid microemulsions: III. Pseudo-ternary phase diagrams of systems containing water-lecithin-isopropyl myristate and either an alcanoic acid, amine, alkanediol, polyethylene glycol alkyl ether or alcohol as cosurfactant. *Int J Pharm.* 1994; 111:63-72.
16. Mokhtar M, Hammad M, El-Ghamry A, Abu-Zaid S. Phase study and characterization of certain developed multicomponent colloidal systems and their potential application as carriers for antimicrobial agent. *Alex J Pharm Sci.* 2005; 19:131-140.
17. Warisnoicharoen W, Lansley AB, Lawrence MJ. Nonionic oil-in-water microemulsions: The effect of oil type on phase behavior. *Int J Pharm.* 2000; 198:7-27.
18. Ktistis G. A viscosity study on oil-in-water microemulsions. *Int J Pharm.* 1990; 61:213-218.
19. von Corswant C, Thorén P, Engström S. Triglyceride-based microemulsion for intravenous administration of sparingly soluble substances. *J Pharm Sci.* 1998; 87:200-208.
20. de Gennes PG, Taupin C. Microemulsions and the flexibility of oil/water interfaces. *J Phys Chem.* 1982; 86:2294-2304.
21. Safran SA, Grest GS, Bug ALM, Webma I. Percolation in interacting systems. In: *Microemulsion Systems* (Rosano HL, Clause M, eds.). Marcel Dekker, New York, NY, USA, 1987; pp. 238-245.
22. Mahmoud El-Badry. Performance of propranolol hydrochloride in certain ophthalmic formulations (M. Sc. Thesis). Faculty of Pharmacy, Assiut University, Egypt, 1991.

(Received March 21, 2010; Revised April 6, 2010; Re-revised May 27, 2010; Accepted May 27, 2010)

Original Article**Preparation, characterization, and stability studies of piroxicam-loaded microemulsions in topical formulations**

Fathy I. Abd-Allah*, Hamdy M. Dawaba, Ahmed M. S. Ahmed

Department of Pharmaceutics and Industrial Pharmacy, Faculty of Pharmacy, Al-Azhar University, Nasr City, Cairo, Egypt.

ABSTRACT: The main purpose of this work was to determine the *in vitro* release of piroxicam in microemulsion formulations from different pharmaceutical topical preparations including different gel bases, such as, methyl cellulose (MC), carboxy methyl cellulose (CMC), hydroxypropyl methyl cellulose (HPMC), Carbopol 934, Carbopol 940, and Pluronic F-127 bases. The effect of the employed gel bases on the *in vitro* release profiles of piroxicam was examined to choose the base which gave the highest *in vitro* release. The kinetic treatments and parameters derived from *in vitro* release of piroxicam formulations were calculated according to different kinetic orders or systems. These gel formulations were selected for rheological and stability studies. Stability studies were conducted to investigate the change in drug content, viscosity, and pH of the semisolid formulations. The results showed that, the incorporation of piroxicam in microemulsion formulas could lead to enhancement of piroxicam release profiles by allowing constant and regular *in vitro* release. Three percent MC gel base showed the highest release of piroxicam-microemulsion after 180 min (97.70%) followed by 3% HPMC (94.0%) when compared to bases containing piroxicam alone. All the medicated gel bases containing piroxicam exhibit pseudoplastic flow with thixotropic behavior. The degradation of piroxicam from its topical formulations was found to be a zero-order reaction based on the mean value of correlation coefficients. All formulations were quite stable. The shelf life of the gel containing HPMC base was about 2.85 years. Considering the *in vitro* release, rheological properties and shelf life, HPMC gel base containing 0.5% piroxicam in a microemulsion formula was the best among the studied formulations.

Keywords: Piroxicam, topical, microemulsion, gel, hydroxypropyl methyl cellulose

1. Introduction

Piroxicam is a non steroidal anti-inflammatory drug (NSAID) that exhibits anti-inflammatory, anti-rheumatoid arthritis (1), analgesic (2), and antipyretic activities in animal models. Piroxicam like other non steroidal anti-inflammatory drugs causes side-effects on the gastro-intestinal system and other systems of the body. Piroxicam has a number of undesirable physicochemical properties including its poor solubility in water (3). Various strategies have been used to overcome the problems arising from its poor aqueous solubility and to improve bioavailability. Among these strategies were the use of penetration enhancers and a prodrug approach (4). Thus for this reason, topical administration of piroxicam have been studied as a way to minimize these side effects.

Microemulsions which are optically isotropic and thermodynamically stable systems of water, oil, surfactant and cosurfactant, have been studied as drug delivery systems because of their solubilization capacity for poorly water soluble drugs as well as their enhancement effects on topical and systemic availability. For example, oral microemulsion formulations have been successfully developed for cyclosporine, a highly lipophilic and poorly aqueous soluble drug for improving oral absorption and reducing absorption variation (5,6).

It is considered that the improved absorption from microemulsions is due to incorporation of drug into microemulsion droplets, the smaller size of microemulsion droplets, the increased specific surface area, and the increased membrane permeability towards the drug *via* solubilization of certain membrane components and pore formation. All these factors resulted in enhancing contact with the gastro-intestinal tract. Another important factor is the inner polarity of droplets governed by the hydrophilic lipophilic balance of surfactant used. The change in droplet polarity

*Address correspondence to:

Dr. Fathy Ibrahim Abd-Allah, Pharmaceutics Department, Faculty of Pharmacy (Boys), Al-Azhar University, Cairo, Egypt.
e-mail: Fathy_fet@hotmail.com

affects the arrangement of drug and surfactant on the droplet interface and alters drug transdermal (9), and parenteral drug delivery systems (10). A very few studies have reported the use of microemulsions as nasal drug delivery systems (11).

There are different types of topical administration including ointments, creams, and gel preparations. Gels are semisolid preparations containing large proportions of water. They are used pharmaceutically as lubricants and also used as carriers for many drugs because of their local effects and percutaneous absorption (12). Gels are particularly suitable for water soluble medicaments and are less satisfactory for insoluble substances which are often difficult to be incorporated uniformly. They are easy to be applied and the evaporation of the water content produces a pleasant sensation. The residual film usually adheres well and gives protection but it is easily removed by washing when the treatment is complete (13).

Some of the gelling agents are available in different grades with a different viscosity at a definite concentration (14). According to the nature of the colloidal properties, gel bases are classified into: inorganic gel bases, *e.g.* Bentonite magma; organic gel bases which were further subdivided according to the nature of the dispersed organic molecule (15), polypeptides, *e.g.* gelatin; synthetic block copolymers, *e.g.* poloxamers (16), and semi-synthetic polymers, *e.g.* effective cellulose derivatives including sodium carboxy methyl cellulose (CMC), hydroxyl propyl cellulose and hydroxyl propyl methyl cellulose (HPMC) (17,18).

The objective of this study was to determine the *in vitro* release of piroxicam in microemulsion formulations from different pharmaceutical topical preparations including different gel bases such as methyl cellulose (MC), CMC, HPMC, Carbopol 934, Carbopol 940, and Pluronic F-127 bases. The effect of the employed gel bases on the *in vitro* release profiles of piroxicam was studied to choose the base which gave the highest *in vitro* release. The kinetic treatments and parameters derived from the *in vitro* release of piroxicam formulations were calculated according to different kinetic orders or systems. These gel formulations were selected for rheological and stability studies. Stability studies were conducted to see the change in drug content, viscosity, and pH of the semisolid formulations. Finally, the composition of the formulation with best overall properties was determined.

2. Materials and Methods

2.1. Materials

Piroxicam (Batch No. 20030202) and CMC were purchased from El-Nasr Pharmaceutical Chemicals (Cairo, Egypt). Methyl cellulose, HPMC, triethanolamine

(TEA), and Pluronic F-127 were from Sigma-Aldrich (St Louis, MO, USA). Carbopol 934 and 940 were from Goodrich Chemical Co. (London, England). All other materials were of analytical grade and they were used without any further purification.

2.2. Microemulsion formulation and phase diagram construction

The selected oil (oleic acid), surfactant (Tween-80) and cosurfactant (propylene glycol) from the solubility studies (22) were used in this method. The microemulsion domains were distinguished using the corresponding phase diagrams. The microemulsion phases were identified as the area in the phase diagram where clear and transparent formulations were produced based on visual inspection of many samples.

The domains of existing transparent, isotropic systems were considered to correspond to the microemulsion phases. Phase diagrams were constructed at room temperature, approximately 25°C as outlined by Li *et al.* (11) with slight modifications. The ternary phase diagrams of surfactant, cosurfactant, and oil were developed at a constant water percent from 0 to 400% of total initial weight of surfactant, cosurfactant, and oil mixtures, with mixtures containing 0% water referring to premicroemulsion.

For initial determination of microemulsion phase areas within the entire phase diagram, about 36 sample mixtures (based on 10% change in weight) of oil, surfactant, and cosurfactant were carefully weighed, mixed with the aid of a vortex and visually inspected for phase clarity and flowability. For more exact determination of the areas corresponding to premicroemulsions additional mixtures of surfactant, co-surfactant, and oil were prepared with a concentration change rate of 5% for each component at the boundary obtained from the previous step. Samples were then titrated with water in a drop-wise manner and mixed thoroughly by vortexing until clear and transparent microemulsion phase regions could be identified. Once the microemulsion phase was identified additional samples were prepared to determine the boundary regions. No heating was used during the preparation.

The clear areas corresponding to either pre-microemulsions or diluted microemulsions were constructed inside the triangular phase diagram using the Microsoft program AutoCAD 2000.

2.3. Preparation of microemulsions containing piroxicam

Piroxicam was accurately weighed and added simply to the selected premicroemulsion bases from the constructed phase diagrams. Vortexing was required to dissolve piroxicam completely in microemulsion

systems. The final piroxicam concentration was adjusted to be 0.5% (w/v).

2.4. Determination of particle size

The determination of the particle was done for both premicroemulsion formulas (*i.e.*, piroxicam free formulas) and microemulsions containing piroxicam using a JEOL Transmission Electron Microscope (JTEM) model 1010 (JEOL, Ltd., Tokyo, Japan).

2.4.1. Preparation of plain cellulosic gel bases

The weighed amounts of the cellulosic polymer powder was sprinkled gently on a vortex in a 100 mL beaker containing distilled water, and magnetically stirred at high speed. Stirring was continued until a thin hazy dispersion, without lumps, was formed. For complete gel dispersion it was necessary to leave samples overnight in the refrigerator (19,20). The same method was used for all cellulosic substances except boiling distilled water was used for the MC gel, and a portion of hot distilled water at 80°C was used for the HPMC gel preparation while the remaining amount of cold water was added and mixing was continued until a smooth homogenous HPMC gel was formed (21).

2.4.2. Preparation of cellulosic gel bases containing piroxicam

The formulas for cellulosic gel bases were prepared by addition of piroxicam in microemulsion form (22), or piroxicam alone was added during the stirring process and the steps were completed as mentioned above for plain cellulosic gel bases.

2.4.3. Preparation of plain Carbopols (934 and 940) gel bases

Carbopol 934 or 940 gel bases were prepared by homogenizing 0.5% (w/v) Carbopol dispersion in sufficient water using a magnetic stirrer for 30 min and leaving it to equilibrate for 24 h. After that, pH was adjusted to 5-7 with triethanolamine (23).

2.4.4. Preparation of Carbopols (934 and 940) gel bases containing piroxicam

Formulas of both Carbopol 934 and 940 gel bases were prepared by addition of piroxicam in microemulsion form or piroxicam alone during the stirring process and the steps were completed as mentioned for Carbopol plain gel bases.

2.4.5. Preparation of plain Pluronic F-127 gel base

The required amount of Pluronic F-127 powder was

slowly added to cold distilled water (5-10°C) while maintaining constant agitation with a magnetic stirrer. The dispersion was left overnight in a refrigerator to form a clear viscous solution (19,20).

2.4.6. Preparation of Pluronic F-127 gel bases containing piroxicam

The formulas of Pluronic F-127 gel bases were prepared by addition of piroxicam in microemulsion form or piroxicam alone to the gel and mixing is done while the gel is liquid. The poloxamer gels exhibit thermal behavior and therefore are fluid at lower temperatures (19,20).

2.5. *In vitro* release of piroxicam from different gel bases

The release pattern of the drug from the gel bases was examined using a cell diffusion model as described elsewhere (24), holding the temperature of the water bath at $37 \pm 2^\circ\text{C}$. The dissolution apparatus (USP dissolution test apparatus II, version DT 600, Heusenstamm, Germany) adapted for semi-solid formulations was set up, containing 300 mL phosphate buffer pH 7.4, at a speed of 120 rpm: the diffusion system had a static cell. A synthetic cellulose acetate membrane (7.54 cm) previously treated with distilled water at 100°C for 5 min and maintained at 4°C was fixed at the end of the glass tube of the diffusion cell. The experimental procedure was carried out using 2 g of gel base. The analysis was performed with 2 mL samples withdrawn from the dissolution medium at 15 min intervals. The removed samples were replaced with equal volumes of phosphate buffer at the same pH to maintain a constant volume for the receiving medium.

Control samples with the same composition of oil, surfactant, and cosurfactant in gel bases were treated as before in order to eliminate the effect of microemulsion components on the UV absorption of piroxicam. The amount of the drug released from the bases was determined spectrophotometrically at 350 nm by measuring the test samples against blank samples. Experiments were done in triplicate and mean results were reported (25).

2.6. Kinetic analysis of drug release data

The kinetic data for the *in vitro* release of piroxicam was estimated using different kinetic orders (zero-, first-, and second-order) or systems such as Higuchi's diffusion model (26), the Hixson-Crowel cup root law (27), and the Baker-Lonsdale equation (28). A special computer program was used to calculate the kinetic treatments, kinetic parameters and kinetic data for the *in vitro* release from piroxicam microemulsions.

2.7. Rheological properties of semisolid preparations

A Brookfield LVT DV-II Programmable Viscometer of Engineering Laboratories, Inc. (Middleboro, MA, USA) was connected to a thermostatic water bath adjusted to 25°C. The viscosity of the plain gel bases and the medicated bases containing piroxicam which gave the highest *in vitro* release was determined. Measurements were carried out to determine the most suitable gel bases.

Viscosity was measured on each base by using spindle 40. A defined amount (0.5 g) of each gel base was placed inside the plate and carefully closed. The measurement was started by operating the viscometer at 0.6 rpm, the speed was gradually increased and the measurement was recorded when the torque reached 10%. The speed was gradually increased at a constant rate for all tested samples until the torque reached 90%, with 30 sec between each successive speed. The rheological parameters, including viscosity, shear rate, shear stress, and yield value, were directly obtained from the monitor. The speed was then reduced gradually, using the same order as the increasing speeds, until reaching the starting rpm.

A complete rheogram was obtained by either plotting the shear rate as a function of the shear stress or plotting the viscosity as a function of shear rate.

The flow properties of microemulsion formulas can be determined by using the equation for non-Newtonian systems as follows. For plastic flow, plastic viscosity (η) was described in the following equation.

$$\eta = (F - f)/G \quad \text{----- Ex. 1}$$

Where, f is the yield value or intercept, on the shear stress axis is dyne cm^{-2} , F is the shear stress and G is the rate of shear. For pseudoplastic flow, several approaches have been used to obtain meaningful parameters that will allow different pseudoplastic materials to be compared (29). Of those, the exponential formula has been used most frequently.

$$\eta' = (F^N)/G \quad \text{----- Ex. 2}$$

The exponent N (Farrow's constant) rises as the flow becomes increasingly non-Newtonian. The term η' represents viscosity coefficient. By arrangement of the above equation,

$$\log G = N \log F - \log \eta' \quad \text{----- Ex. 3}$$

An equation for a straight line is obtained. Many pseudoplastic systems fit this equation when $\log G$ is plotted as a function of $\log F$.

2.8. Measurement of thixotropy

Measurement of thixotropic behavior of both plain and

medicated gel bases was determined using the cut and weight method (30) in order to calculate the hysteresis loop between the upward curve and downward curve of each plain and medicated gel base using calc paper (70 g, 21 × 29.7 cm).

2.9. Stability studies of semisolid preparations

The prepared plain and medicated gel bases were stored in well stoppered polyvinyl chloride (PVC) plastic containers in the dark for 6 months at room temperature. They were checked for drug content, viscosity, and pH change bimonthly throughout the period. The method used by Tas *et al.* (31) to investigate the stability of chlorpheniramine maleate in gels prepared using different cellulose derivatives were followed in the present studies.

2.9.1. Piroxicam content study

An accurately weighted quantity of each gel base (about 100 mg) was dissolved in about 50 mL of phosphate buffer (pH 7.4). These solutions were quantitatively transferred to volumetric flasks and appropriate dilutions were made with the same buffer solution. The resulting solutions were then filtered through 0.45 μm membrane filters before subjecting the solution to spectrophotometric analysis for piroxicam at 350 nm (20,32).

2.9.2. Viscosity measurements

A Brookfield Viscometer was used to measure the viscosity of the prepared gel bases. The spindle was rotated at 10 rpm. Samples of the bases were allowed to settle over 30 min at room temperature before the measurements were taken (20,32).

2.9.3. pH measurements

The pH was measured in each base using a pH meter that was calibrated before each use with buffered solutions at pH 4, 7, and 10. A defined amount of each tested base was taken and diluted with calibrated distilled water and mixed well. The electrode of the pH meter was immersed in the prepared base solution for pH determination (33).

3. Results and Discussion

3.1. Preparation of topical formulations

Preliminary screening using different concentration of polymers in the gel formulations (3% methyl cellulose, 2% carboxy methylcellulose, 3% hydroxypropyl methylcellulose, 0.5% Carbopols (934 and 940), and 20% Pluronic F-127) was performed before the present

study. The lowest concentration of each polymer needed to form gels was used to prepare the formulations for dissolution, rheological, and stability studies. It was found that drug release decreased with higher polymer concentration. One obvious reason for this would be the increase in viscosity due to the increase in polymer concentration. It is also possible that at higher polymer concentrations the active substance was trapped by the polymer molecules and by its close proximity to polymer molecules. This increased the resistance to diffusion more than expected. Additionally the density of chain structures which has been observed in gels microstructure increased at higher polymer concentrations and this limits the active substance movement area (34-37).

3.2. *In vitro* release of piroxicam from gel bases

The previously mentioned concentrations of gel bases were selected since they gave the best release with most previously studied drugs and it is apparent that drug release rate decreases as the concentration of the gel increases (38-41).

An explanation for this behavior is the increased number of micelles at higher gel concentration as in the case of Pluronic F-127, resulting in a more entangled system and a more rigid gel (40). Also, decreased drug release by an increase in the concentration of the gel may be attributed to the differences in the viscosity of the polymers (38,41). As shown in Figures 1 and 2, piroxicam in its microemulsion form clearly exhibited a higher *in vitro* release as compared with plain piroxicam.

3.2.1. Release of piroxicam from cellulose derivative gel bases

The direct addition of MC and HPMC into water causes

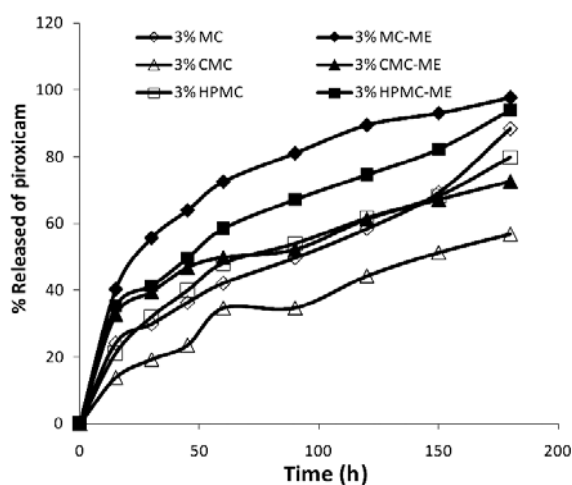


Figure 1. Percentage of piroxicam released from plain and microemulsion gel base. Open circle, 3% MC; Closed circle, 3% MC-ME; Open triangle, 3% CMC; Closed triangle, 3% CMC-ME; Open square, 3% HPMC; Closed square, 3% HPMC-ME.

coagulation and subsequent dissolution is slow and difficult. Both MC and HPMC are soluble in hot water, consequently the initial uniform dispersion can be done in hot water followed by cooling (42). As shown in Figure 1, it was clear that the release of piroxicam from 3% MC gel bases was higher than that from other tested cellulose derivative gel bases (CMC and HPMC). The *in vitro* release of piroxicam-microemulsion formulas from different cellulose derivative gel bases could be arranged in a descending manner as follows: 3% MC > 3% HPMC and finally 3% CMC. By combining the two previous arrangements, the *in vitro* release of piroxicam from plain drug and drug-microemulsion cellulose derivative gel bases could be arranged in a descending manner as follows: 3% MC-ME > 3% HPMC-ME > 3% MC > 3% HPMC > 3% CMC-ME and finally 3% CMC gel base.

3.2.2. Release of piroxicam from Carbopols and Pluronic F-127 gel bases

The least concentration of both Carbopols 934 and 940 and Pluronic F-127 was used since the decreased release encountered by increasing the concentration of the gel may be attributed to the difference in the viscosity of the polymers (40,41,43). As shown in Figure 2, Carbopol 934 gels showed a higher release than Carbopol 940 gels. These results were attributed to the fact that Carbopol 934 gel base exhibited a lower viscosity than the Carbopol 940 gel base (44).

The *in vitro* release of piroxicam from different Carbopols and Pluronic F-127 gel bases can be arranged in a descending manner as follows: 0.5% Carbopol 934 > 0.5% Carbopol 940 and Pluronic F-127. The *in vitro* release of the piroxicam-microemulsion formula from different Carbopols and Pluronic F-127 gel bases could be arranged in a descending manner as follows:

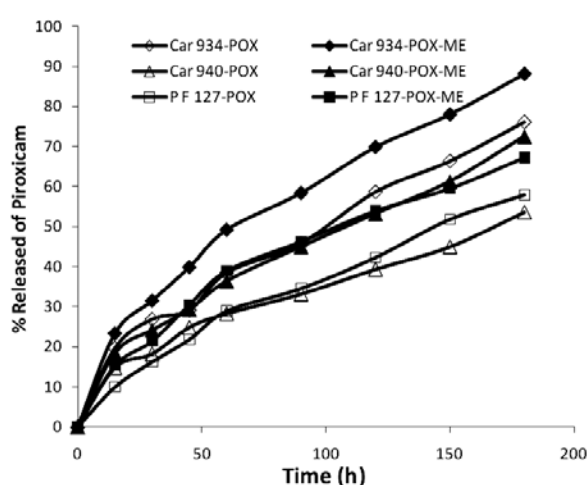


Figure 2. Percentage of piroxicam released from Carbopol and Pluronic F-127 from plain and microemulsion gel base. Open circle, Carbopol 934; Closed circle, Carbopol 934-ME; Open triangle, Carbopol 940; Closed triangle, Carbopol 940-ME; Open square, Pluronic F-127; Closed square, Pluronic F-127-ME.

0.5% Carbopol 934 > 0.5% Carbopol 940 and Pluronic F-127. By combining the two previous arrangements, the *in vitro* release of piroxicam from plain drug and drug-microemulsion could be arranged in a descending manner as follows: 0.5% Carbopol 934-ME > 0.5% Carbopol 934 > 0.5% Carbopol 940-ME > Pluronic-ME > Pluronic and finally 0.5% Carbopol 940 gel base.

3.3. Kinetic data of piroxicam *in vitro* release

According to the results obtained from the *in vitro* release data for all gel bases, the bases that gave the best release were chosen to study kinetic behavior. In order to develop an ideal kinetic model to interpret the diffusion data in terms of meaningful parameters, various kinetic models including zero-order, first-order, and the Higuchi diffusion model were applied to obtain the best fit for the results. As shown in Table 1, it was found that *in vitro* release of piroxicam-microemulsion formulas followed zero-order for Carbopol 940, first-order for 3% MC and Pluronic F-127, and Higuchi diffusion order for 3% CMC, 3% HPMC, and 0.5% Carbopol 934. The kinetic data showed that the *in vitro* release of piroxicam followed different kinetic orders and that no single kinetic order could be used to express drug release from specific types of topical formulations.

3.4. Rheological properties of topical formulations

The rheological evaluation of pharmaceutical semisolids is useful since it provides a method of quality control during and after the manufacturing process and information about the structure of the phases present in a product and the influence of various agents used in its formulation. All the investigated gel bases (plain or medicated) were subjected to rheological examination. All the studied gel bases exhibited pseudoplastic behavior with thixotropic character. The results are shown in Table 2. Gel formulations containing piroxicam micremulsion in MC and HPMC bases were at the top in terms of thixotropy. Thixotropy is a desirable property in liquid pharmaceutical systems because these systems retain their high consistency in the container yet can be poured from the containers precisely and spread on the skin easily (45). Besides, thixotropy improves product stability by decreasing the rate of sedimentation, which may be crucial for parenteral products.

3.5. Stability studies

Shelf storage stability tests of semisolid preparations based on storing the preparation at room temperature

Table 1. Kinetic parameters of piroxicam released from cellulosic derivatives, Carbapols and Pluronic F-127 gel bases containing piroxicam-microemulsion formulae

Bases	Kinetic order or model	Intercept (a)	Slope (b)	Correlation (r^2)	Rate constant (k)	$t_{1/2}$ (min)
MC (3%)	Zero	46.66	0.319	0.9497	0.319	156.6
	First	1.92	-0.018	0.9872	-0.018	38.2
	Diff.	23.07	5.852	0.9858	5.852	73.0
CMC (3%)	Zero	27.97	0.234	0.9934	0.224	213.7
	First	1.88	-0.021	0.9964	-0.005	143.2
	Diff.	11.89	4.144	0.9966	4.143	154.6
HPMC (3%)	Zero	33.42	0.341	0.9908	0.341	146.5
	First	1.96	-0.006	0.9572	-0.013	54.7
	Diff.	9.36	6.056	0.9958	6.056	68.2
Carbopol 934 (0.5%)	Zero	21.81	0.383	0.9920	0.383	130.5
	First	1.99	-0.005	-0.9862	-0.011	65.2
	Diff.	4.63	6.809	0.9985	6.809	53.9
Carbopol 940 (0.5%)	Zero	15.16	0.318	0.9978	0.318	157.4
	First	1.97	-0.003	0.9899	-0.006	111.5
	Diff.	6.20	5.579	0.9929	5.580	80.3
Pluronic F-127 (20%)	Zero	25.34	0.305	0.9813	0.305	163.9
	First	1.91	-0.003	-0.9997	-0.007	99.9
	Diff.	3.86	5.466	0.9968	5.466	83.7

Higuchi model was written in the table as diffusion model (Diff.).

Table 2. Viscosity and thixotropic behavior of piroxicam prepared from microemulsion in different gel bases

Formulae	Viscosity (cp)		Thixotropic behavior (cm^2)	Farrow's constant
	Max	Min		
3% MC	289	63	2.36	1.74
3% CMC	9,310	1,210	5.34	1.42
3% HPMC	74	35	2.16	1.92
0.5% Carbopol 934	6,630	784	1.63	1.42
0.5% Carbopol 940	9,550	337	2.10	1.31

were carried out to detect any changes in drug content, viscosity, and pH of the preparations through 6 months. The results are summarized in Table 3. All of the gel samples showed excellent results in these studies. Drug degradation was found to be in the range 3.3-7.9% after 6 months. Viscosity values after 6 months compared to the initial viscosity were in the range 2-52%, while pH changed 0.08-0.23 units only. In all cases, MC and HPMC showed the smallest changes in these parameters (Table 3).

According to the results obtained from the kinetic analysis of the stability tests, it was obvious that the degradation of piroxicam was found to obey a zero-order reaction for all the tested gel bases, based on the values of the correlation coefficient (r) (Table 4). After knowing the half-life ($t_{1/2}$) of all the investigated gel bases, it was possible to calculate the time after which the gel bases lose 10% of their initial content (t_{90}). This is a direct calculation of the length of time through which the gel bases would remain and complies with the official requirement of drug content. From these results, it was obvious that 3% HPMC and 3% MC gave the longest t_{90} in years of 2.85 and 2.08, respectively.

4. Conclusion

The incorporation of piroxicam in microemulsion formulas could lead to enhancement of piroxicam

release profiles by allowing constant and regular *in vitro* release as well as reduction in piroxicam microemulsion particle size. Thus usage of the microemulsion technique led to improvement in piroxicam availability which can offer many promising features for its use as a topical vehicle for piroxicam delivery. Various gel bases containing piroxicam-microemulsion were studied for drug release, rheologic behavior, and stability of the topical formulations. Three percent MC gel base showed the highest release of piroxicam-microemulsion after 180 min (97.7%) followed by 3% HPMC (94.0%) when compared to bases containing piroxicam alone. All the medicated gel bases containing piroxicam exhibited pseudoplastic flow with thixotropic behavior. The degradation of piroxicam from its topical formulations was found to be a zero-order reaction based on the mean values of correlation coefficients. All formulations were quite stable. The shelf life of the gel containing HPMC base were about 2.85 years. Considering *in vitro* release, rheological properties and shelf life, the HPMC gel base containing 0.5% piroxicam in microemulsion formula was the best among the studied formulations.

Acknowledgements

The authors would like to thank the EL-Nasr Pharmaceutical Chemical Company, Cairo, Egypt, for their donation of piroxicam.

Table 3. Various parameters for shelf storage stability tests for up to 6 months

Parameters	Storage periods (Months)						
	0	1	2	3	4	5	6
Piroxicam content (%)							
3% MC	100	99.6	99.2	98.3	97.5	96.5	95.8
3% CMC	100	99.4	98.7	97.4	96.1	94.5	92.1
3% HPMC	100	99.5	99.0	98.5	97.9	97.1	96.7
Viscosity (dyne/cm)							
3% MC	265	266	268	268	269	269	270
3% CMC	2,914	2,907	2,898	2,895	2,887	2,879	2,862
3% HPMC	69	67	67	66	66	65	65
pH values							
3% MC	7.28	7.28	7.25	7.25	7.22	7.19	7.19
3% CMC	7.80	7.84	7.88	7.92	7.96	7.98	8.03
3% HPMC	7.71	7.77	7.77	7.68	7.66	7.63	7.63

Table 4. Kinetic parameters for shelf stability testing of piroxicam released from different gel bases

Formulae	Kinetic order	Intercept (a)	Slope (b)	Correlation (r^2)	Rate constant (k)	$t_{1/2}$ (min)
3% MC	Zero	-0.593	0.401	0.9957	0.401	124.6
	First	2.003	-0.002	-0.9954	-0.004	-168.6
	Second	0.009	0.001	0.9951	< 0.001	237.8
3% CMC	Zero	-1.350	0.714	0.9833	0.714	70.0
	First	2.006	-0.003	-0.9812	-0.008	-93.0
	Second	0.009	< 0.001	0.9791	< 0.001	128.8
3% HPMC	Zero	-0.154	0.293	0.9968	0.293	170.9
	First	2.001	-0.001	-0.9966	-0.003	-232.1
	Second	0.009	< 0.001	0.9964	< 0.001	328.5

References

- Hedner T, Samulesson O, Wahrborg P, Wadenvik H, Ung KA, Ekbom A. Nabumetone: Therapeutic use and safety profile in the management of osteoarthritis and rheumatoid arthritis. *Drugs*. 2004; 64:2315-2343.
- Izdes S, Orhun S, Turanii S, Erkilic E, Kanbak O. The effects of preoperative inflammation on the analgesic efficacy of intra-articular piroxicam for outpatient knee arthroscopy. *Anesth Analg*. 2003; 97:1016-1019.
- TenHoor C, Bakatselou V, Dressman J. Solubility of mefenamic acid under simulated fed- and fasted-state conditions. *Pharm Res*. 1991; 8:1203-1205.
- Schwenker G, Chen J. 1,2-Dihydro-3,1-benzoxazin-4-one and 4H-1,2-dihydro-pyrido-[2,3-d]- [1,3]-oxazin-4-one derivatives as potential prodrugs. Part III: Permeability through excised human skin *in vitro*. *Arch Pharm (Weinheim)*. 1991; 324:891-894.
- Cooney GF, Jeevanandam V, Choudhury S, Feutren G, Mueller EA, Eisen HJ. Comparative bioavailability of Neoral and Sandimmune in cardiac transplant recipients over 1 year. *Transplant Proc*. 1998; 30:1892-1894.
- Kim CK, Ryuu SA, Park KM, Lim SJ, Hwang SJ. Preparation and physicochemical characterization of phase inverted water/oil microemulsion containing cyclosporin A. *Int J Pharm*. 1997; 147:131-134.
- Shah NH, Carvajal MT, Patel CI, Infeld MH, Malick AW. Self-emulsifying drug delivery systems (SEDDS) with polyglycolized glycerides for improving *in vitro* dissolution and oral absorption of lipophilic drugs. *Int J Pharm*. 1994; 106:15-23.
- García-Celma MJ, Azemar N, Pes MA, Solans C. Solubilization of antifungal drugs in water/POE(20) sorbitan monooleate/oil systems. *Int J Pharm*. 1994; 105:77-81.
- Thevenin MA, Grossiord JL, Poelman MC. Sucrose esters/cosurfactant microemulsion systems for transdermal delivery: assessment of bicontinuous structures. *Int J Pharm*. 1996; 137:177-186.
- von Corswant C, Thorén P, Engström S. Triglyceride-based microemulsion for intravenous administration of sparingly soluble substances. *J Pharm Sci*. 1998; 87:200-208.
- Li L, Nandi I, Kim KH. Development of an ethyl laurate-based microemulsion for rapid-onset intranasal delivery of diazepam. *Int J Pharm*. 2002; 237:77-85.
- Nishihata T, Rytting JH, Takahashi K, Sakai K. Effects of dithiothreitol and ascorbate on the penetration of diclofenac across excised rat dorsal skin. *Pharm Res*. 1988; 5:738-740.
- Carter SJ. Cooper and Gunn's Dispensing for Pharmaceutical Students. 12th ed., Pitman Medical, London, UK, 1982; pp. 214-223.
- Block L. Medicated Application. In: Remington. The Science and Practice of Pharmacy, (Gennaro AR, ed.). 19th ed., Mack Publishing, Easton, PA, USA, 1995.
- Fox C. An introduction to the formulation of shampoos. *Cosmet Toilet*. 1988; 103:25-58.
- Chen-Chow PC, Frank SG. *In vitro* release of lidocaine from Pluronic F-127 gels. *Int J Pharm*. 1981; 8:89-99.
- Rufe RG. Cellulose polymers in cosmetics and toiletries. *Cosmet Perfum*. 1975; 90:93-94.
- Teng JT, Lucas JM, Scallet BL. *Cosmet Perfum*. 1975; 90:30-32.
- Badran M, Ahmed S, Ibrahim E. Pharmaceutical studies on percutaneous drug delivery of certain medicaments (M. Sc. Thesis). Faculty of Pharmacy, Al-Azhar University, Cairo, Egypt, 2004.
- Abd EL-Napy T, Fetouh I, Ahmed S. Preformulation studies on the release of non-steroidal anti-inflammatory drug from different pharmaceutical topical preparations (M. Sc. Thesis). Faculty of Pharmacy, Al-Azhar University, Cairo, Egypt, 2007.
- Handbook of Pharmaceutical Excipients. American Pharmaceutical Association, Washington, DC, USA; Royal Pharmaceutical Society of Great Britain, London, UK, 2000; pp. 79, 252, 336.
- Abd-Allah F, Dawaba H, Ahmed S. Development of microemulsion based formula for improving the availability of poorly water soluble drug. *Az J Pharm Sci*. 2009; 40:94-110.
- Gallardo V, Zouaki Y, Parera A, Ruiz MA. Effect of cellulose polymer on the release of salicylates in topical formulations. *React Funct Polym*. 2001; 50:33-40.
- USP 24/NF 19. Dissolution Apparatus Description. Prepared by the Committee of Revision and Published by the Board of Trustees, 1995; pp. 1791-1793.
- Dalmora ME, Dalmora SL, Oliveira AG. Inclusion complex of piroxicam with beta-cyclodextrin and incorporation in cationic microemulsion. *In vitro* drug release and *in vivo* topical anti-inflammatory effect. *Int J Pharm*. 2001; 222:45-55.
- Higuchi WI, Bernardo PD, Mehta SC. Polymorphism and drug availability. II. Dissolution rate behavior of the polymorphic forms of sulfathiazole and methylprednisolone. *J Pharm Sci*. 1967; 56:200-207.
- Hixson AW, Crowell JH. Dissolution of Tablets. In: *Pharmaceutics of solids and solid dosage form*. John Wiley & Sons, New York, NY, USA, 1977; p. 163.
- Baker RW, Lonsdale HK. Controlled release: mechanisms and rates. In: *Controlled Release of Biologically Active Agents* (Tanquary AC, Lacey RE, eds.). Plenum press, New York, NY, USA, 1974; pp. 15-71.
- Martin AN, Banker GS, Chun AHC. Rheology. In: *Advances in Pharmaceutical Sciences* (Bean HS, ed.), Chap. 1. Academy Press, London, England, 1964.
- Lipatov YS. Studies of polymer-filler interaction: VI. Some rheological properties of polymer solutions in the presence of fillers. *Polymer Science USSR*. 1963; 4:490-500.
- Tas C, Ozkan Y, Savaşer A, Baykara T. *In vitro* release studies of chlorpheniramine maleate from gels prepared by different cellulose derivatives. *Farmaco*. 2003; 58:605-611.
- Taş C, Ozkan Y, Savaşer A, Baykara T. *In vitro* and *ex vivo* permeation studies of chlorpheniramine maleate gels prepared by carbomer derivatives. *Drug Dev Ind Pharm*. 2004; 30:637-647.
- Elkababi S. Formulation, stability and rheological studies of certain creams of antifungal and local acting drugs (Ph. D. Thesis). Cairo University, Cairo, Egypt, 2000.
- Fang JY, Sung KC, Hu OY, Chen HY. Transdermal delivery of nalbuphine and nalbuphine pivalate from hydrogels by passive diffusions and iontophoresis. *Arzneimittelforschung*. 2001; 51:408-413.
- Wang YY, Hong CT, Chiu WT, Fang JY. *In vitro* and *in vivo* evaluations of topically applied capsaicin and nonivamide from hydrogels. *Int J Pharm*. 2001; 224:89-104.

36. Osborne DW, Amann AH. Topical Drug Delivery Formulations, Vol. 42. Marcel Dekker, New York, NY, USA, 1990.
37. Al-Khamis KI, Davis SS, Hadgraft J. Microviscosity and drug release from topical gel formulations. *Pharm Res.* 1986; 3:214-217.
38. Stubberud L, Arwidsson HG, Hjortsberg V, Graffner C. Water-solid interactions. III. Effect of glass transition temperature, T_g, and processing on tensile strength of compacts of lactose and lactose/polyvinyl pyrrolidone. *Pharm Dev Technol.* 1996; 1:195-204.
39. Mowafy H, Fetouh I, Ahmed S. Pharmaceutical Studies on the Release of Certain Medicament using Different Dermatological Formulations (M. Sc. Thesis). Faculty of Pharmacy, Al-Azhar University, Cairo, Egypt, 2000.
40. Moore T, Croy S, Mallapragada S, Pandit N. Experimental investigation and mathematical modeling of Pluronic F127 gel dissolution: Drug release in stirred systems. *J Control Release.* 2000; 67:191-202.
41. Ilango R, Kavimani K, Kumar S, Deepa KR, Jaykar B. Formulation and evaluation of transdermal preparations of nimesulide gel. *East Pharm.* 1998; 41:123-125.
42. Mowafy H, Fetouh I, Ahmed S, Christal C. Pharmaceutical studies on the release of certain non-steroidal anti-inflammatory drug (Ph.D. Thesis). Faculty of Pharmacy, Al-Azhar University, Cairo, Egypt, 2004.
43. Miyazaki S, Takecuchi C, Takada M. Pluronic F-127 gels as a vehicle for topical administration of anticancer agents. *Chem Pharm Bull (Tokyo).* 1984; 32:4205-4208.
44. Macedoa T, Blocka LH, Shuklab AJ. Release of tolmetin from carbomw gel systems. *Drug Dev Ind Pharm.* 1993; 19:887-902.
45. Sinko P. *Martin's Physical Pharmacy and Pharmaceutical Sciences.* Lippincott Williams & Wilkins, Philadelphia, PA, USA, 2006.

(Received April 1, 2010; Revised April 16, 2010; Re-revised May 27, 2010; Accepted June 3, 2010)

Original Article**The potential therapeutic effect of nitric oxide modulators in experimentally-induced gastric ulcers****Ebtehal El-Demerdash¹, Hala O. El-Mesallamy², Noha M. Abu-Zaid³, Mohamed Z. Gad^{2,*}**¹ Pharmacology & Toxicology Department, Faculty of Pharmacy, Ain Shams University, Cairo, Egypt;² Biochemistry Department, Faculty of Pharmacy, Ain Shams University, Cairo, Egypt;³ Quality Assurance Department, The Holding Company for Biological Products and Vaccines (VACSERA), Giza, Egypt.

ABSTRACT: Nitric oxide (NO) appears to play a critical role in modulating gastric mucosal defense. Administration of NO donors has been reported to protect the gastrointestinal mucosa against damage induced by several irritants. However, the possible role of NO in healing existing ulcers must be clarified further. Therefore, the present study was designed to assess the effect of modulation of NO on the healing of an indomethacin-induced peptic ulcer using a NO precursor, L-arginine, and a competitive inhibitor of NO synthase, L-NAME. Results of administering L-arginine were compared to those using nitroglycerin (NTG), an NO donor. Rats were injected with a single oral dose of indomethacin (30 mg/kg) and then treated with L-arginine (200 mg/kg, *i.p.*), NTG (1 mg/kg, *i.p.*) or L-NAME (15 mg/kg, *i.p.*) once daily for 7 d starting 4 h after the indomethacin injection. Gross lesion examination and histological assessment were done. NO, prostaglandin (PGE₂), and mucin content in gastric tissue were detected. In addition, oxidative stress markers including glutathione (GSH) and lipid peroxides were measured. L-arginine and NTG almost completely healed indomethacin-induced ulceration as indicated by macroscopic and histological examination, restoration of normal levels of NO and GSH, and a significant attenuation of the increase in PGE₂ and lipid peroxides induced by indomethacin. In contrast, L-NAME was found to exacerbate mucosal damage. In conclusion, the present study provides further evidence for the role of NO in gastric ulcer healing and it suggests an alternative path to treating the universal problem of non-steroidal anti-inflammatory-drug-induced gastropathy.

Keywords: Indomethacin, L-arginine, nitroglycerin, L-NAME, nitric oxide, gastric ulcer

*Address correspondence to:

Dr. Mohamed Z. Gad, Biochemistry Department, Faculty of Pharmacy, The German University in Cairo, El-Tagmoa El-Khamis, New Cairo, Egypt.
e-mail: mohamed.gad@guc.edu.eg

1. Introduction

Peptic ulcers represent a serious medical problem due to their frequency among different socioeconomic classes. They affect 5-10% of the world's population and are characterized by ulceration of the stomach, duodenum, or both (1). Peptic ulcers are generally believed to result from an imbalance between aggressive factors and counteracting defense mechanisms. Foremost among aggressive factors is the use of non-steroidal anti-inflammatory drugs (NSAIDs). NSAIDs have been found to produce gastroduodenal ulcers in 25% of users, often with bleeding and perforation (2).

A diminished mucosal blood flow is generally believed to be a major factor underlying the mechanism of NSAID-induced gastric damage (3). Microcirculatory perfusion comprises the epithelial defense mechanism that provides energy, oxygen, nutrients, gastrointestinal (GI) peptide hormones, as well as other substrates necessary for maintaining epithelial cell integrity. In addition, the circulating blood in the surface mucosa removes waste materials and irritating substances and maintains mucus production and bicarbonate secretion. Thus, it helps to sustain the mucosal barrier (4). Furthermore, surface mucosal blood flow has been found to play an important role in the ulcer healing process (1,5). Therefore, a reduced blood flow leads to the mucosa's increased vulnerability to damaging agents.

The key factor in modulating microcirculation is nitric oxide (NO). When the mucosa is exposed to an irritant, a rapid increase in mucosal flow occurs. This response is initiated by sensory nerves underlying the epithelium, and its stimulation results in activation of endothelial nitric oxide synthase (eNOS) and subsequent production of NO. Vascular smooth muscle relaxes and mucosal blood flow thus increases (6). Moreover, Ma and Wallace (7) determined the relative effects of endothelial and inducible NOS on gastric ulcer healing and found that eNOS plays a significant role in gastric ulcer healing while its inducible isoform do not. Several studies have reported that administration of NO donors may protect the GI mucosa against

damage induced by several irritants, suggesting the potential use of these compounds in situations in which the GI mucosa is exposed to noxious substances or in which mucosal defense is impaired (8-10). Furthermore, a recent study used the NO precursor L-arginine to augment the gastroprotective effect of simvastatin, an antihyperlipidemic drug (11). However, the possible role of NO in treating the existing ulcers must be clarified further.

The present study was thus designed to assess the effect of modulation of NO on healing indomethacin-induced peptic ulcers using the NO precursor L-arginine and a competitive inhibitor of NOS, L-NAME. Results of administering L-arginine were also compared to those of administering nitroglycerin (NTG), an NO donor. Ulcer healing was evaluated macroscopically and histologically, and changes in PGE₂, NO, and mucin were also detected. In addition, the pathogenesis of NSAID-induced GI damage is also known to depend on hyperproduction of reactive oxygen species (ROS) and thus induction of oxidative stress injury (10). Thus, the present study evaluated the effect of modulation of NO on the oxidative stress induced by indomethacin.

2. Materials and Methods

2.1. Drugs and chemicals

Indomethacin (Liometacen ampule) was obtained from the Nile Company for Pharmaceuticals and Chemical Industries, Cairo, Egypt. A single dose of 30 mg/kg was given by oral intubation in order to induce ulcers in accordance with the study of Bhattacharya *et al.* (12). L-Arginine (Merck, Germany) was dissolved in saline and used in a dose of 200 mg/kg (*i.p.*). This dose is suggested to protect against ulcer induction (13). NTG was obtained from G. Pohl-Boskamp GmbH & Co., (Hohenlockstedt, Germany) and used in a dose of 1 mg/kg (*i.p.*) (14). L-NAME (Sigma Chemical Co., St. Louis, Mo, USA) was dissolved in saline and injected in a dose of 15 mg/kg (*i.p.*) (7).

Bovine serum albumin (BSA), *n*-butanol, 5,5'-dithiobis (2-nitrobenzoic acid) (DTNB), reduced glutathione (GSH), Folin reagent, Griess reagent, 1,1,3,3-tetramethoxypropane, thiobarbituric acid (TBA), trichloroacetic acid, and vanadium(III) chloride were all purchased from Sigma Chemical Co., Ltd. All other chemicals were of analytical grade.

2.2. Animals

This study involved eighty-five male albino rats weighing 150-200 g obtained from the Nile Co. for Pharmaceutical and Chemical Industries. The animals were housed in cages with wide mesh wire bottoms to prevent coprophagy and kept on a standard diet and water *ad libitum*. The standard food pellets (El-Nasr

Co., Abu Zaabal, Egypt) contained a mixture of no less than 20% protein, 5% fiber, 3.5% fat, 6.5% ash, and vitamins. Rats were deprived of food but had free access to water 24 h before ulcer induction. The study protocol was approved by the local ethics committee.

2.3. Experimental design

Rats were divided into six groups. To induce gastric ulcers, the 1st and 2nd groups were given a single dose of indomethacin 30 mg/kg by oral intubation. The 1st group was sacrificed 4 h after indomethacin injection and designated the group with indomethacin-induced ulceration on day 0. The 2nd group was injected *i.p.* with saline, once daily for 7 d starting 4 h after indomethacin injection and this group was designated the group with indomethacin-induced ulceration on day 7. The 3rd, 4th, and 5th groups were injected *i.p.* with L-arginine (200 mg/kg, *i.p.*), NTG (1 mg/kg, *i.p.*), or L-NAME (15 mg/kg, *i.p.*) once daily for 7 d starting 4 h after the indomethacin injection. The last group was the control group and was given saline only.

After 7 d of treatment, rats were sacrificed under ether anesthesia. Their stomachs were excised, opened along the greater curvature, rinsed extensively with saline to remove attached debris, and then pinned flat on cardboard for evaluation of gross lesions. The length of individual lesions in the mucosa was measured and the sum of lengths of all lesions in each stomach served as the ulcer index (15). The severity of gastric lesions was scored in accordance with the method of Yamamoto *et al.* (16) as follows: **1** (ulcerated area: 1-6 mm²), **2** (ulcerated area: 7-12 mm²), **3** (ulcerated area: 13-18 mm²), **4** (ulcerated area: 19-24 mm²), and **5** (ulcerated area: > 24 mm²).

Immediately after gross lesion examination, the stomach was placed on an ice-cold surface. The stomach tissue was cut into pieces, weighed, and homogenized in 0.1 M Tris-HCl buffer (pH 7.4) to obtain 20% (w/v) homogenate. Tissue homogenate was used for determination of GSH, lipid peroxides, and PGE₂. Part of the homogenate was centrifuged at 1,000 × g for 10 min to remove cell debris and nuclei and the resultant supernatant was used for estimation of NO. Specimens from stomachs of each group were fixed in alcoholic fixative material for histological examination and mucin assessment.

2.4. Biochemical analysis

Oxidative stress markers, GSH, and lipid peroxides were estimated by the methods of Ellman (17) and Uchiyama and Mihara (18), respectively. As an index of NO production, total nitrate/nitrite was estimated in the cytosolic fraction after protein precipitation using an equal volume of ethanol in accordance with the method of Miranda (19). In accordance with the

method described elsewhere (20), PGE₂ was determined by competitive enzyme-linked immunosorbent assay (ELISA) using a PGE₂ kit (Parameter™) provided by R & D Systems Inc., USA. Tissue protein was assessed in accordance with the method of Lowry *et al.* (21).

2.5. Histological assessment

Sections of 5 µm were obtained and stained with haematoxylin and eosin (H&E) stain for standard histological examination in accordance with the method of Drury and Wallington (22). Qualitative assessment of mucin was carried out in accordance with the method of McManus (23).

2.6. Statistical analysis

Data are presented as mean ± S.E.M. For statistical analysis of the data, multiple comparisons were carried out using one-way analysis of variance (ANOVA) followed by a Tukey-Kramer test for post-hoc analysis. Statistical significance was acceptable at a level of $p < 0.05$. Data analysis was achieved using the software program GraphPad InStat.

3. Results

3.1. Macroscopic and histological examination of gastric ulcers

Oral injection of a single dose of indomethacin in rats fasted for 24 h caused gastric ulceration in the glandular portion of the stomach. The group with indomethacin-induced ulceration on day 7 had a significantly higher number of ulcers than did the group with indomethacin-induced ulceration on day 0. However, there was no significant difference in the ulcer index and ulcer score for the two groups with ulceration (Table 1). Treatment of rats with either L-arginine or NTG after ulcer induction tended to return the stomach mucosa to normal (Table 1). In contrast, treatment with L-NAME for 7 d after ulcer induction further aggravated ulcer formation, as reflected by a 29% increase in the

number of ulcers, a 22% increase in ulcer index, and a 26% increase in the ulcer score for rats receiving this treatment in comparison to those receiving indomethacin (Table 1). In addition, indomethacin caused the death of three animals. The highest number of animal deaths, five animals, occurred in the group treated with indomethacin + L-NAME; these deaths were attributed to severe hemorrhaging as was revealed by gross examination of the gastric ulcers. The lowest number of deaths, one animal, occurred in the group treated with indomethacin + L-arginine. No deaths occurred in the control group.

As shown in Figure 1A, specimens from control rats revealed the normal histological structure of the glandular stomach for both the fundus and pylorus. Indomethacin treatment induced severe macroscopic gastric mucosal damage that was not accompanied by self-healing during the 7 d of the experiment. Gastric mucosal damage was characterized by focal necrosis and ulceration (Figure 1B). The inner area of the mucosa and lamina propria showed inflammatory cell infiltration as well as focal aggregation (Figure 1C). Edema with severe congested blood vessels was also detected in the lamina propria and submucosa. After treatment with L-arginine for 7 d, the gastric mucosa had an almost normal mucosal layer with little inflammatory cell infiltration. However, edema and congested blood vessels were detected in the lamina propria along with edema present only in the muscularis (Figure 1D). The stomachs of rats receiving NTG showed only focal desquamation in the lining mucosal epithelium along with little inflammatory cell infiltration in the lamina propria, although the muscularis was still edematous (Figure 1E). In contrast, rats treated with L-NAME had multiple gastric ulcers and necrobiotic changes were noted in the mucosal epithelium and glandular structure along with inflammatory cell infiltration and congested blood vessels in the lamina propria (Figure 1F).

Qualitative assessment of mucin revealed that specimens from the control group showed positive reaction to periodic acid Schiff's staining (PAS) in the periphery and in the mid zone of the glandular mucosal layer of the stomach, although the groups

Table 1. Gross examination of the effect of daily administration of L-arginine (200 mg/kg, *i.p.*), NTG (1 mg/kg, *i.p.*), or L-NAME (15 mg/kg, *i.p.*) for 7 d on gastric ulcers induced with indomethacin in rats

Group ^a	No. of dead rats	No. of ulcers	Ulcer index (mm)	Ulcer score
Control	0/15	0	---	---
Indomethacin (group with indomethacin-induced ulceration on day 0)	0/10	10.80 ± 0.49	17.0 ± 0.79	3.40 ± 0.16
Indomethacin (group with indomethacin-induced ulceration on day 7)	3/15	13.25 ^a ± 0.75	19.0 ± 1.45	3.63 ± 0.26
Indomethacin + L-arginine	1/15	0	---	---
Indomethacin + NTG	2/15	0	---	---
Indomethacin + L-NAME	5/15	17.11 ± 0.66 ^{***}	23.2 ± 1.15 ^{***}	4.55 ± 0.18 ^{***}

^a Values given are means of 10-15 observations ± S.E.M. Gastric lesions were scored according to their severity on a scale of 1 to 5: **1** (ulcerated area: 1-6 mm²), **2** (ulcerated area: 7-12 mm²), **3** (ulcerated area: 13-18 mm²), **4** (ulcerated area: 19-24 mm²), and **5** (ulcerated area: > 24 mm²). ^{***} Significant difference with respect to groups with indomethacin-induced ulceration on day 0 and 7, respectively, at $p < 0.05$ using ANOVA followed by Tukey-Kramer for multiple comparisons.

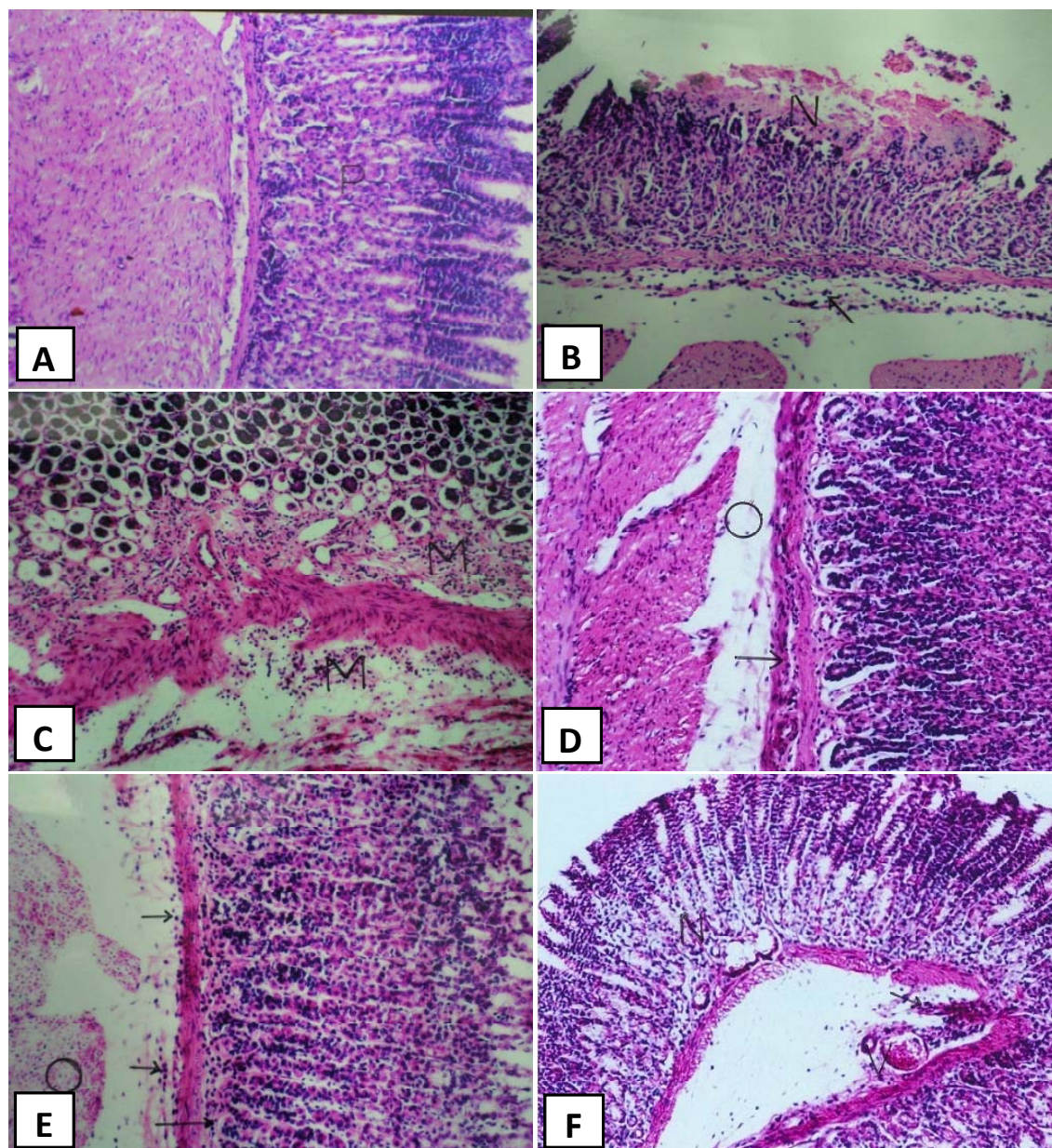


Figure 1. Photomicrographs of sections in the glandular stomach stained with hematoxylin-eosin stain. Panel A ($\times 40$) represents a section taken from the stomach of a rat treated with saline and shows the normal histological structure of mucosal layer (P). Panels B and C represent sections taken from the stomach of a rat treated with indomethacin and panel B ($\times 40$) shows focal necrosis and ulceration in the mucosal layer (N) and panel C ($\times 24$) shows inflammatory cell infiltration in the base of mucosal layer and lamina propria (M). Panel D ($\times 40$) represents a section taken from the stomach of a rat treated with indomethacin and L-arginine (200 mg/kg, *i.p.*) for 7 d and shows a normal mucosal layer with little inflammatory cell infiltration in the lamina propria (arrow) and edema (O). Panel E ($\times 40$) represents a section taken from the stomach of a rat treated with indomethacin and NTG (1 mg/kg, *i.p.*) for 7 d and shows desquamation of the mucosal epithelium and little inflammatory cell infiltration in the lamina propria (arrow) and muscular edema (O). Panel F ($\times 40$) represents a section taken from the stomach of a rat treated with indomethacin and L-NAME (15 mg/kg, *i.p.*) for 7 d and shows necrobiotic changes in the mucosal layer and glands (N) with hyperemia in blood vessels and inflammatory cell infiltration in the lamina propria (arrow).

with indomethacin-induced ulceration on day 0 and 7 showed a positive PAS reaction in the ulcerated area of the mucosa (Figures 2A-2C). Rats treated with L-NAME showed a positive PAS reaction in the ulcerated area of mucosal epithelium (Figure 2F). After treatment with either L-arginine or NTG, positive PAS was noted in the edges of the mucosa (Figures 2D and 2E).

3.2. Stomach content of NO and PGE₂

In comparison to the control group, a single dose of indomethacin induced a significant reduction in NO content of 28% 4 h after injection and a similar reduction of 40% 7 d after injection. Treatment of animals with L-arginine after ulcer induction significantly increased NO content by 80% in comparison to the group with indomethacin-induced ulceration on day 7 and even caused significant elevation of 8% above normal (Table 2). Animals treated with NTG also had a significant

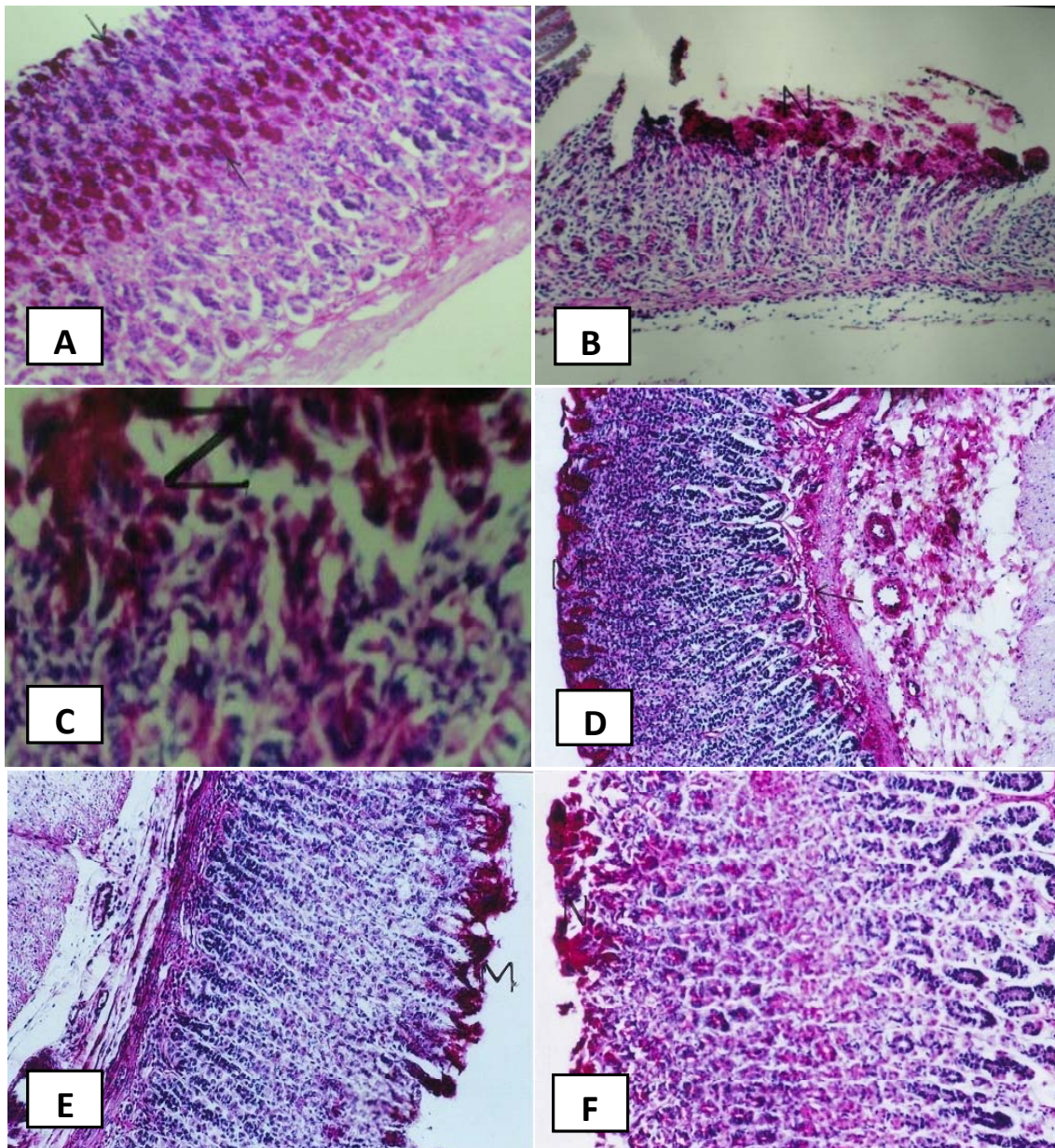


Figure 2. Photomicrographs of sections in the glandular stomach after periodic acid Schiff's staining (PAS). Panel A ($\times 40$) represents a section taken from the stomach of a rat treated with saline and shows a positive PAS reaction in the peripheral and mid zonal portions of the mucosa. Panels B and C ($\times 40$) represent sections taken from the stomach of rats treated with indomethacin after 4 h and 7 d, respectively, and the panels show a positive PAS reaction around the necrotic and ulcerated area of the mucosal layer. Panels D and E ($\times 40$) represent a section taken from the stomach of rats treated with indomethacin and either L-arginine or NTG, respectively, and show a positive PAS reaction in the edges of the mucosa. Panel F ($\times 40$) represents a section taken from the stomach of a rat treated with indomethacin and L-NAME and shows a positive PAS reaction in the ulcerated area of the mucosa.

Table 2. Effect of daily administration of L-arginine (200 mg/kg, *i.p.*), NTG (1 mg/kg, *i.p.*), or L-NAME (15 mg/kg, *i.p.*) for 7 d on NO content and PGE₂ level in gastric tissue of rats subjected to indomethacin-induced gastric ulcers

Group ^a	NO ($\mu\text{mol/g}$ tissue)	PGE ₂ (pg/mg protein)
Control	381.5 \pm 12.94	254.2 \pm 7.35
Indomethacin (group with indomethacin-induced ulceration on day 0)	274.1 \pm 3.78*	78.3 \pm 2.00*
Indomethacin (group with indomethacin-induced ulceration on day 7)	229.7 \pm 2.57***	330.4 \pm 6.06***
Indomethacin + L-arginine	413.2 \pm 5.44*****	266.5 \pm 4.86*****
Indomethacin + NTG	327.5 \pm 5.58*****	288.1 \pm 1.43*****
Indomethacin + L-NAME	184.2 \pm 9.21*****	394.8 \pm 4.34*****

^a Values given are means of 8-10 observations \pm S.E.M. ***** Significant difference with respect to the control group and groups treated with indomethacin on d 0 and d 7, respectively, at $p < 0.05$ using ANOVA followed by Tukey-Kramer for multiple comparisons.

increase in NO content of 42.5% in comparison to the group with indomethacin-induced ulceration on day 7. However, the level was still significantly lower than normal. It was about 86% of that for the control group (Table 2). On the other hand, treatment of rats with L-NAME caused a further lowering of NO content (20%) in comparison to the group with indomethacin-induced ulceration on day 7 (Table 2).

A single dose of indomethacin induced a significant decrease in PGE₂ that reached 78.31 pg/mg protein after 4 h. However, the group with ulceration on day 7 had a significant increase in PGE₂ of 30% in comparison to the control group. Treatment with either L-arginine or NTG for 7 d after ulcer induction induced a significant decrease in the PGE₂ level of 19 and 13%, respectively, in comparison to the group with indomethacin-induced ulceration on day 7. Worthy of mention is the fact that the PGE₂ level in the group treated with NTG was still significantly higher than the control group while there was no significant difference in this level for the group treated with L-arginine and the control group (Table 2). In the group treated with L-NAME, a further significant increase in the PGE₂ level of 19% was observed in comparison to the group with indomethacin-induced ulceration on day 7 (Table 2).

3.3. Oxidative stress markers (GSH and lipid peroxides)

The control level of GSH was found to be 3.65 ± 0.104 $\mu\text{mol/g}$ of tissue. Table 3 shows that in comparison to the control group indomethacin induced a significant decrease in the GSH level of about 40% 4 h and 7 d after injection. Both L-arginine and NTG treatment for 7 d succeeded in increasing GSH content by 1.6- and 1.4-fold, respectively, in comparison to GSH content in the group with indomethacin-induced ulceration on day 7. However, the level of GSH in the group treated with NTG was still significantly lower than normal. In contrast, treatment with L-NAME resulted in a further decrease in GSH content of 26% in comparison to the group with indomethacin-induced ulceration on day 7.

Assessment of stomach lipid peroxides revealed that the control level was 13.73 ± 0.63 nmol/g tissue. Table 3 illustrates the effects of different treatments on the level of stomach lipid peroxides. In comparison to

the control value, the level of lipid peroxides increased up to 149 and 157% in the groups with indomethacin-induced ulceration on day 0 and 7, respectively. The effect of indomethacin was significantly attenuated by treatment with either L-arginine or NTG (reaching 48 and 35%, respectively) in comparison to the group with indomethacin-induced ulceration on day 7. However, the level of stomach lipid peroxides was still significantly higher than normal. In contrast, animals treated with L-NAME had a further significant increase in lipid peroxides of 57% in comparison to the group with indomethacin-induced ulceration on day 7.

4. Discussion

NO appears to play an important role in gastric mucosal defense (5). However, the possible role of NO in treating existing ulcers must be clarified further. The present study assessed the effect of modulation of NO on peptic ulcer healing using a NO precursor, L-arginine, an NO donor, NTG, and a competitive inhibitor of NOS, L-NAME. Indomethacin was chosen to induce gastric ulcers because it is widely used as an experimental model to study the pathophysiological mechanisms underlying the formation of mucosal lesions and to evaluate the potential therapeutic effects of drugs (24). A single dose of indomethacin produced marked damage to the gastric mucosa, as macroscopic and histological examinations revealed. Similar results have been previously reported (12,25,26). To better understand the role played by NO in healing indomethacin-induced gastric ulcers, the concentration of NO was measured in the gastric tissue and results revealed that indomethacin significantly reduced the gastric NO content in comparison to the NO content in the control group. The reduction in NO content was significantly higher 7 d after injection than 4 h after injection. This reduction in NO content might be explained by the fact that indomethacin induces a reduction in eNOS activity (27).

The reduction in endogenous NO tissue content by indomethacin was supported by studying the effect of L-arginine, NTG, and L-NAME on gastric ulcer healing. Macroscopic and histological examination revealed that L-arginine and NTG accelerated the healing

Table 3. Effect of daily administration of L-arginine (200 mg/kg, i.p.), NTG (1 mg/kg, i.p.), or L-NAME (15 mg/kg, i.p.) for 7 d on oxidative stress markers in rats subjected to indomethacin-induced gastric ulcers

Group ^a	GSH ($\mu\text{mol/g}$ tissue)	Lipid peroxides (nmol/g tissue)
Control	3.65 ± 0.10	13.73 ± 0.63
Indomethacin (group with indomethacin-induced ulceration on day 0)	$2.22 \pm 0.07^*$	$34.17 \pm 0.57^*$
Indomethacin (group with indomethacin-induced ulceration on day 7)	$2.15 \pm 0.04^*$	$35.28 \pm 0.61^*$
Indomethacin + L-arginine	$3.39 \pm 0.11^{***}$	$18.34 \pm 0.74^{*****}$
Indomethacin + NTG	$3.04 \pm 0.05^{*****}$	$22.84 \pm 0.66^{*****}$
Indomethacin + L-NAME	$1.58 \pm 0.02^{*****}$	$55.49 \pm 1.48^{*****}$

^a Values given are means of 8-10 observations \pm S.E.M. ***** Significant difference with respect to the control group and groups treated with indomethacin on day 0 and 7, respectively, at $p < 0.05$ using ANOVA followed by Tukey-Kramer for multiple comparisons.

of indomethacin-induced ulcers but that L-NAME exacerbated mucosal damage. In addition, both L-arginine and NTG significantly restored the gastric NO level while L-NAME induced a further decrease in NO tissue content. As a consequence of the increased NO level, the complete recovery of gastric mucosa as a result of L-arginine or NTG probably depends on either drug's direct vasodilating action. This action increases mucosal blood flow and promotes angiogenesis, a key factor in ulcer healing (13).

Furthermore, NO not only improves blood flow and angiogenesis but also plays a role in stimulating mucus secretion, which is believed to constitute one of the primary levels of mucosal defense (28). Therefore, mucus secretion was assessed in the present study. However, treatment with indomethacin alone and with L-NAME was unexpectedly found to increase mucin in the ulcerated area. This interesting result agrees with the finding of Luo *et al.* (29), who found that mucus thickness at the ulcer margin increased profoundly after ulcer induction. This could be a positive biological feedback mechanism to protect the ulcer from further ulceration (20,29). Treatment with either L-arginine or NTG once daily for 7 d after ulcer induction clearly increased the mucus layer at the edges of the gastric mucosa. The increase in mucus production usually assists the healing process by protecting the ulcer crater against irritant stomach secretions, thereby enhancing the rate of the local healing process (12).

Since the mechanism of NSAID-induced gastric damage is generally believed to be related to inhibition of gastric PG generation (3), studying the effect of NO donors and inhibitors on the level of gastric PGs generated was crucial. A single dose of indomethacin induced a significant decrease in PGE₂ that reached 78.31 pg/mg protein after 4 h, a finding that agrees with several previous studies (3,25). However, 7 d after indomethacin injection the PGE₂ level was found to have significantly increased (30%) in comparison to the PGE₂ level in the control group. This finding agrees with a study by Luo *et al.* (29) that reported an increase in PGE₂ formation at the ulcer margin 7 d after ulcer induction in comparison to the control group.

Indeed, peptic ulcer healing is an active and complex process that includes the reconstruction of the mucosa by formation of granulation tissue at the ulcer base, formation of new blood vessels, and re-establishment of the glandular architecture (30). PGs generated particularly at the ulcer margin by COX-2 appear to play a crucial role in ulcer healing by triggering cell proliferation, promoting angiogenesis, and repairing mucosal injury (31). In contrast, PGs generated by COX-1 are constitutively expressed in intact gastric mucosa to regulate mucosal blood flow and epithelial secretions. Of interest is the fact that PGs generated from COX-1 suppress COX-2 activity in the GI tract. When the mucosa is exposed to potentially

damaging agents or when ulceration occurs, COX-2 is rapidly up-regulated. Therefore, higher amounts of PGE₂ are detected at the site of ulceration than in non-ulcerated mucosa (32,33). Thus, an important finding of the present study is that histopathological examination of the rats with ulcers revealed the presence of multiple sites of inflammatory cell infiltration in the base of the mucosal layer and lamina propria, providing a suitable inflammatory environment for COX-2 expression and consequently resulting in a significant increase in PGE₂ generation as was detected.

With regard to the effect of NO modulation on the elevated level of PGE₂, the current study revealed that treatment with either L-arginine or NTG for 7 d after ulcer induction inhibited the inflammatory signs associated with indomethacin to different degrees. Rats treated with L-arginine had a normal PGE₂ level, while those treated with NTG had a significant decrease in the elevated PGE₂ level. However, this level was still significantly higher than normal. In contrast, treatment with L-NAME further increased the PGE₂ level. These results can be explained by the inhibitory role of NO in the inflammation process (34). NO is an important modulator of leukocyte adherence to the vascular endothelium, a rate-controlling step in the inflammatory process, and using NO donors results in a reduction in myeloperoxidase activity (an indicator of the neutrophil count) and thus tissue injury (35). NO also appears to down-regulate the release of a number of inflammatory mediators from mast cells (36). Similarly, Calatayud *et al.* (37) found that transdermal NTG protected against indomethacin-induced ulceration by maintenance of mucosal blood flow and reduction of leukocyte endothelial cell rolling and adherence. In contrast, Barrachina *et al.* (34) found that NOS inhibitors enhanced inflammation by increasing leukocyte endothelium interactions.

Several studies have recognized the role of oxidative stress in the development of mucosal ulceration caused by NSAIDs. Therefore, the present study involved two potential oxidative stress markers, namely GSH and malondialdehyde (MDA). Indomethacin was found to induce a significant decrease in the gastric content of GSH along with a significant increase in gastric MDA content in both groups with indomethacin-induced ulceration on day 0 and 7 in comparison to gastric content of GSH and MDA in the control group. These findings might be attributed to the pro-oxidant activity of indomethacin, which initiates generation of ROS and thus interferes with the endogenous antioxidant systems of mucosal cells (38). The decreased concentration of GSH may also contribute to increased lipid peroxidation as the loss of this important cellular antioxidant will lead to the accumulation of ROS (39). Treatment with either L-arginine or NTG for 7 d after ulcer induction significantly increased gastric GSH content and decreased the MDA level, but these values did not

return to normal. In contrast, L-NAME caused a further reduction in GSH content and significant elevation in the MDA level in comparison to the GSH content and MDA level in the group with indomethacin-induced ulceration on day 7. These findings are in accordance with previous studies that investigated the protective role of NO during the induction of gastric ulcers. Kwiecien *et al.* (40) found that NO donors reduced gastric lesions and they found that this effect was accompanied by a fall in oxidative stress parameters. That said, NOS inhibitors have also been found to induce an increase in gastric mucosal lipid peroxidation (6).

In conclusion, L-arginine and NTG almost completely healed indomethacin-induced ulceration. Less healing by NTG than by L-arginine may be a result of the different doses. However, the advantages of L-arginine as a natural dietary supplement and immediate precursor of NO should not be ignored. Thus, the present study provides further evidence for the role of NO in gastric ulcer healing and it suggests an alternative path to treating the universal problem of NSAID-induced gastropathy.

Acknowledgements

The authors wish to thank Professor Adel B. Kholoussy (Department of Pathology, Faculty of Veterinary Medicine, Cairo University) for his help with the pathology portion of this work.

References

- Spechler SJ. Peptic ulcer disease and its complications. In: *Gastrointestinal and Liver Disease Pathophysiology/Diagnosis/Management* (Feldman M, Friedman LS, Sleisenger M, eds.). 7th ed., Saunders Company, Philadelphia, USA, 2002; pp. 747-781.
- Sivri B. Trends in peptic ulcer pharmacotherapy. *Fundam Clin Pharmacol.* 2004; 18:23-31.
- Santos CL, Souza MH, Gomes AS, Lemos HP, Santos AA, Cunha FQ, Wallace JL. Sildenafil prevents indomethacin-induced gastropathy in rats: Role of leukocyte adherence and gastric blood flow. *Br J Pharmacol.* 2005; 146:481-486.
- Petersson J, Phillipson M, Jansson EA, Patzak A, Lundberg JO, Holm L. Dietary nitrate increases gastric mucosal blood flow and mucosal defense. *Am J Physiol Gastrointest Liver Physiol.* 2007; 292:G718-G724.
- Gyires K. Gastric mucosal protection: From prostaglandins to gene-therapy. *Curr Med Chem.* 2005; 12:203-215.
- Hsu DZ, Liu MY. Involvement of nitric oxide in gastrin protection of epinephrine in endotoxin intoxication in rats. *Toxicology.* 2004; 204:203-208.
- Ma L, Wallace JL. Endothelial nitric oxide synthase modulates gastric ulcer healing in rats. *Am J Physiol Gastrointest Liver Physiol.* 2000; 279:G341-G346.
- Gürbüz V, Alican I, Berrak, Yegen C, Bozkurt A, Oktar B, Haklar G, Yüksel M, Kurtel H. Role of nitric oxide in indomethacin-induced gastric mucosal dysfunction in the rat. *Exp Physiol.* 1999; 84:319-332.
- Khattab MM, Gad MZ, Abdallah D. Protective role of nitric oxide in indomethacin-induced gastric ulceration by a mechanism independent on gastric acid secretion. *Pharmacol Res.* 2001; 43:463-467.
- Dengiz GO, Odabasoglu F, Halici Z, Suleyman H, Cadirci E, Bayir Y. Gastroprotective and antioxidant effects of amiodarone on indomethacin-induced gastric ulcers in rats. *Arch Pharm Res.* 2007; 30:1426-1434.
- Heeba GH, Hassan MK, Amin RS. Gastroprotective effect of simvastatin against indomethacin-induced gastric ulcer in rats: Role of nitric oxide and prostaglandins. *Eur J Pharmacol.* 2009; 607:188-193.
- Bhattacharya S, Banerjee D, Bauri AK, Chattopadhyay S, Bandyopadhyay SK. Healing property of piper betel phenol, allylpyrocatechol against indomethacin-induced stomach ulceration and mechanism of action. *World J Gastroenterol.* 2007; 13:3705-3713.
- Konturek SJ, Brzozowski T, Majka J, Pytko-Polonczyk J, Stachura J. Inhibition of nitric oxide synthase delays healing of chronic gastric ulcers. *Eur J Pharmacol.* 1993; 239:215-217.
- Sen S, Doger FK, Sen S, Aydin ON, Karul A, Dost T. The protection effect of nitroglycerin on gastrointestinal and renal side effects of lornoxicam in rats. *Eur J Pharmacol.* 2006; 41:191-197.
- Valcavi U, Caponi R, Brambilla A, Palmira M, Minoja F, Bernini F, Musanti R, Fumagalli R. Gastric antisecretory, antiulcer and cytoprotective properties of 9-hydroxy-19,20-bis-nor-prostanoic acid in experimental animals. *Arzneimittelforschung.* 1982; 32:657-663.
- Yamamoto O, Okada Y, Okabe S. Effects of a proton pump inhibitor, omeprazole, on gastric secretion and gastric and duodenal ulcers or erosions in rats. *Dig Dis Sci.* 1984; 29:394-401.
- Ellman M. A spectrophotometric method for determination of reduced glutathione in tissues. *Anal Biochem.* 1959; 74:214-226.
- Uchiyama M, Mihara M. Determination of malondialdehyde precursor in tissues by thiobarbituric acid test. *Anal Biochem.* 1978; 86:271-278.
- Miranda KM, Espey MG, Wink DA. A rapid, simple spectrophotometric method for simultaneous detection of nitrate and nitrite. *Nitric oxide.* 2001; 5:62-71.
- Ma L, Wang WP, Chow JY, Lam SK, Cho CH. The role of polyamines in gastric mucus synthesis inhibited by cigarette smoke or its extract. *Gut.* 2000; 47:170-177.
- Lowry OH, Rosebrough NJ, Farr AL, Randall RJ. Protein measurement with the folin phenol reagent. *J Biol Chem.* 1951; 64:95-102.
- Drury RA, Wallington EA. *Carlton's Histological Technique.* 5th ed., Oxford University Press, New York, USA, 1980; pp. 139-200.
- McManus JFA. Histological demonstration of mucin after periodic acid. *Nature.* 1946; 158:202.
- Ilahi M, Khan J, Inayat Q, Abidi TS. Histological changes in parts of foregut of rat after indomethacin administration. *J Ayub Med Coll Abbottabad.* 2006; 18:29-34.
- Banerjee D, Bauri AK, Guha RK, Bandyopadhyay SK, Chattopadhyay S. Healing properties of malabaricone B and malabaricone C against indomethacin-induced gastric ulceration and mechanism of action. *Eur J Pharmacol.* 2008; 578:300-312.
- Bhattacharya S, Chaudhuri SR, Chattopadhyay S,

- Bandyopadhyay SK. Healing properties of some indian medicinal plants against indomethacin induced gastric ulceration of rats. *J Clin Biochem Nutr.* 2007; 41:106-114.
27. Slomiany BL, Piotrowski J, Slomiany A. Endothelin-1, interleukin-4 and nitric oxide synthase modulators of gastric mucosal injury by indomethacin: Effect of antiulcer agents. *J Physiol Pharmacol.* 1999; 50:197-210.
 28. Wallace JL, Ma L. Inflammatory mediators in gastrointestinal defense and injury. *Exp Biol Med (Maywood).* 2001; 226:1003-1015.
 29. Luo JC, Shin VY, Liu ES, So WH, Ye YN, Chang FY, Cho CH. Non-ulcerogenic doses of dexamethasone delays gastric ulcer healing in rats. *J Pharmacol Exp Ther.* 2003; 307:692-698.
 30. Perini RF, Ma L, Wallace JL. Mucosal repair and COX-2 inhibition. *Curr Pharm Des.* 2003; 9:2207-2211.
 31. Tatsuguchi A, Sakamoto C, Wada K, Akamatsu T, Tsukui T, Miyake K, Futagami S, Kishida T, Fukuda Y, Yamanaka N, Kobayashi M. Localisation of cyclooxygenase 1 and cyclooxygenase 2 in *Helicobacter pylori* related gastritis and gastric ulcer tissues in humans. *Gut.* 2000; 46:782-789.
 32. Lesch CA, Gilbertsen RB, Song Y, Dyer RD, Sehrier D, Kraus ER, Sanchez B, Guglietta A. Effect of novel anti-inflammatory compounds on healing of acetic acid-induced gastric ulcer in rats. *J Pharmacol Exp Ther.* 1998; 287:301-306.
 33. Poonam D, Vinay CS, Gautam P. Cyclo-oxygenase-2 expression and prostaglandin E2 production in experimental chronic gastric ulcer healing. *Eur J Pharmacol.* 2005; 519:277-284.
 34. Barrachina MD, Panes J, Esplugues JV. Role of nitric oxide in gastrointestinal inflammatory and ulcerative diseases: perspective for drugs and development. *Curr Pharm Des.* 2001; 7:31-48.
 35. Kubes P, Wallace JL. Nitric oxide as a mediator of gastrointestinal mucosal injury? – Say it ain't so. *Mediators Inflamm.* 1995; 4:397-405.
 36. Salvemini D, Masini E, Anggard E, Mannaioni PF, Vane J. Synthesis of nitric oxide-like factor from L-arginine by rat serosal mast cells: Stimulation of guanylate cyclase and inhibition of platelet aggregation. *Biochem Biophys Res Commun.* 1990; 169:596-601.
 37. Calatayud S, Sanz MJ, Canet A, Bello R, de Rojas FD, Esplugues JV. Mechanisms of gastroprotection by transdermal nitroglycerin in the rat. *Br J Pharmacol.* 1999; 127:1111-1118.
 38. Naito Y, Yoshikawa T, Yoshida N, Kondo M. Role of oxygen radical and lipid peroxidation in indomethacin-induced gastric mucosal injury. *Dig Dis Sci.* 1998; 43:30S-34S.
 39. Othman AI, El-Missiry MA, Amer MA. The protective action of melatonin on indomethacin-induced gastric and testicular oxidative stress in rats. *Redox Rep.* 2001; 6:173-177.
 40. Kwiecień S, Brzozowski T, Konturek PCh, Konturek SJ. The role of reactive oxygen species in action of nitric oxide-donors on stress-induced gastric mucosal lesions. *J Physiol Pharmacol.* 2002; 53:761-773.

(Received March 17, 2010; Revised April 6, 2010; Accepted April 15, 2010)

Original Article**Effect of trazodone and nefazodone on hepatic injury induced by carbon tetrachloride**Omar M. E. Abdel Salam^{1,2,*}, Amany A. Sleem¹, Nermeen Shafee³¹ Department of Pharmacology, National Research Centre, Cairo, Egypt;² Department of Toxicology, National Research Centre, Cairo, Egypt;³ Department of Pathology, National Research Centre, Cairo, Egypt.

ABSTRACT: The present study aimed to evaluate the effect of the serotonin antagonists and reuptake inhibitors trazodone and nefazodone on liver injury induced by treatment with carbon tetrachloride (CCl₄) in rats. Liver damage was induced in rats by oral administration of CCl₄ (2.8 mL/kg in olive oil). Nefazodone (5, 10, or 20 mg/kg), trazodone (5, 10, or 20 mg/kg), silymarin (25 mg/kg), or saline (control) was orally administered once daily in association with CCl₄ and for one week thereafter. Liver damage was assessed by determining serum enzyme activities and hepatic histopathology. In CCl₄-treated rats, treatment with trazodone (5, 10, 20 mg/kg), reduced serum alanine aminotransferase (ALT) levels by 24, 38.6, and 49.3%. Serum aspartate aminotransferase (AST) levels were decreased by 18.1, 37.9, and 42.2%, and alkaline phosphatase (ALP) levels decreased by 25.7, 32.6, and 39.7%, respectively. Nefazodone (5, 10, 20 mg/kg) in a dose-dependent manner reduced the elevation of ALT levels by 15.6, 36.5, and 45.9%, AST levels by 16.7, 17.3, and 43%, and ALP by 30.5, 37.5, and 42.9%, respectively. Silymarin treatment reduced the levels of ALT, AST, and ALP by 56.1-62.8, 56.0-64.0, and 50.1-58.2%, respectively. The administration of CCl₄ decreased levels of reduced glutathione in blood compared to the vehicle-treated group. In CCl₄-treated rats, reduced glutathione levels increased after trazodone in a dose-dependent manner. Reduced glutathione was increased by nefazodone at concentrations of 5 and 10 mg/kg, but not after 20 mg/kg nefazodone. Reduced glutathione levels were increased by the administration of silymarin to near normal values. The administration of CCl₄ resulted in a marked increase in nitric oxide levels in serum (the concentrations of nitrite/nitrate) as

compared to the control group. Treatment with trazodone or nefazodone caused a dose-dependent decrease in serum nitric oxide levels compared with the CCl₄ control group. Histopathological and histomorphometric examinations also indicated that CCl₄-induced liver injury was less severe in trazodone and nefazodone-treated groups than in the CCl₄ control groups. Metabolic perturbations caused by CCl₄ in the form of decreased intracellular protein and mucopolysaccharide content in hepatocytes were improved by treatment with trazodone and nefazodone. It is concluded that administration of serotonin antagonists and reuptake inhibitors trazodone and nefazodone is associated with a reduction in experimental liver injury induced by CCl₄.

Keywords: Trazodone, nefazodone, serotonin antagonists, liver injury, rats

1. Introduction

The effect of drugs acting on serotonin (5-HT) neurotransmission or serotonin modulators on liver function is of particular interest for several reasons. First, these drugs are widely prescribed for the pharmacotherapy of depression and accordingly their effect on liver in healthy patients and more importantly in patients with liver disease is of clear clinical significance. In patients with hepatitis C viral infection, these agents have been used for the treatment of depression especially that observed after treatment with interferon-alpha/ribavirin combination therapy (1,2). Second, serotonin has been linked to liver disease in man, where in patients with liver cirrhosis, a significant fall of serotonin concentration in sera and urine has been noted, which might contribute to development of the hyperdynamic state of circulation observed in this condition (3). In addition, alterations of the serotonin system have been implicated in the

*Address correspondence to:

Dr. Omar M. E. Abdel Salam, Department of Pharmacology, National Research Centre, Tahrir St., Dokki, Cairo, Egypt.
e-mail: omasalam@hotmail.com

pathogenesis of hepatic encephalopathy, a serious neuropsychiatric complication of chronic liver disease (4) and therapeutic approaches aiming at the normalization of serotonin turnover could be beneficial in the prevention and treatment of early neuropsychiatric symptoms of hepatic encephalopathy (5). Third, changes in levels of neuropeptides in the brain can have substantial effects on liver function. For example, intracisternal administration of thyrotropin-releasing hormone has been shown to protect the liver (6), while intracisternal injection of corticotropin releasing factor exacerbated hepatic injury induced by CCl₄ in rats (7). Consequently, increased central serotonergic activity could affect liver function. Fourth, serotonin appears to play an important role in liver regeneration (8-10).

Trazodone is a phenylpiperazine with complex pharmacological actions, possessing antidepressant, anxiolytic and hypnotic activities. Trazodone is primarily a serotonergic antidepressant, blocking the reuptake of 5-HT presynaptically, thereby, increasing its availability in the synapse (11,12). In the brain, this latter effect accounts for the alleviation of the symptoms of depression (13). It also blocks postsynaptic 5-HT₂ receptors leading to facilitated neurotransmission through 5-HT_{1A} receptors, which reduces anxiety levels (12). Nefazodone which is chemically related to trazodone is also a 5-HT₂ receptor antagonist and a reuptake inhibitor. It has a weak affinity for cholinergic and noradrenaline alpha 1-adrenergic receptors (12,14-16). In view of their mixed serotonin effects, these agents can be described as serotonin modulators. Both trazodone and nefazodone are also capable of inducing hepatotoxicity (17-20), with the result that nefazodone was withdrawn from the US market (21).

The aim of the present study was to examine whether trazodone and nefazodone would modulate the development of hepatic injury caused by CCl₄ in the rat. Hepatic injury was determined *via* liver enzymes and histological analysis of necrotic areas as well as histochemical investigation of intracellular protein and mucopolysaccharide content. The effect of trazodone and nefazodone on CCl₄-induced hepatic damage was compared to that of silymarin, a herbal remedy widely used for its hepatoprotective effects (22).

2. Materials and Methods

2.1. Animals

Sprague-Dawley rats of both sexes, weighing 120-130 g were used throughout the experiments and fed with standard laboratory chow and water *ad libitum*. All animal procedures were performed in accordance to the Institutional Ethics Committee and in accordance with the recommendations for the proper care and use of laboratory animals (NIH publication No. 85-23, revised 1985). The drug doses for rats used were based

upon the human dose after conversion to that of the rat according to Paget and Barnes conversion tables (23).

2.2. Drugs and chemicals

Carbon tetrachloride (BDH Chemicals, Poole, UK), silymarin (Sedico Pharmaceutical Co., Giza, Egypt), nefazodone hydrochloride (Bristol-Myers Squibb, Cairo, Egypt) and trazodone hydrochloride (Egyptian International Pharmaceutical Industries Co., Cairo, Egypt) were used. All drugs were dissolved in isotonic (0.9% NaCl) saline solution immediately before use.

2.3. CCl₄-induced hepatic injury

Two separate studies evaluated the effect of trazodone and nefazodone on CCl₄-induced hepatic damage. In each study rats were divided into 6 equal groups (6 rats each). Groups 1-5 received CCl₄ in olive oil (1:1, v/v) at a dose of 2.8 mL/kg through an orogastric tube. Starting on the first day of CCl₄ administration, rats were also treated with the test drug (trazodone or nefazodone) at doses of 5, 10, and 20 mg/kg, silymarin (25 mg/kg) or saline only (positive control, treated with CCl₄ and not receiving drugs) once daily orally and for one week thereafter. All treated rats were administered half the initial dose of CCl₄ (0.14 mL/100 g body weight) 3 days after the first administration of CCl₄ so as to maintain hepatic damage. In addition, a 6th group of rats (*n* = 6) received the vehicle (olive oil) at 2.8 mL/kg followed 3 days later by an additional dose of 1.4 mL/kg olive oil. Rats had free access to food and drinking water during the study. After 7 days of CCl₄ or olive oil administration, rats were killed under ether anaesthesia.

In a third study, the effect of the highest dose (20 mg/kg) of trazodone or nefazodone was examined on serum aminotransferases in normal rats (*n* = 6/group). Drugs were given once daily orally for one week.

2.4. Biochemical assessment

At the end of the experiments, blood samples were obtained from the retro-orbital vein plexuses, under ether anaesthesia. Alanine aminotransferase (ALT) and aspartate aminotransferase (AST) activities in serum were measured according to the Reitman-Frankel colorimetric transaminase procedure (24), whereas colorimetric determination of alkaline phosphatase (ALP) activity was done according to the method of Belfield and Goldberg (25), using commercially available kits (BioMérieux, Craponne, France). Blood reduced glutathione (GSH) level was estimated spectrophotometrically by the method of Beutler *et al.* (26) using a commercial kit (Biodiagnostic, Giza, Egypt). Glutathione levels were expressed as mg/dL. Nitric oxide estimated as nitrite/nitrate, was determined in serum according to the method of Miranda *et al.* (27). The level of total nitrite/nitrate in

serum samples was expressed in μM and was calculated using the standard curve constructed with the prepared serial dilutions of sodium nitrite.

2.5. Histological and histochemical studies

At the end of the treatment period, rats were killed, livers excised and fixed in 10% formalin saline. Sections were prepared and stained with haematoxylin and eosin stain (H&E) for histological examination. Livers of all animals were dissected immediately after death. The specimens were then fixed in 10% neutral-buffered formal saline for at least 72 h. All specimens were washed in tap water for half an hour and then dehydrated using increasing grades of alcohol, cleared in xylene and embedded in paraffin. Serial sections 6 μm thick were cut and stained with H&E for histopathological investigation (28). Protein (29) and mucopolysaccharide (30) staining were also performed. All sections were investigated using the light microscope. Further histopathological evaluation was done with morphometry. The percentage of liver tissue affected by necrosis and fibrosis (damaged area) were determined using a computer assisted automated image analyzer. The Qwin Leica image processing and analysis system (Cambridge, UK) was used for interactive automatic measurement of the percentage of damaged areas on slides stained with H&E by analyzing 15 random fields per slide.

The image analyzer was also used to evaluate the DNA content. The image analysis system automatically expresses the DNA content of each individual cell measured then gives the percentage of each cell out of the total number of cells examined. Also, it classifies the cells into 4 groups; diploid (2C), proliferating cells (3C), tetraploid (4C) and aneuploid cells (> 5C). The proliferating cells were further classified according to Lee *et al.* (31) into: (< 10%) low proliferating index, (10-20%) medium proliferating index, and (> 20%) high proliferating index.

2.6. Statistical analysis

All results are expressed as means \pm S.E. Multiple group comparisons were performed by one way ANOVA followed by Duncan test. $p < 0.05$ was considered statistically significant.

3. Results

3.1. Biochemical changes

In normal rats, trazodone or nefazodone administered at a dose of 20 mg/kg had no effect on serum ALT, AST, or ALP (Table 1). In rats treated with CCl_4 , the levels of ALT, AST, and ALP in plasma were markedly raised indicating the severity of hepatic injury and cholestasis

Table 1. Effect of trazodone and nefazodone on serum ALT, AST, and ALP in normal rats

Treatments	ALT (U/L)	AST (U/L)	ALP (U/L)
Vehicle	61.0 \pm 3.1	66.4 \pm 2.5	59.0 \pm 1.9
Vehicle + trazodone 20 mg/kg	57.4 \pm 1.5	55.8 \pm 2.1	53.3 \pm 3.1
Vehicle + nefazodone 20 mg/kg	55.4 \pm 3.4	57.2 \pm 1.7	50.3 \pm 2.4

Data are means \pm S.E.

caused by CCl_4 . Trazodone (5, 10, or 20 mg/kg) given at the time of CCl_4 administration caused a dose-dependent reduction of raised ALT by 24, 38.6, and 49.3%, AST by 18.1, 37.9, and 42.2%, and ALP levels by 25.79, 32.6, and 39.7%, respectively. Meanwhile, silymarin treatment reduced the levels of ALT, AST, and ALP by 62.8, 64.0, and 50.1%, respectively (Table 2). In CCl_4 -treated rats, glutathione level in blood was reduced by 40.9% compared with vehicle-treated control group (21.4 \pm 0.7 vs. 36.2 \pm 0.1 mg/dL). Reduced glutathione was increased by 19.6, 37.8, and 54.2% by trazodone administered at doses of 5, 10, and 20 mg/kg, respectively, compared with the CCl_4 -control group. Meanwhile, reduced glutathione increased after silymarin treatment by 62.1% compared with the CCl_4 -control group (Table 2). The administration of CCl_4 induced a significant increase in serum concentrations of nitric oxide (nitrite/nitrate). Treatment with trazodone significantly protected against the CCl_4 -induced elevation in nitric oxide level which decreased by 27.7, 45.6, and 52.6% after 5, 10, and 20 mg/kg trazodone, respectively, as compared to control CCl_4 . On the other hand, silymarin significantly lowered the raised nitric oxide level by 57.4% as compared to CCl_4 control group (Table 2).

Nefazodone administered to CCl_4 -treated rats at doses of 5, 10, or 20 mg/kg, reduced the elevation of ALT levels by 15.6, 36.5, and 45.9%, AST levels by 16.7, 17.3, and 43.0%, and ALP by 30.5, 37.5, and 42.9%, respectively. On the other hand, ALT, AST, and ALP decreased by 56.1, 56.0, and 58.2%, respectively, by treatment with silymarin. In CCl_4 -treated rats, glutathione level in blood was reduced compared with vehicle-treated control group (21.0 \pm 0.6 vs. 36.6 \pm 0.8 mg/dL). Reduced glutathione was increased to 30.9 \pm 0.8 and 29.95 \pm 1.3 mg/dL by nefazodone given at doses of 5 or 10 mg/kg, respectively (47.1% and 42.6% increase vs. CCl_4 control group). With nefazodone at 20 mg/kg, reduced glutathione levels were reduced again to 24.3 \pm 0.8 mg/dL (15.7% increase vs. CCl_4 control group). In contrast, reduced glutathione in blood increased by 66.2% after silymarin treatment compared with the CCl_4 -control group (34.9 \pm 0.6 vs. 21.0 \pm 0.6 mg/dL) (Table 3). Treatment with nefazodone at 10 or 20 mg/kg also resulted in a significant decrease of the CCl_4 -induced elevation in nitric oxide level by 27.5 and 54.0%, respectively, as compared to control CCl_4 . Nitric oxide level decreased by 61.2% after silymarin treatment compared to the CCl_4 control group (Table 3).

Table 2. Effect of trazodone on serum ALT, AST, ALP, nitric oxide (NO), blood GSH, and histological area of damage in carbon tetrachloride-treated rats

Treatment groups	ALT (U/L)	AST (U/L)	ALP (U/L)	NO (μ M)	GSH (mg/dL)	Area of damage (%)
Vehicle	52.0 \pm 6.0	57.2 \pm 4.8	60.2 \pm 3.6	53 \pm 3.2	36.2 \pm 0.1	0.21 \pm 0.1
CCl ₄ (control)	144.3 \pm 11.1 ^{a,c}	155.4 \pm 12.1 ^{a,c}	116.2 \pm 7.0 ^{a,c}	512 \pm 17.8 ^{a,c}	21.4 \pm 0.8 ^{a,c}	56.96 \pm 6.5 ^{a,c}
CCl ₄ + trazodone 5 mg/kg	109.7 \pm 5.5 ^{a,b,c} (-24.0%)	127.2 \pm 8.5 ^{a,b,c} (-18.1%)	86.3 \pm 6.2 ^{a,b,c} (-25.7%)	370 \pm 16.1 ^{a,b,c} (-27.7%)	25.6 \pm 0.5 ^{a,b,c} (19.6%)	47.76 \pm 1.4 ^{a,c} (-16.2%)
CCl ₄ + trazodone 10 mg/kg	88.6 \pm 4.9 ^{a,b,c} (-38.6%)	96.5 \pm 3.6 ^{a,b,c} (-37.9%)	78.3 \pm 6.1 ^{a,b,c} (-32.6%)	278.3 \pm 16.0 ^{a,b,c} (-45.6%)	29.5 \pm 0.6 ^{a,b,c} (37.8%)	34.87 \pm 3.9 ^{a,b,c} (-38.8%)
CCl ₄ + trazodone 20 mg/kg	73.1 \pm 4.3 ^{a,b,c} (-49.3%)	89.8 \pm 7.5 ^{a,b,c} (-42.2%)	70.1 \pm 6.7 ^b (-39.7%)	242.6 \pm 18.0 ^{a,b} (-52.6%)	33.0 \pm 0.7 ^{a,b} (54.2%)	17.10 \pm 2.0 ^{a,b,c} (-69.9%)
CCl ₄ + silymarin 25 mg/kg	53.6 \pm 2.4 ^b (-62.8%)	56.0 \pm 3.9 ^b (-64.0%)	58.0 \pm 3.6 ^b (-50.1%)	218.2 \pm 15.0 ^{a,b} (-57.4%)	34.7 \pm 0.1 ^{a,b} (62.1%)	10.90 \pm 1.3 ^{a,b} (-80.9%)

Data are means \pm S.E. Six rats were used for each group. The percent change from the CCl₄-control group is also shown in parenthesis. Data were analyzed by one way ANOVA and means of different groups were compared by Duncan's multiple range test. $p < 0.05$ was considered statistically significant. ^a $p < 0.05$ vs. vehicle control group. ^b $p < 0.05$ vs. CCl₄ control group. ^c $p < 0.05$ vs. silymarin-treated group. Serum ALT, AST, and NO levels were significantly less in CCl₄ + trazodone 10 mg/kg- and CCl₄ + trazodone 20 mg/kg-treated groups than CCl₄ + trazodone 5 mg/kg-treated group.

Table 3. Effect of nefazodone on serum ALT, AST, ALP, NO, blood GSH, and histological area of damage in carbon tetrachloride-treated rats

Treatment groups	ALT (U/L)	AST (U/L)	ALP (U/L)	NO (μ M)	GSH (mg/dL)	Area of damage (%)
Vehicle	58.4 \pm 3.9	62.2 \pm 6.1	51.0 \pm 4.3	58.0 \pm 2.6	36.6 \pm 0.8	0.16 \pm 0.2
CCl ₄ (control)	134.9 \pm 8.7 ^a	148.2 \pm 12.8 ^a	115.9 \pm 8.1 ^a	531.1 \pm 19.0 ^{a,b}	21.0 \pm 0.6 ^{a,b}	43.5 \pm 4.5 ^{a,b}
CCl ₄ + nefazodone 5 mg/kg	113.8 \pm 9.9 ^{a,b,c} (-15.6%)	123.4 \pm 4.1 ^{a,b,c} (-16.7%)	80.5 \pm 7.3 ^{a,b,c} (-30.5%)	503.9 \pm 24.5 ^{a,c} (-5.3%)	30.9 \pm 0.8 ^b (47.1%)	37.53 \pm 2.6 ^{a,c} (-13.7%)
CCl ₄ + nefazodone 10 mg/kg	85.6 \pm 6.3 ^{a,b,c} (-36.5%)	122.5 \pm 6.8 ^{a,b,c} (-17.3%)	72.2 \pm 6.3 ^{a,b,c} (-37.7%)	385.3 \pm 8.0 ^{a,b,c} (-27.5%)	29.95 \pm 1.3 ^{a,b} (42.6%)	24.5 \pm 3.0 ^{a,b,c} (-43.7%)
CCl ₄ + nefazodone 20 mg/kg	72.9 \pm 6.1 ^b (-45.9%)	84.4 \pm 5.1 ^{a,b,c} (-43.0%)	66.2 \pm 6.0 ^{a,b,c} (-42.9%)	244.0 \pm 15.5 ^{a,b} (-54.0%)	24.3 \pm 0.8 ^{a,c} (15.7%)	20.4 \pm 1.8 ^{a,b,c} (-53.1%)
CCl ₄ + silymarin 25 mg/kg	59.2 \pm 3.1 ^b (-56.1%)	65.2 \pm 6.2 ^b (-56.0%)	48.4 \pm 4.2 ^b (-58.2%)	206.0 \pm 8.3 ^{a,b} (-61.2%)	34.9 \pm 0.6 ^b (66.2%)	9.6 \pm 1.3 ^{a,b} (-77.9%)

Results are means \pm S.E. Six rats were used for each group. The percent change from the CCl₄-control group is also shown in parenthesis. Data were analyzed by one way ANOVA and means of different groups were compared by Duncan's multiple range test. $p < 0.05$ was considered statistically significant. ^a $p < 0.05$ vs. vehicle control group. ^b $p < 0.05$ vs. CCl₄ control group. ^c $p < 0.05$ vs. silymarin-treated group. Serum ALT and NO levels were significantly less in CCl₄ + trazodone 10 mg/kg- and CCl₄ + trazodone 20 mg/kg-treated groups than CCl₄ + trazodone 5 mg/kg-treated group. Serum AST level was significantly less in CCl₄ + trazodone 20 mg/kg-treated group than CCl₄ + trazodone 5 mg/kg-treated group.

3.2. Histological and histochemical results

Trazodone (20 mg/kg) or nefazodone (20 mg/kg) only treated rats showed a normal hepatic appearance (Figure 1). Treatment of rats with CCl₄ led to marked liver tissue damage in the form of complete distortion of the tissue architecture, a variable degree of vacuolar degeneration in many of the hepatocytes, cellular infiltration as well as hemorrhage (Figure 2A). Examination of sections from the liver of rats treated with trazodone and CCl₄ revealed that trazodone administered at 20 mg/kg had a protective effect against the damaging effect of CCl₄ (Figure 2D). With trazodone at 5 and 10 mg/kg, a variable degree of vacuolar degeneration was still present in many of the hepatocytes. Also, cellular infiltration was marked (Figures 2B and 2C). The highest dose caused regain of normal tissue architecture although mild cellular infiltration was noticed (Figure 2D). Histochemical

investigation for protein and mucopolysaccharide confirmed these results as only at the highest dose of trazodone did their levels return to normal (Figures 3 and 4).

Examination of liver sections from CCl₄ + nefazodone-treated rats revealed a dose-dependent improvement in hepatic architecture compared to the CCl₄ control group (Figure 5). In sections from rats treated with 5 mg/kg nefazodone, vacuolar degeneration and pyknotic nuclei were present in most of the hepatocytes. These findings became less prominent after 10 mg/kg nefazodone, while marked improvement of liver tissue except for slight dilatation and congestion of some blood sinusoids was observed with the highest dose (20 mg/kg) of nefazodone examined (Figure 5). Histochemical investigation for protein and mucopolysaccharide content in hepatocytes were in agreement with these findings (Figures 6 and 7). Sections taken from the liver of silymarin + CCl₄-

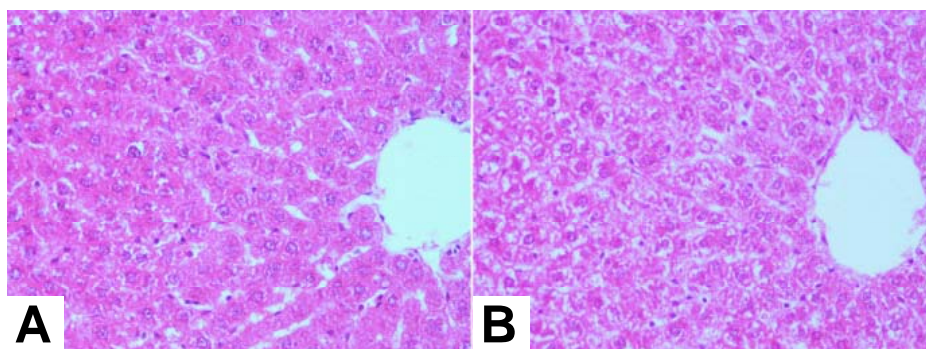


Figure 1. Typical liver tissue sections from rats treated with trazodone (20 mg/kg) (A) and nefazodone (20 mg/kg) (B). Each tissue stained with H&E showed normal hepatic architecture.

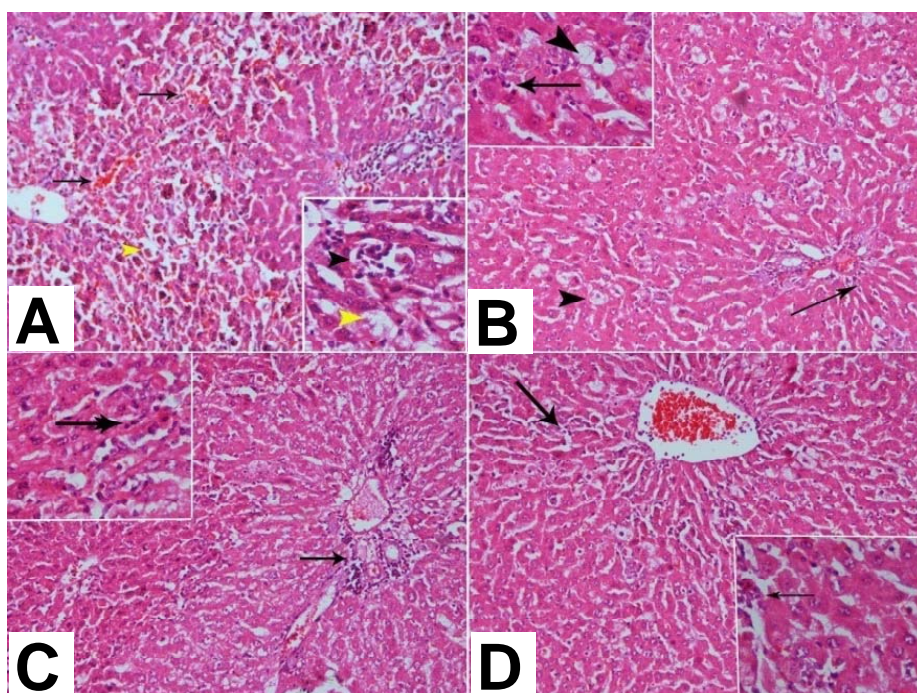


Figure 2. H&E stain of liver tissue sections from rats treated with CCl_4 and various doses of trazodone. (A) section of liver tissue from a rat treated with CCl_4 alone showing complete distortion of the liver architecture, variable degrees of vacuolar degeneration in many of the hepatocytes (yellow arrow head), cellular infiltration (black arrow head), and areas of hemorrhage (arrow) over the hepatic lobule. (B) section of liver tissue from a rat given CCl_4 and trazodone (5 mg/kg) showing that the liver tissue architecture was still distorted with mild degree of fibrosis and cellular infiltrate around the main vessels (arrow). The cellular infiltrate was also seen in the blood sinusoids. Many of the hepatocytes showed vacuolar degeneration (arrow head). (C) section of liver tissue from a rat treated with CCl_4 and trazodone (10 mg/kg) showing no vacuolar degeneration observed in hepatocytes, while marked cellular infiltrate was still present in the blood sinusoids and around the main blood vessels. (D) section of liver tissue from a rat that received CCl_4 and trazodone (20 mg/kg) showing regain of normal architecture of liver tissue, although diffuse cellular infiltrate was still observed in blood sinusoids (arrow). No fibrosis was noticed.

treated rats showed almost normal hepatic architecture (Figures 5-7).

3.3. Quantitative analysis of the area of damage

A significant increase in the percentage of damaged areas was observed in CCl_4 -treated rats when compared to normal animals. Morphometric analysis of liver sections showed that trazodone or nefazodone administration to CCl_4 -treated rats resulted in a dose-dependent decrease in damaged areas compared with the CCl_4 control group (Tables 2 and 3).

3.4. Quantitative analysis of the DNA content

Normal distribution of DNA content in the liver of the control group showed that 22.5% of the examined cells contained DNA at a value $< 1.5C$, 60.0% of the examined cells contained a diploid DNA value of $2C$, 16.66% of the examined cells contained a $3C$ DNA value (medium proliferating index) and 0.83% of the examined cells were at a $4C$ level. The group subjected to CCl_4 showed that 0.0% of the examined cells contained DNA ($< 1.5C$), which means a decrease in DNA content (hypoploidy) compared to the control group (Table 4).

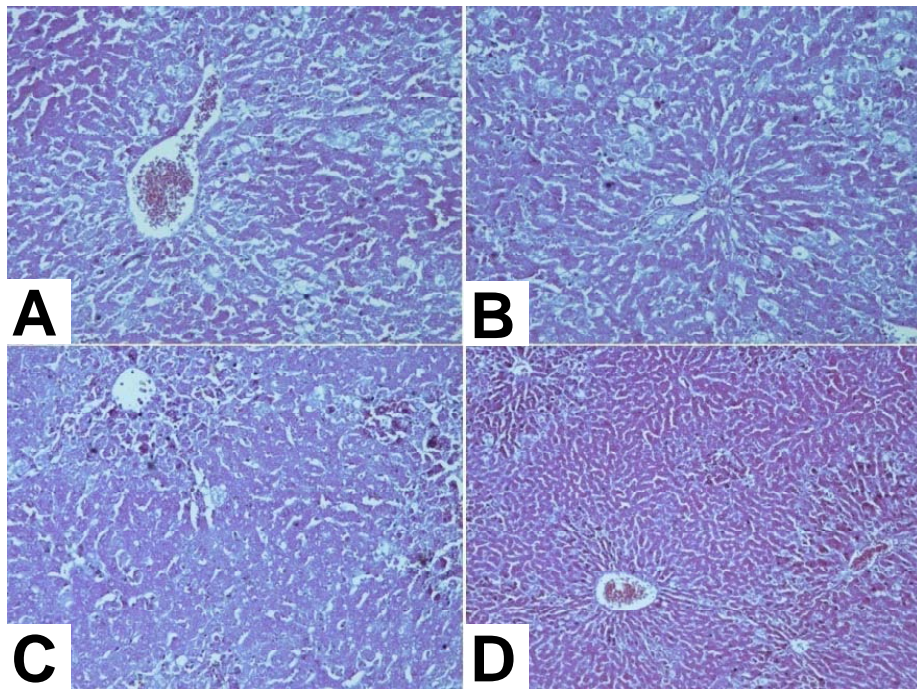


Figure 3. Protein stain of liver tissue sections from rats treated with CCl₄ and various doses of trazodone. (A) section of liver tissue from a rat treated with CCl₄ alone showing marked decrease in protein content of hepatocytes in a patchy manner over the hepatic lobule. (B) section of liver tissue from a rat that received CCl₄ and trazodone (5 mg/kg) showing that the protein content of liver tissue was still much less than normal compared with control levels. (C) section of liver tissue from a rat that received CCl₄ and trazodone (10 mg/kg) showing improvement of protein content level in hepatocytes, although the areas around the central vein still suffered from protein deficiency. (D) section of liver tissue from a rat that received CCl₄ and trazodone (20 mg/kg) showing normalization of protein content level.

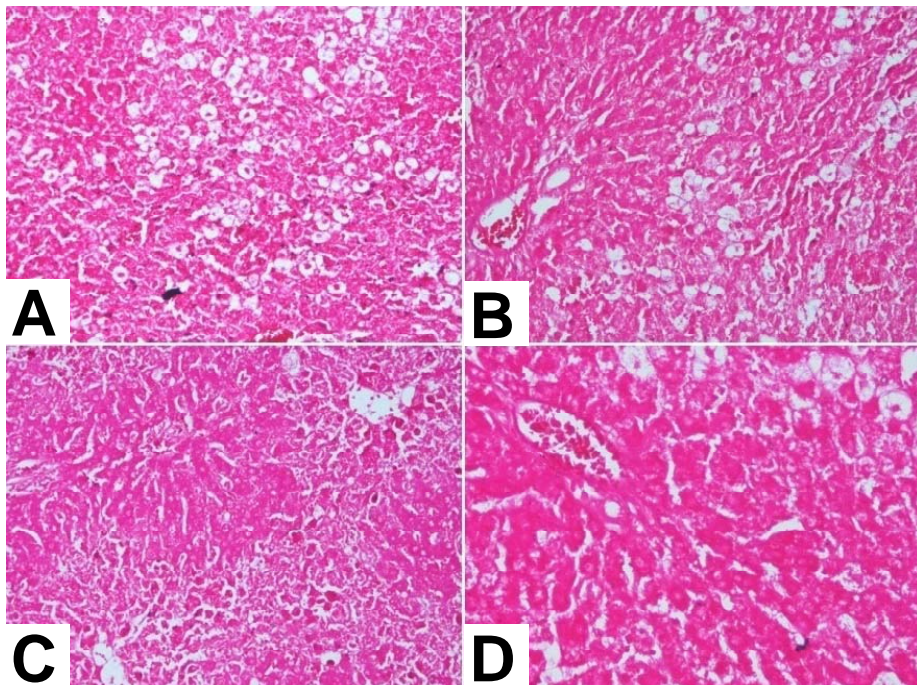


Figure 4. Mucopolysaccharide stain of liver tissue sections from rats treated with CCl₄ and various doses of trazodone. (A) section of liver tissue from a rat treated with CCl₄ alone showing marked decrease in mucopolysaccharide content over the hepatic lobule that appeared completely distorted. (B) section of liver tissue from a rat that received CCl₄ and trazodone (5 mg/kg) showing marked decrease in mucopolysaccharide content specially in cells suffering from vacuolar degeneration. (C) section of liver tissue from a rat given CCl₄ and trazodone (10 mg/kg) showing mild improvement of mucopolysaccharide content. (D) section of liver tissue from a rat treated with CCl₄ and trazodone (20 mg/kg) showing marked increase in mucopolysaccharide content level.

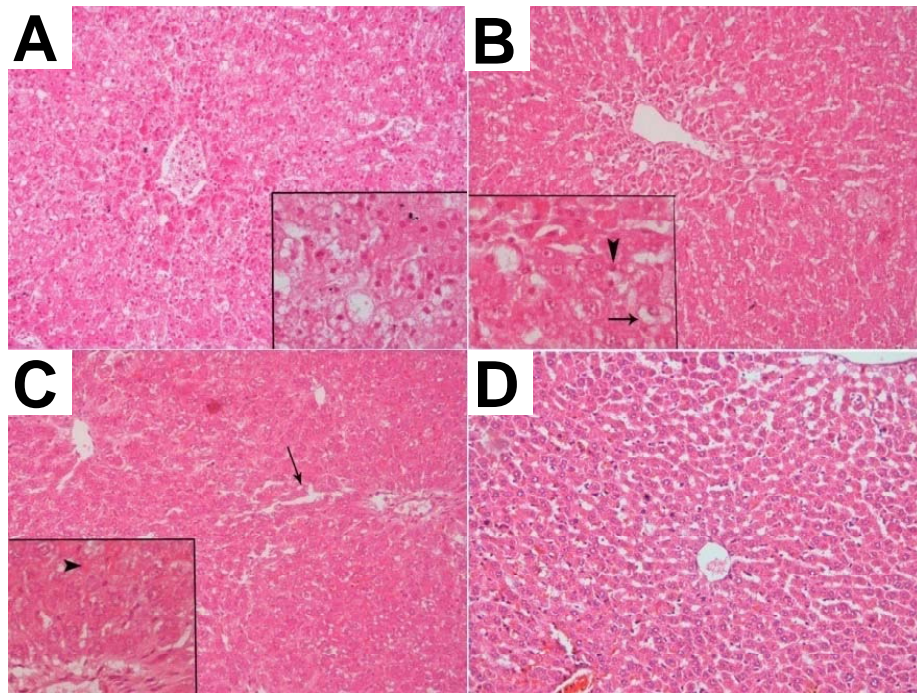


Figure 5. H&E stain of liver tissue sections from rats treated with CCl_4 and various doses of nefazodone. (A) section of liver tissue from a rat treated with CCl_4 and nefazodone (5 mg/kg) showing vacuolar degeneration of variable degrees and pyknotic nuclei in most of the cells. (B) section of liver tissue from a rat that received CCl_4 and nefazodone (10 mg/kg) showing noticeable improvement although there was cellular infiltrate around the central vein (arrow head) and vacuolar degeneration in a few cells. (C) section of liver tissue from a rat given CCl_4 and nefazodone (20 mg/kg) showing marked improvement of liver tissue except for slight dilatation of some blood sinusoids (arrow) and congestion in others (arrow head). (D) section of liver tissue from a rat treated with silymarin showing normal liver tissue architecture.

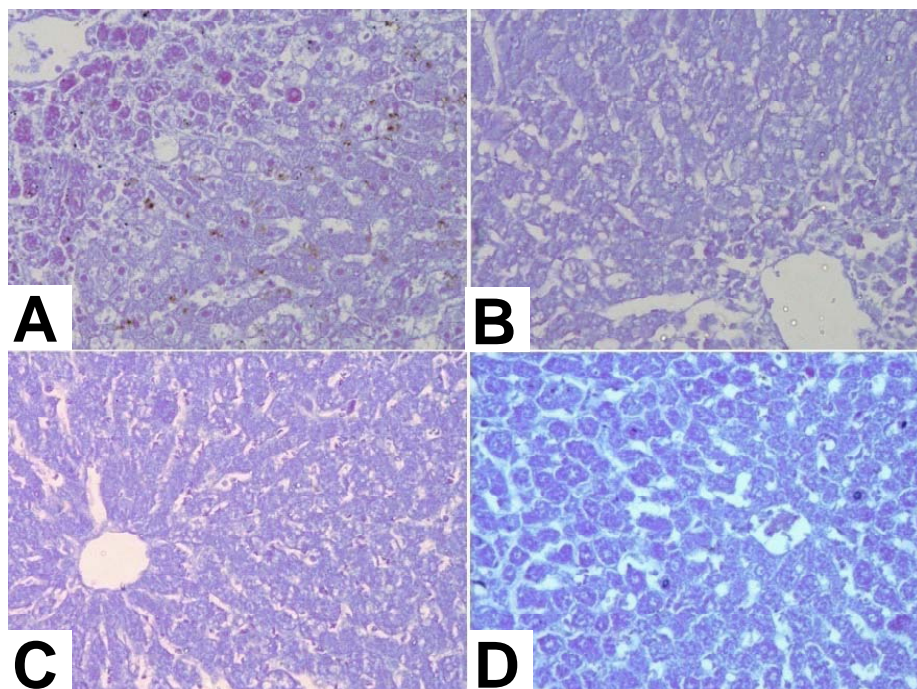


Figure 6. Protein stain of liver tissue sections from rats treated with CCl_4 and various doses of nefazodone. (A) section of liver tissue from a rat treated with CCl_4 and nefazodone (5 mg/kg) showing marked decrease in protein content in most of the hepatocytes mainly due to vacuolar degeneration. (B) section of liver tissue from a rat given CCl_4 and nefazodone (10 mg/kg) showing mild increase in protein content. (C) section of liver tissue from a rat that received CCl_4 and nefazodone (20 mg/kg) showing marked increase in protein content in most of the hepatocytes. (D) section of liver tissue from a rat treated with silymarin showing normal protein content of hepatocytes.

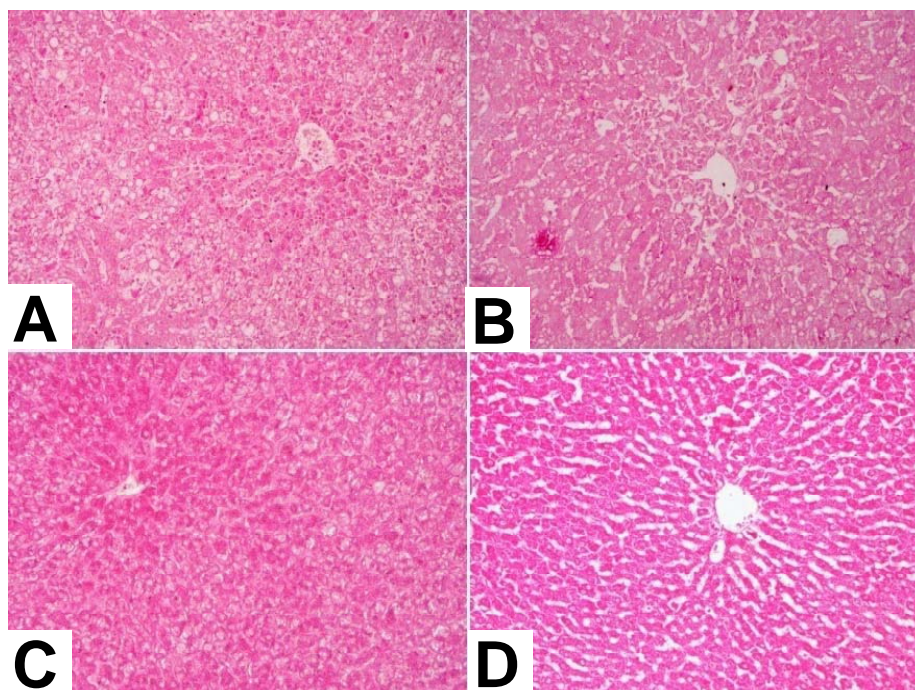


Figure 7. Mucopolysaccharide stain of liver tissue sections from rats treated with CCl₄ and various doses of nefazodone. (A) section of liver tissue from a rat treated with CCl₄ and nefazodone (5 mg/kg) showing that the mucopolysaccharide content in most of the hepatocytes was still very low compared to control levels. (B) section of liver tissue from a rat that received CCl₄ and nefazodone (10 mg/kg) showing mild increase in stain density. (C) section of liver tissue from a rat treated with CCl₄ and nefazodone (20 mg/kg) showing marked increase in mucopolysaccharide content. (D) section of liver tissue from a rat given silymarin showing normal mucopolysaccharide content of hepatocytes.

Table 4. Effect of trazodone and nefazodone on DNA content of hepatocytes (% cells) in carbon tetrachloride-treated rats

Treatment groups	< 1.5C	DNA index	1.5C-2.5C	DNA index	2.5C-3.5C	DNA index	3.5C-4.5C	DNA index	> 4.5C	DNA index
Vehicle	22.5 ± 0.13	0.63	60.0 ± 0.27	0.99	16.67 ± 0.08	1.46	0.83 ± 0.12	1.93	0	0
CCl ₄ (control)	0	0	1.96 ± 0.08 ^a	1.02	9.80 ± 0.30 ^a	1.57	25.5 ± 0.19 ^a	2.07	62.74 ± 0.34 ^a	2.89
CCl ₄ + trazodone 5 mg/kg	1.89 ± 0.15 ^{a,b}	0.06	0 ^{a,b}	0	1.89 ± 0.13 ^{a,b}	1.60	13.21 ± 0.21 ^{a,b}	2.09	83.02 ± 1.45 ^{a,b}	3.34
CCl ₄ + trazodone 10 mg/kg	0	0	3.57 ± 0.13 ^{a,b}	1.06	14.27 ± 0.12	1.62	25.0 ± 0.12	2.04	57.14 ± 1.17 ^a	3.09
CCl ₄ + trazodone 20 mg/kg	0	0	0 ^{a,b}	0	20.75 ± 0.13 ^b	1.57	24.53 ± 0.23 ^a	2.07	54.72 ± 1.04 ^a	3.02
CCl ₄ + nefazodone 5 mg/kg	2.9 ± 0.13 ^{a,b}	0.64	1.5 ± 0.01 ^a	1.91	7.24 ± 0.19 ^a	0.63	11.30 ± 0.23 ^{a,b}	1.32	77.06 ± 0.25 ^{a,b}	0.94
CCl ₄ + nefazodone 10 mg/kg	0	0	5.21 ± 0.11 ^{a,b}	1.79	18.75 ± 0.16 ^b	1.38	20.0 ± 0.14 ^a	0.63	56.04 ± 0.29 ^a	0.94
CCl ₄ + nefazodone 20 mg/kg	2.2 ± 0.08 ^{a,b}	0.64	0 ^{a,b}	0	26.87 ± 0.15 ^{a,b}	1.40	18.46 ± 0.06 ^{a,b}	1.35	52.47 ± 0.26 ^a	1.01

Data are means ± S.E. Data were analyzed by one way ANOVA and means of different groups were compared by Duncan's multiple range test. $p < 0.05$ was considered statistically significant. ^a $p < 0.05$ vs. vehicle control group. ^b $p < 0.05$ vs. CCl₄ control group.

3.4.1. Effect of trazodone

Treatment of rats with CCl₄ + trazodone 5 mg/kg showed that 1.88% of the examined hepatocytes contained DNA at < 1.5C, 1.96% of the examined cells contained a diploid DNA value of 2C, 9.8% of the examined cells contained a 3C DNA value (low proliferating index) and 25.49% of the examined cells were in the 4C area. After treatment with trazodone 10 mg/kg, 0.0% of

the examined cells contained DNA at < 1.5C, 3.57% contained a diploid DNA value of 2C, 14.28% of the examined cells contained a 3C DNA value (medium proliferating index) and 25% of the examined cells were in the 4C area. Following treatment with trazodone at 20 mg/kg, 0.0% of the examined cells contained DNA at < 1.5C, 0.0% of the examined cells contained a diploid DNA value of 2C, 20.75% of the examined cells contained a 3C DNA value (high proliferating

index) and 24.52% of the examined cells were in the 4C area. These results indicated that treatment with 5, 10, and 20 mg/kg trazodone resulted in a low, medium and high proliferating index, respectively, while the group treated with only CCl₄ showed decreased DNA values (hypoploidy) (Table 4).

3.4.2. Effect of nefazodone

After treatment with CCl₄ along with 5 mg/kg nefazodone, 2.9% of the examined hepatocytes contained DNA that was < 1.5C, 1.5% of the examined cells contained diploid DNA value of 2C, 7.24% of the examined cells contained DNA of a 3C value (low proliferating index) and 11.30% of the examined cells were in the 4C area. The group treated with CCl₄ + nefazodone 10 mg/kg showed that 0.0% of the examined cells contained DNA at < 1.5C, 5.21% contained a diploid DNA value of 2C, 18.75% of the examined cells contained a 3C DNA value (medium proliferating index), and 20% of the examined cells were in the 4C area. Following treatment with CCl₄ + nefazodone 20 mg/kg, 2.2% of the examined cells contained DNA at < 1.5C, 0.0% of the examined cells contained diploid DNA value of 2C, 26.87% of the examined cells contained a DNA value of 3C (high proliferating index) and 18.46% of the examined cells were in the 4C area. Thus treatment with nefazodone resulted in a dose-dependent increase in proliferating index in contrast to the CCl₄ control group that exhibited decreased DNA values (hypoploidy) (Table 4).

4. Discussion and Conclusion

The present study provided evidence that in the CCl₄ model of hepatic toxicity, the systemic administration of nefazodone or trazodone, two drugs that are in use in pharmacotherapy of depression, was associated with a decrease in the extent of hepatic damage. In CCl₄-treated rats, the serum levels of hepatocellular enzymes ALT and AST decreased after the administration of either drug in a dose-dependent fashion, which is an indication of improved liver function and preserved liver architecture in the face of the toxic insult to the liver. Plasma levels of alkaline phosphatase, a cell wall enzyme induced by stagnation of bile flow, also showed a marked and significant decrease. Histopathological and histochemical investigations were in agreement with the biochemical findings and indicated that cellular perturbations evoked by the hepatotoxin in the form of decreased protein and mucopolysaccharide content in hepatocytes were ameliorated by either drug. Thus in circumstances of acute toxic insult to the liver, these two drugs did not exacerbate liver injury, but in fact lessened the development of hepatocellular injury. These observations might be unexpected in view of the ability of the two drugs to cause hepatotoxicity

in humans, that appeared to be more evident and more serious in the case of nefazodone, leading to its withdrawal from the US market in 2004 (21).

Both trazodone and nefazodone enhance serotonin synaptic transmission by blocking postsynaptic 5-HT₂ receptors and by inhibiting the reuptake of 5-HT (11,12,14-16). In the brain the increase in serotonergic neuronal activity is thought to have a major role in the alleviation of symptoms of depression (13). Most serotonin (95%), however, is found in the gut in the mucosal enterochromaffin cells and within the enteric nervous system, where it is involved in the control of smooth muscle tone and motility (32). Serotonin is also stored in platelets and it is this aspect of serotonin which has been implicated in liver regeneration (9,10), but also in aggravation of liver injury (33,34).

Selective serotonin reuptake inhibitors as well as trazodone significantly reduce the concentration of 5-HT in platelets and inhibit platelet aggregation (35-38). This is one mechanism which might underlie the propensity of these drugs to cause gastrointestinal bleeding events alone or especially in combination with NSAIDs and aspirin (39,40) and also a mechanism which is likely to explain their cardiovascular benefit (35). Since these drugs reduce platelet serotonin, then a possible explanation for their beneficial effect upon experimental liver injury may be by lessening the vasoconstrictor effect of platelet-derived serotonin in the hepatic microcirculation. Studies have shown that serotonin provokes constriction of sinusoids and decreased sinusoidal and central venous perfusion after endoport application (41). Alternatively, the inhibition of the serotonin transporter by these agents (42) will likely result in increased extracellular serotonin. In mucosal preparations of the rat ileum, blockade of the serotonin transporter mechanism by fluoxetine increased both the stimulated serotonin release as well as background levels of 5-HT in the mucosa (43). Serotonin might then act in a paracrine way by binding to presynaptic 5-HT₄ receptors to stimulate the release of acetylcholine and calcitonin gene-related peptide release from nerve terminals between the submucosal intrinsic primary afferent neurons and adjacent interneurons (44) or to affect hepatic stellate cell functions, the principal cell involved in liver fibrogenesis. Hepatic stellate cells express 5-HT receptors and the serotonin antagonist ketanserin was capable of suppressing the proliferation of hepatic stellate cells as well as increasing their rate of apoptosis (45). *In vitro*, serotonin acted as a potent hepatocyte mitogen and induced DNA synthesis in primary cultures of rat hepatocytes (8). Serotonin is also involved in liver regeneration induced by estrogen in rats (10). Inhibitors of serotonin reuptake might also alleviate hepatic injury by preventing metabolic derangement due to CCl₄. In the present study, histochemical investigations revealed that the decrease in intracellular protein and mucopolysaccharide

content in hepatocytes evoked by CCl_4 was reduced by treatment with trazodone and nefazodone. Indeed, these agents appear to have significant effects on glucose regulation and hepatic glycogen distribution (46,47).

Glutathione (GSH) is an intracellular tripeptide (glycyl-glutamic acid-cysteine) common in all tissues, that provides a major antioxidant defense mechanism and which is important in protecting the liver against toxic injury (48). In the present study, blood reduced glutathione was significantly decreased in CCl_4 -treated rats. A dose-dependent increase in reduced glutathione was registered after treatment with trazodone. It was noted, however, that after treatment with nefazodone even at the highest dose examined *i.e.*, 20 mg/kg, blood glutathione did not show a further decrease beyond that caused by the toxic agent alone. Moreover, blood glutathione was increased by the lower doses of the drug which did not substantially reduce hepatic damage, thereby indicating in this case that the protective effect is unrelated to glutathione levels in blood. This, however, does not exclude the possibility that toxicity reported in many clinical instances with higher doses of the drug (19) might be caused by depletion of liver glutathione.

Nitric oxide production can be estimated from determining the concentrations of nitrite and nitrate end products (27). Nitric oxide is generated by inflammatory cytokines due to the action of inducible nitric oxide (iNOS) and iNOS overexpression was observed after the administration of CCl_4 (49,50). In the present study, nitrite/nitrate concentration in serum was markedly raised in CCl_4 -treated rats, in accordance with other studies (51). Treatment with trazodone or nefazodone significantly protected against the CCl_4 -induced increase in serum nitric oxide level, possibly due to a decrease in the inflammatory response caused by the drugs.

Serotonin antagonists and reuptake inhibitors such as trazodone and nefazodone might also alleviate hepatic injury *via* central mechanisms such as enhanced serotonergic neurotransmission or through vagal-mediated mechanisms. Brain neuropeptides have been shown to modulate liver injury. For example, the intracisternal administration of thyrotropin-releasing hormone stimulated hepatic DNA synthesis (52), enhanced liver blood flow (53) and inhibited hepatocellular necrosis and the elevation of serum alanine aminotransferase level induced by CCl_4 (6). This latter effect was abolished by hepatic branch vagotomy, atropine, and indomethacin and also by the nitric synthase inhibitor N(G)-nitro-L-arginine methyl ester (6). In contrast, intracisternal injection of corticotropin releasing factor was found to exacerbate the development of CCl_4 -induced acute liver injury. This effect was mediated through the sympathetic-noradrenergic nervous systems (7). There is also evidence to suggest that increased serotonin content

in cerebral cortex and brain stem induced hepatic proliferation through sympathetic stimulation (54). The present study showed that treatment with CCl_4 resulted in 0.0% of the examined cells containing DNA were $< 1.5C$, which meant a decrease in DNA content (hypoploidy) compared to normal rats. Meanwhile, treatment with either trazodone or nefazodone resulted in a dose-dependent increase in proliferating index in contrast to the CCl_4 control group that exhibited decreased DNA values. In a previous study, it was demonstrated that fluoxetine, a prototype selective serotonin reuptake inhibitor, led to the amelioration of liver injury caused by CCl_4 in the rat (55), suggesting a common mechanism(s) for drugs potentiating serotonergic neurotransmission in protecting against liver injury.

Cases of hepatotoxic reactions due to trazodone and nefazodone have been reported in the literature (17-19). Hepatotoxicity has also been observed after treatment with monoamine oxidase inhibitors and tricyclic antidepressants and among the serotonin reuptake inhibitors, paroxetine has the largest number of cases of hepatotoxicity recorded (56,57). In other instances *e.g.* in alcohol-dependent subjects (58) or in the case of chronic hepatitis C with interferon/ribavirin therapy (2), nefazodone was not associated with hepatotoxicity. In the past few years, there have been attempts at explaining nefazodone hepatotoxicity. *In vitro*, nefazodone (and not trazodone) inhibited mitochondrial respiration in isolated rat liver mitochondria and in intact HepG2 cells. The target was mitochondrial complex I (59). Inhibition of bile acid transport may be another mechanism of nefazodone-induced hepatotoxic reactions, an effect which is not shared by trazodone (60). It has been suggested that the low oral bioavailability of nefazodone of $\sim 20\%$ and short half-life of ~ 1 h due to extensive first pass metabolism mediated by P4503A4 in the small intestine and liver and the resultant high daily dose (200-400 mg/day) increase the total body burden to reactive metabolite exposure which might exceed a threshold needed to cause toxicity (61). The optimum therapeutic dosage of nefazodone appears to be between 300 and 600 mg/day (14) and doses in the range of 200-600 mg/day were associated with acute hepatic reactions (19). Liver toxicity with markedly elevated serum transaminases have also been observed following a dose of 150 mg nefazodone twice daily for 20 weeks in an alcoholic patient. Symptoms resolved completely after discontinuation of nefazodone (18). Nefazodone is extensively metabolized in the liver and plasma concentrations of the drug are increased in severe hepatic impairment and in the elderly, especially in elderly females (15), which requires lowering the dose in patients with liver disease. Notably, in most instances of nefazodone or trazodone hepatotoxicity, drugs were administered for a prolonged time (6-12 months)

before the onset of symptoms (17-20). The present study, however, examined only the short term effect of trazodone or nefazodone administration.

Trazodone and nefazodone undergo bioactivation in human liver microsomes to a reactive quinone-imine and an epoxide intermediate, and these react with glutathione, which might represent a rate-limiting step in the initiation of trazodone- or nefazodone-mediated hepatotoxicity (62,63). Toxicity due to nefazodone or trazodone can thus be interpreted in terms of as an imbalance between a detrimental affect of the drug itself on hepatocytes and the beneficial effect of increased serotonin levels in the periphery and centrally. This is due to overwhelming metabolites and exceeding the capacity of the liver to deal with *e.g.* an increased rate of liver regeneration. With lower doses the beneficial effects maintaining hepatic integrity and promoting regeneration are likely to prevail.

In summary, the present study has shown that both nefazodone and trazodone, two drugs which block postsynaptic 5-HT₂ receptors and inhibit the reuptake of 5-HT, lessened hepatocellular injury in rats caused by administration of CCl₄. The involvement of enhanced central serotonergic neurotransmission or peripheral serotonergic mediated mechanisms is suggested.

References

- Gleason OC, Yates WR, Isbell MD, Philipsen MA. An open-label trial of citalopram for major depression in patients with hepatitis C. *J Clin Psychiatry*. 2002; 63:194-198.
- Schäfer M, Schmidt F, Amann B, Schlösser S, Loeschke K, Grunze H. Adding low-dose antidepressants to interferon alpha treatment for chronic hepatitis C improved psychiatric tolerability in a patient with schizoaffective psychosis. *Neuropsychobiology*. 2000; 42 (Suppl 1):43-45.
- Culafic D, Dukic V, Mirkovic D, Karamarkovic A. Hyperdynamic circulation and serotonin levels in patients with liver cirrhosis. *Jugoslav Med Biochem*. 2004; 23:31-35.
- Albrecht J, Jones EA. Hepatic encephalopathy: molecular mechanisms underlying the clinical syndrome. *J Neurol Sci*. 1999; 170:138-146.
- Lozeva V, Montgomery JA, Tuomisto L, Rocheleau B, Pannunzio M, Huet PM, Butterworth RF. Increased brain serotonin turnover correlates with the degree of shunting and hyperammonemia in rats following variable portal vein stenosis. *J Hepatol*. 2004; 40:742-748.
- Sato Y, Yoneda M, Nakamura K, Makino I, Terano A. Protective effect of central thyrotropin-releasing hormone on carbon tetrachloride-induced acute hepatocellular necrosis in rats. *J Hepatol*. 2003; 39:47-54.
- Shiro Y, Yoneda M, Nakamura K, Makino I. Effect of central corticotropin-releasing factor on carbon tetrachloride-induced acute liver injury in rats. *Am J Physiol*. 1999; 276:G622-G628.
- Balasubramanian S, Paulose CS. Induction of DNA synthesis in primary cultures of rat hepatocytes by serotonin: Possible involvement of serotonin S₂ receptor. *Hepatology*. 1998; 27:62-66.
- Lesurtel M, Graf R, Aleil B, Walther DJ, Tian Y, Jochum W, Gachet C, Bader M, Clavien PA. Platelet-derived serotonin mediates liver regeneration. *Science*. 2006; 312:104-107.
- Kitagawa T, Yokoyama Y, Kokuryo T, Kawai T, Watanabe K, Kawai K, Nagino M. Estrogen promotes hepatic regeneration *via* activating serotonin signal. *Shock*. 2009; 31:615-620.
- Haria M, Fitton A, McTavish D. Trazodone: A review of its pharmacology, therapeutic use in depression and therapeutic potential in other disorders. *Drugs Aging*. 1994; 4:331-355.
- Gibbons SS. Antidepressants. In: *Pharmacology for the Primary Care Provider* (Edmunds MW, Mayhew MS, eds.). Mosby INC, St. Louis, MO, USA, 2000; pp. 602-620.
- Vaswani M, Linda FK, Ramesh S. Role of selective serotonin reuptake inhibitors in psychiatric disorders: A comprehensive review. *Prog Neuropsychopharmacol Biol Psychiatry*. 2003; 27:85-102.
- Davis R, Whittington R, Bryson HM. Nefazodone. A review of its pharmacology and clinical efficacy in the management of major depression. *Drugs*. 1997; 53:608-636.
- Greene DS, Barbhuiya RH. Clinical pharmacokinetics of nefazodone. *Clin Pharmacokinet*. 1997; 33:260-275.
- Lader MH. Tolerability and safety: Essentials in antidepressant pharmacotherapy. *J Clin Psychiatry*. 1996; 57 (Suppl 2):39-44.
- Fernandes NF, Martin RR, Schenker S. Trazodone-induced hepatotoxicity: A case report with comments on drug-induced hepatotoxicity. *Am J Gastroenterol*. 2000; 95:532-535.
- Eloubeidi MA, Gaede JT, Swaim MW. Reversible nefazodone-induced liver failure. *Dig Dis Sci*. 2000; 45:1036-1038.
- Stewart DE. Hepatic adverse reactions associated with nefazodone. *Can J Psychiatry*. 2002; 47:375-377.
- Beck PL, Bridges RJ, Demetrick DJ, Kelly JK, Lee SS. Chronic active hepatitis associated with trazodone therapy. *Ann Intern Med*. 1993; 118:791-792.
- Choi S. Nefazodone (Serzone) withdrawn because of hepatotoxicity. *CMAJ*. 2003; 169:1187.
- Flora K, Hahn M, Rosen H, Benner K. Milk thistle (*Silybum marianum*) for the therapy of liver disease. *Am J Gastroenterol*. 1998; 93:139-143.
- Paget GE, Barnes JM. Toxicity tests. In: *Evaluation of Drug Activities Pharmacometrics* (Laurence DR, Bacharach AL, eds.). Academic Press, London, UK, 1964; pp. 1-135.
- Crowley LV. The Reitman-Frankel colorimetric transaminase procedure in suspected myocardial infarction. *Clin Chem*. 1967; 13:482-487.
- Belfield A, Goldberg DM. Revised assay for serum phenyl phosphatase activity using 4-amino-antipyrine. *Enzyme*. 1971; 12:561-573.
- Beutler E, Duron O, Kelly BM. Improved method for the determination of blood glutathione. *J Lab Clin Med*. 1963; 61:882-888.
- Miranda KM, Espey MG, Wink DA. A rapid, simple spectrophotometric method for simultaneous detection of nitrate and nitrite. *Nitric Oxide*. 2001; 5:62-71.
- Drury RAB, Walligton EA. *Carlton's Histological Techniques*. 5th ed., Oxford University Press, New York,

- NY, USA, 1980; p. 206.
29. McManus JF, Cason JE. Carbohydrate histochemistry studied by acetylation techniques. *J Exp Med.* 1950; 91:651-654.
 30. Mazia D, Brewer PA, Alfert M. The cytochemical staining and measurement of protein with mercuric bromophenol blue. *Biol Bull.* 1953; 104:57-67.
 31. Lee KH, Lee JS, Lee JH, Kim SW, Suh C, Kim WK, Kim SH, Min YI, Kim BS, Park KC, Lee MS, Sun HS. Prognostic value of DNA flow cytometry in stomach cancer: A 5-year prospective study. *Br J Cancer.* 1999; 79:1727-1735.
 32. Beattie DT, Smith JA. Serotonin pharmacology in the gastrointestinal tract: A review. *Naunyn Schmiedeberg Arch Pharmacol.* 2008; 377:181-203.
 33. Murata R, Hamada N, Nakamura N, Kobayashi A, Fukueda M, Taira A, Sakata R. Serotonin activity and liver dysfunction following hepatic ischemia and reperfusion. *In Vivo.* 2003; 17:567-572.
 34. Lang PA, Contaldo C, Georgiev P, *et al.* Aggravation of viral hepatitis by platelet-derived serotonin. *Nat Med.* 2008; 14:756-761.
 35. Maurer-Spurej E, Pittendreigh C, Solomons K. The influence of selective serotonin reuptake inhibitors on human platelet serotonin. *Thromb Haemost.* 2004; 91:119-128.
 36. Healy D, Carney PA, Leonard BE. Biochemical correlates of antidepressant response. Results of a trazodone versus amitriptyline trial. *Psychopathology.* 1984; 17 (Suppl 2):82-87.
 37. McCloskey DJ, Postolache TT, Vittone BJ, Nghiem KL, Monsale JL, Wesley RA, Rick ME. Selective serotonin reuptake inhibitors: Measurement of effect on platelet function. *Transl Res.* 2008; 151:168-172.
 38. Abdelmalik N, Ruhé HG, Barwari K, van den Dool EJ, Meijers JC, Middeldorp S, Büller HR, Schene AH, Kamphuisen PW. Effect of the selective serotonin reuptake inhibitor paroxetine on platelet function is modified by a SLC6A4 serotonin transporter polymorphism. *J Thromb Haemost.* 2008; 6:2168-2174.
 39. de Abajo FJ, Rodriguez LA, Montero D. Association between selective serotonin reuptake inhibitors and upper gastrointestinal bleeding: Population based case-control study. *BMJ.* 1999; 319:1106-1109.
 40. Wessinger S, Kaplan M, Choi L, Williams M, Lau C, Sharp L, Crowell MD, Keshavarzian A, Jones MP. Increased use of selective serotonin reuptake inhibitors in patients admitted with gastrointestinal haemorrhage: A multicentre retrospective analysis. *Aliment Pharmacol Ther.* 2006; 23:937-944.
 41. Reilly FD, Cilento EV, McCuskey RS. Hepatic microvascular regulatory mechanisms. V. Effects of lodoxamide tromethamine or phentolamine-HCl on vascular responses elicited by serotonin. *Microcirc Endothelium Lymphatics.* 1984; 1:671-689.
 42. Owens MJ, Ieni JR, Knight DL, Winders K, Nemeroff CB. The serotonergic antidepressant nefazodone inhibits the serotonin transporter: *In vivo* and *ex vivo* studies. *Life Sci.* 1995; 57:PL373-PL380.
 43. Bertrand PP, Hu X, Mach J, Bertrand RL. Serotonin (5-HT) release and uptake measured by real-time electrochemical techniques in the rat ileum. *Am J Physiol Gastrointest Liver Physiol.* 2008; 295:G1228-G1236.
 44. Gershon MD, Tack J. The serotonin signaling system: From basic understanding to drug development for functional GI disorders. *Gastroenterology.* 2007; 132:397-414.
 45. Ruddell RG, Oakley F, Hussain Z, Yeung I, Bryan-Lluka LJ, Ramm GA, Mann DA. A role for serotonin (5-HT) in hepatic stellate cell function and liver fibrosis. *Am J Pathol.* 2006; 169:861-876.
 46. Moore MC, DiCostanzo CA, Dardevet D, Lautz M, Farmer B, Neal DW, Cherrington AD. Portal infusion of a selective serotonin reuptake inhibitor enhances hepatic glucose disposal in conscious dogs. *Am J Physiol Endocrinol Metab.* 2004; 287:E1057-E1063.
 47. An Z, Moore MC, Winnick JJ, Farmer B, Neal DW, Lautz M, Smith M, Rodewald T, Cherrington AD. Portal infusion of escitalopram enhances hepatic glucose disposal in conscious dogs. *Eur J Pharmacol.* 2009; 607:251-257.
 48. Cnubben NHP, Rietjens IMCM, Wortelboer H, van Zanden J, van Bladeren PJ. The interplay of glutathione-related processes in antioxidant defense. *Environ Toxicol Pharmacol.* 2001; 10:141-152.
 49. Mizumoto M, Arai S, Furutani M, Nakamura T, Ishigami S, Monden K, Ishiguro S, Fujita S, Imamura M. NO as an indicator of portal hemodynamics and the role of iNOS in increased NO production in CCl₄-induced liver cirrhosis. *J Surg Res.* 1997; 70:124-133.
 50. Iwai S, Karim R, Kitano M, Sukata T, Min W, Morimura K, Wanibuchi H, Seki S, Fukushima S. Role of oxidative DNA damage caused by carbon tetrachloride-induced liver injury – enhancement of MeIQ-induced glutathione S-transferase placental form-positive foci in rats. *Cancer Lett.* 2002; 179:15-24.
 51. Muriel P. Nitric oxide protection of rat liver from lipid peroxidation, collagen accumulation, and liver damage induced by carbon tetrachloride. *Biochem Pharmacol.* 1998; 56:773-779.
 52. Yoneda M, Tamori K, Sato Y, Yokohama S, Nakamura K, Makino I. Central thyrotropin-releasing hormone stimulates hepatic DNA synthesis in rats. *Hepatology.* 1997; 26:1203-1208.
 53. Tamori K, Yoneda M, Nakamura K, Makino I. Effect of intracisternal thyrotropin-releasing hormone on hepatic blood flow in rats. *Am J Physiol.* 1998; 274:G277-G282.
 54. Pyroja S, Joseph B, Paulose CS. Increased 5-HT_{2C} receptor binding in the brain stem and cerebral cortex during liver regeneration and hepatic neoplasia in rats. *J Neurol Sci.* 2007; 254:3-8.
 55. Abdel Salam OME, Sleem AA, Shaffie NM. Effect of the selective serotonin reuptake inhibitor fluoxetine on carbon tetrachloride induced hepatic damage in rats. *J Pharmacol Toxicol.* 2006; 1:395-406.
 56. Carvajal García-Pando A, García del Pozo J, Sánchez AS, Velasco MA, Rueda de Castro AM, Lucena MI. Hepatotoxicity associated with the new antidepressants. *J Clin Psychiatry.* 2002; 63:135-137.
 57. DeSanty KP, Amabile CM. Antidepressant-induced liver injury. *Ann Pharmacother.* 2007; 41:1201-1211.
 58. Hernandez-Avila CA, Modesto-Lowe V, Feinn R, Kranzler HR. Nefazodone treatment of comorbid alcohol dependence and major depression. *Alcohol Clin Exp Res.* 2004; 28:433-440.
 59. Dykens JA, Jamieson JD, Marroquin LD, Nadanaciva S, Xu JJ, Dunn MC, Smith AR, Will Y. *In vitro* assessment of mitochondrial dysfunction and cytotoxicity of nefazodone, trazodone, and buspirone. *Toxicol Sci.* 2008; 103:335-345.

60. Kostrubsky SE, Strom SC, Kalgutkar AS, Kulkarni S, Atherton J, Mireles R, Feng B, Kubik R, Hanson J, Urda E, Mutlib AE. Inhibition of hepatobiliary transport as a predictive method for clinical hepatotoxicity of nefazodone. *Toxicol Sci.* 2006; 90:451-459.
61. Bauman JN, Frederick KS, Sawant A, Walsky RL, Cox LM, Obach RS, Kalgutkar AS. Comparison of the bioactivation potential of the antidepressant and hepatotoxin nefazodone with aripiprazole, a structural analog and marketed drug. *Drug Metab Dispos.* 2008; 36:1016-1029.
62. Kalgutkar AS, Henne KR, Lame ME, Vaz AD, Collin C, Soglia JR, Zhao SX, Hop CE. Metabolic activation of the nontricyclic antidepressant trazodone to electrophilic quinone-imine and epoxide intermediates in human liver microsomes and recombinant P4503A4. *Chem Biol Interact.* 2005; 155:10-20.
63. Wen B, Ma L, Rodrigues AD, Zhu M. Detection of novel reactive metabolites of trazodone: Evidence for CYP_{2D6}-mediated bioactivation of *m*-chlorophenylpiperazine. *Drug Metab Dispos.* 2008; 36:841-850.

(Received March 19, 2010; Revised May 22, 2010; Accepted June 8, 2010)

Drug Discoveries & Therapeutics

Guide for Authors

1. Scope of Articles

Drug Discoveries & Therapeutics mainly publishes articles related to basic and clinical pharmaceutical research such as pharmaceutical and therapeutical chemistry, pharmacology, pharmacy, pharmacokinetics, industrial pharmacy, pharmaceutical manufacturing, pharmaceutical technology, drug delivery, toxicology, and traditional herb medicine. Studies on drug-related fields such as biology, biochemistry, physiology, microbiology, and immunology are also within the scope of this journal.

2. Submission Types

Original Articles should be reports new, significant, innovative, and original findings. An Article should contain the following sections: Title page, Abstract, Introduction, Materials and Methods, Results, Discussion, Acknowledgments, References, Figure legends, and Tables. There are no specific length restrictions for the overall manuscript or individual sections. However, we expect authors to present and discuss their findings concisely.

Brief Reports should be short and clear reports on new original findings and not exceed 4,000 words with no more than two display items. *Drug Discoveries & Therapeutics* encourages younger researchers and doctors to report their research findings. Case reports are included in this category. A Brief Report contains the same sections as an Original Article, but Results and Discussion sections must be combined.

Reviews should include educational overviews for general researchers and doctors, and review articles for more specialized readers.

Policy Forum presents issues in science policy, including public health, the medical care system, and social science. Policy Forum essays should not exceed 2,000 words.

News articles should not exceed 500 words including one display item. These articles should function as an international news source with regard to topics in the life and social sciences and medicine. Submissions are not restricted to journal staff - anyone can submit news articles on subjects that would be of interest to *Drug Discoveries & Therapeutics'* readers.

Letters discuss material published in *Drug Discoveries & Therapeutics* in the last 6 months or issues of general interest. Letters should not exceed 800 words and 6 references.

3. Manuscript Preparation

Preparation of text. Manuscripts should be written in correct American English and submitted as a Microsoft Word (.doc) file in a single-column format. Manuscripts must be paginated and double-spaced throughout. Use Symbol font for all Greek characters. Do not import the figures into the text file but indicate their approximate locations directly on the manuscript. The manuscript file should be smaller than 5 MB in size.

Title page. The title page must include 1) the title of the paper, 2) name(s) and affiliation(s) of the author(s), 3) a statement indicating to whom correspondence and proofs should be sent along with a complete mailing address, telephone/fax numbers, and e-mail address, and 4) up to five key words or phrases.

Abstract. A one-paragraph abstract consisting of no more than 250 words must be included. It should state the purpose of the study, basic procedures used, main findings, and conclusions.

Abbreviations. All nonstandard abbreviations must be listed in alphabetical order, giving each abbreviation followed by its spelled-out version. Spell out the term upon first mention and follow it with the abbreviated form in parentheses. Thereafter, use the abbreviated form.

Introduction. The introduction should be a concise statement of the basis for the study and its scientific context.

Materials and Methods. Subsections under this heading should include sufficient instruction to replicate experiments, but well-established protocols may be simply referenced. *Drug Discoveries & Therapeutics* endorses the principles of the Declaration of Helsinki and expects that all research involving humans will have been conducted in accordance with these principles. All laboratory animal studies must be approved by the authors' Institutional Review Board(s).

Results. The results section should provide details of all of the experiments that are required to support the conclusions of the paper. If necessary, subheadings may be used for an orderly presentation. All figures, tables, and photographs must be referred in the text.

Discussion. The discussion should include conclusions derived from the study and supported by the data. Consideration should be given to the impact that these conclusions have on the body of knowledge in which context the experiments were conducted. In Brief Reports, Results and Discussion sections must be combined.

Acknowledgments. All funding sources should be credited in the Acknowledgments section. In addition, people who contributed to the work but who do not fit the criteria for authors should be listed along with their contributions.

References. References should be numbered in the order in which they appear in the text. Cite references in text using a number in parentheses. Citing of unpublished results and personal communications in the reference list is not recommended but these sources may be mentioned in the text. For all references, list all authors, but if there are more than fifteen authors, list the first three authors and add "*et al.*" Abbreviate journal names as they appear in PubMed. Web references can be included in the reference list.

Example 1:

Hamamoto H, Akimitsu N, Arimitsu N, Sekimizu K. Roles of the Duffy antigen and glycoporphin A in malaria infectionand erythrocyte. *Drug Discov Ther.* 2008; 2:58-63.

Example 2:

Zhao X, Jing ZP, Xiong J, Jiang SJ. Suppression of experimental abdominal aortic aneurysm by tetracycline: a preliminary study. *Chin J Gen Surg*. 2002; 17:663-665. (in Chinese)

Example 3:

Mizuochi T. Microscale sequencing of *N*-linked oligosaccharides of glycoproteins using hydrazinolysis, Bio-Gel P-4, and sequential exoglycosidase digestion. In: *Methods in Molecular Biology: Vol. 14 Glycoprotein analysis in biomedicine* (Hounsell T, ed.). Humana Press, Totowa, NJ, USA, 1993; pp. 55-68.

Example 4:

Drug Discoveries & Therapeutics. Hot topics & news: China-Japan Medical Workshop on Drug Discoveries and Therapeutics 2007. <http://www.ddtjournal.com/hotnews.php> (accessed July 1, 2007).

Figure legends. Include a short title and a short explanation. Methods described in detail in the Materials and methods section should not be repeated in the legend. Symbols used in the figure must be explained. The number of data points represented in a graph must be indicated.

Tables. All tables should have a concise title and be typed double-spaced on pages separate from the text. Do not use vertical rules. Tables should be numbered with Arabic numerals consecutively in accordance with their appearance in the text. Place footnotes to tables below the table body and indicate them with lowercase superscript letters.

Language editing. Manuscripts submitted by authors whose primary language is not English should have their work proofread by a native English speaker before submission. The Editing Support Organization can provide English proofreading, Japanese-English translation, and Chinese-English translation services to authors who want to publish in *Drug Discoveries & Therapeutics* and need assistance before submitting an article. Authors can contact this organization directly at <http://www.iacmhr.com/iac-eso>.

IAC-ESO was established in order to facilitate manuscript preparation by researchers whose native language is not English and to help edit work intended for international academic journals. Quality revision, translation, and editing services are offered by our staff, who are native speakers of particular languages and who are familiar with academic writing and journal editing in English.

4. Figure Preparation

All figures should be clear and cited in numerical order in the text. Figures must fit a one- or two-column format on the journal page: 8.3 cm (3.3 in.) wide for a single column; 17.3 cm (6.8 in.) wide for a double column; maximum height: 24.0 cm (9.5 in.). Only use the following fonts in the figure: Arial and Helvetica. Provide all figures as separate files. Acceptable file formats are JPEG and TIFF. Please note that files saved in JPEG or TIFF format in PowerPoint lack sufficient resolution for publication. Each Figure file should be smaller than 10 MB in size. Do not compress files. A fee is charged for a color illustration or photograph.

5. Online Submission

Manuscripts should be submitted to *Drug Discoveries & Therapeutics* online at <http://www.ddtjournal.com>. The manuscript file should be smaller than 10 MB in size. If for any reason you are unable to submit a file online, please contact the Editorial Office by e-mail: office@ddtjournal.com

Editorial and Head Office

Wei TANG, MD PhD
Executive Editor
Drug Discoveries & Therapeutics
Pearl City Koishikawa 603,
2-4-5 Kasuga, Bunkyo-ku,
Tokyo 112-0003, Japan
Tel: 03-5840-9697
Fax: 03-5840-9698
E-mail: office@ddtjournal.com

Cover letter. A cover letter from the corresponding author including the following information must accompany the submission: name, address, phone and fax numbers, and e-mail address of the corresponding author. This should include a statement affirming that all authors concur with the

submission and that the material submitted for publication has not been previously published and is not under consideration for publication elsewhere and a statement regarding conflicting financial interests.

Authors may recommend up to three qualified reviewers other than members of Editorial board. Authors may also request that certain (but not more than three) reviewers not be chosen.

The cover letter should be submitted as a Microsoft Word (.doc) file (smaller than 1 MB) at the same time the work is submitted online.

6. Accepted Manuscripts

Proofs. Rough galley proofs in PDF format are supplied to the corresponding author *via* e-mail. Corrections must be returned within 4 working days of receipt of the proofs. Subsequent corrections will not be possible, so please ensure all desired corrections are indicated. Note that we may proceed with publication of the article if no response is received.

Transfer of copyrights. Upon acceptance of an article, authors will be asked to agree to a transfer of copyright. This transfer will ensure the widest possible dissemination of information. A letter will be sent to the corresponding author confirming receipt of the manuscript. A form facilitating transfer of copyright will be provided. If excerpts from other copyrighted works are included, the author(s) must obtain written permission from the copyright owners and credit the source(s) in the article.

Cover submissions. Authors whose manuscripts are accepted for publication in *Drug Discoveries & Therapeutics* may submit cover images. Color submission is welcome. A brief cover legend should be submitted with the image.

Revised June 20, 2009



Drug Discoveries & Therapeutics



Editorial Office

Pearl City Koishikawa 603,
2-4-5 Kasuga, Bunkyo-ku,
Tokyo 112-0003, Japan

Tel: 03-5840-9697
Fax: 03-5840-9698
E-mail: office@ddtjournal.com
URL: www.ddtjournal.com

JOURNAL PUBLISHING AGREEMENT

Ms No:

Article entitled:

Corresponding author:

To be published in Drug Discoveries & Therapeutics

Assignment of publishing rights:

I hereby assign to International Advancement Center for Medicine & Health Research Co., Ltd. (IACMHR Co., Ltd.) publishing Drug Discoveries & Therapeutics the copyright in the manuscript identified above and any supplemental tables and illustrations (the articles) in all forms and media, throughout the world, in all languages, for the full term of copyright, effective when and if the article is accepted for publication. This transfer includes the rights to provide the article in electronic and online forms and systems.

I understand that I retain or am hereby granted (without the need to obtain further permission) rights to use certain versions of the article for certain scholarly purpose and that no rights in patent, trademarks or other intellectual property rights are transferred to the journal. Rights to use the articles for personal use, internal institutional use and scholarly posting are retained.

Author warranties:

I affirm the author warranties noted below.

- 1) The article I have submitted to the journal is original and has not been published elsewhere.
- 2) The article is not currently being considered for publication by any other journal. If accepted, it will not be submitted elsewhere.
- 3) The article contains no libelous or other unlawful statements and does not contain any materials that invade individual privacy or proprietary rights or any statutory copyright.
- 4) I have obtained written permission from copyright owners for any excerpts from copyrighted works that are included and have credited the sources in my article.
- 5) I confirm that all commercial affiliations, stock or equity interests, or patent-licensing arrangements that could be considered to pose a financial conflict of interest regarding the article have been disclosed.
- 6) If the article was prepared jointly with other authors, I have informed the co-authors(s) of the terms of this publishing agreement and that I am signing on their behalf as their agents.

Your Status:

- I am the sole author of the manuscript.
 I am one author signing on behalf of all co-authors of the manuscript.

Please tick one of the above boxes (as appropriate) and then sign and date the document in black ink.

Signature:

Date:

Name printed:

Please return the completed and signed original of this form by express mail or fax, or by e-mailing a scanned copy of the signed original to:

Drug Discoveries & Therapeutics office

Pearl City Koishikawa 603, 2-4-5 Kasuga, Bunkyo-ku, Tokyo 112-0003, Japan

e-mail: proof-editing@ddtjournal.com

Fax: +81-3-5840-9698

